# Haemodynamics and vascular remodeling in vascular access : insights from numerical studies

# Haemodynamics and Vascular Remodeling in Vascular Access

## Insights from Numerical Studies

**Bogdan Ene-Iordache**

# Haemodynamics and Vascular Remodeling in Vascular Access

## Insights from Numerical Studies

A catalogue record is available from the Eindhoven University of Technology Library.
ISBN: 978-90-386-3906-2

Cover design: Davide Martinetti, *Mario Negri* Institute for Pharmacological Research, Ranica, Italy.

Printed by: Cartolibreria *Snoopy* (www.cartolibreriasnoopy.it), Brescia, Italy.

Financial support by the European Commission within the Seventh Framework Programme (ICT-2007-224390-ARCH) is gratefully acknowledged. Additional financial support was generously provided by Fondazione A.R.M.R., Bergamo, Italy.

# Haemodynamics and Vascular Remodeling in Vascular Access

## Insights from Numerical Studies

PROEFSCHRIFT

ter verkrijging van de graad van doctor aan de Technische Universiteit Eindhoven, op gezag van de rector magnificus prof.dr.ir. F.P.T. Baaijens, voor een commissie aangewezen door het College voor Promoties, in het openbaar te verdedigen op maandag 7 september 2015 om 14:00 uur

door

Bogdan Ene-Iordache

geboren te Ploiesti, Roemenië

Dit proefschrift van het proefontwerp is goedgekeurd door de promotoren en de samenstelling van de promotiecommissie is als volgt:

| | |
|---|---|
| voorzitter: | prof.dr. P.A.J. Hilbers |
| 1e promotor: | prof.dr.ir. F.N. van de Vosse |
| 2e promotor: | prof.dr. A. Remuzzi (University of Bergamo) |
| leden: | prof.dr.ir. F.P.T. Baaijens |
| | prof.dr. G. Dubini (Polytechnic University of Milan) |
| | prof.dr. T. Delhaas (UM) |
| | dr. J.H.M. Tordoir (UM-MUMC) |
| | prof.dr.ir. P.D. Anderson |

*To my father*

Table of Contents

# LIST OF ABBREVIATIONS

| | |
|---|---|
| AF | Anastomosis floor |
| AVF | Arteriovenous fistula |
| AVG | Arteriovenous graft |
| BP | Blood pressure |
| $C_p$ | plasma protein concentration (*g/dL*) |
| CDU | color-flow Doppler ultrasound |
| CFD | Computational fluid dynamics |
| CFL | Courant-Friederics-Lewy condition/number |
| CKD | Chronic kidney disease |
| CVC | Central venous catheter |
| DA | Distal artery |
| DNS | Direct numerical simulation |
| DSA | Digital subtraction angiography |
| EBPG | European Best Practice Guidelines |
| EC | Endothelial cells |
| ESRD | End stage renal disease |
| FSI | Fluid-structure interaction |
| GFR | Glomerular filtration rate |
| $H_t$ | Blood hemotocrit (%) |
| IH | Intimal hyperplasia |
| HD | Haemodialysis |
| MRA | Magnetic resonance angiography |
| NH | Neointimal hyperplasia |
| OSI | Oscillatory shear index |
| PA | Proximal artery |
| PIV | Particle image velocimetry |
| PD | Peritoneal dialysis |
| Re | Reynolds number |
| RI | Resistance index |
| RRT | Relative residence time |
| SS | Swing segment |
| transWSS | Transverse wall shear stress |
| US | Ultrasound |
| VA | Vascular access |
| Wo | Womersley number |
| WSS | Wall shear stress |

# CHAPTER 1

# General Introduction

## 1.1. Motivation

A well functioning vascular access (VA) serves as lifeline for the patients with impaired kidney function in order to perform efficient haemodialysis. There is general consensus in the literature on the superiority of arteriovenous fistula (AVF) over arteriovenous graft (AVG) and central venous catheter (CVC) regarding VA survival and related complications. Early failure of a VA occurs either if it never matures adequately to support puncture for dialysis or it fails within the first 3 months after surgery [1]. Despite the availability of clinical guidelines [1]-[3] recommending well-defined criteria preoperatively to create a native AVF, a high early failure rate is complained worldwide due to insufficient flow enhancement induced by development of stenotic lesions downstream of the anastomosis. Maintaining the patency of VA at long term for chronic haemodialysis is challenging. In studies performed between 1977 and 2002 where VA was provided by AVF surgery, the mean early failure rate was 25% (range 2% - 53%) while the mean one-year patency rate was 70% (42% - 90%) [4]. A clinical trial performed in 2012 in four experienced centres in Europe [5] reported an early failure rate of 21% and one-year primary patency rate of 66% [6].

Aimed at reducing these still unacceptably high failure rates, the ARCH FP7 project has built predictive models to simulate haemodynamics following AVF surgery [7], [8] and the VA community has become increasingly interested in such tools [9]. These computational models must be informed by patient-specific data, and where such data are not available, by generic or patient-specific adaptive rules [10]. Specific parameters regarding vascular adaptation, local remodeling (stenosis formation) and anastomosis pressure-drop laws might be obtained by 3-D modeling using computational fluid dynamics (CFD), which allow a more detailed calculation of the velocity and pressure fields and derived quantities like wall shear stress (WSS).

Since the 1990s, numerical modeling on idealized and real geometries was intensively used to assess the WSS in studying the link between haemodynamics and cardiovascular disease. Despite its clinical relevance, this type of method was less used for the study of VA complications.

## 1.2. Clinical background

Chronic kidney disease (CKD) is a progressive condition marked by deteriorating kidney function over time. It is actually a worldwide threat to public health, but the scale of problem is probably not fully appreciated. The number of subjects with CKD requiring renal replacement therapy is rising worldwide so that the global end-stage renal disease (ESRD) population will exceed 2 million patients in the next few years [11]. Continuing provision of adequate facilities, equipment and manpower to assist the growing number of patients with ESRD will pose a substantial burden on health care resources in all countries in the near future. Indeed, the aggregate cost for treatment during the coming decade will be more than US $ 1 trillion [12].

End-stage renal disease is the last phase of CKD when kidney function is impaired and thus it becomes critical for patient's own life to receive some form of renal replacement therapy, which consists primarily of dialysis or kidney transplantation. Dialysis procedure itself can be either haemodialysis (HD), when the process of blood purification takes place in extra corporeal machines called artificial kidneys or peritoneal dialysis (PD), when the waste products are exchanged between blood and the dialysate solution via diffusive transport through the intercellular gaps of patient's peritoneal membrane. This dissertation is focused on the VA for haemodialysis.

### 1.2.1. Haemodialysis

Duration and frequency of HD therapy depends on patient needs, being generally twice or three times weekly, during sessions of 3 to 5 hours, usually in hospital setting or specialized centers. During the HD procedure, patient's blood is pumped into an extracorporeal circuit where it is purified from waste products and the excess of water accumulated in the body. The principle of haemodialysis process is presented in Figure 1.1.

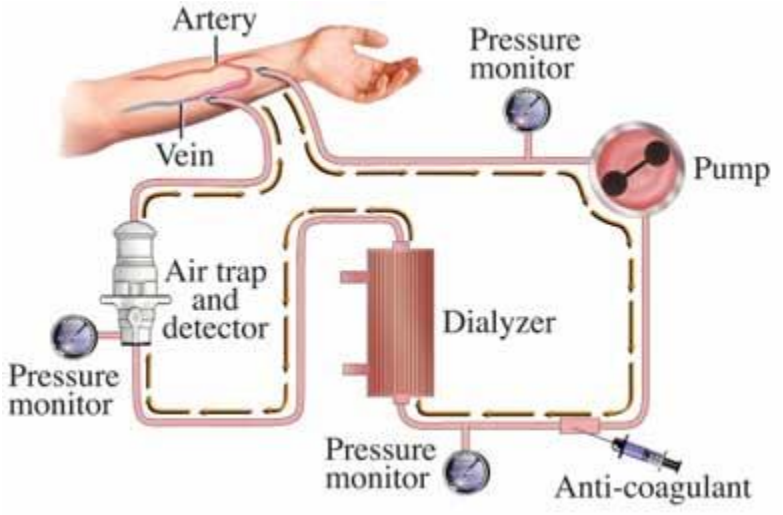


**Figure 1.1. Haemodialysis principle: blood is extracted through a VA and then pumped into an external circuit where it is purified from waste products and excess water accumulated in the body.**

As shown in figure, blood is extracted from patient's body through an arterial needle from the VA by using a roller pump. Then blood flows into the artificial kidney where the waste change take place over a membrane between blood and dialysate. The purified blood is then returned to the patient via the venous needle of VA.

## 1.2.2. The vascular access for haemodialysis

The VA should provide a site for repetitive cannulation, not prone to infections, for the arterial and venous lines and should supply sufficient blood volume flow to the haemodialysis machine. Vascular access can be provisional or permanent. Patients that have acute transitory impaired kidney function can be dialyzed via temporary catheters, like the central venous catheter (CVC). Central venous catheters for haemodialysis are placed into the jugular or subclavian vein to take benefit of the high flow rate in these vessels. Due to the risk of central venous stenosis subsequent to the placement of CVC and the high risk of infection and potential sepsis, CVC are recommended only in acute circumstances for a short period of time. This type of VA is not covered in the present thesis.

### 1.2.2.1. Permanent vascular access

If patients have lost definitively the renal function and needs long term dialysis, a permanent VA should be chosen. Available permanent vascular accesses can be divided into two main groups: autogenous (or native) arteriovenous fistulae (AVF) and prosthetic

arteriovenous grafts (AVG). Arteriovenous fistulae are created by the connection of an artery and a vein (anastomosis), preferable in the lower non-dominant arm. This procedure creates a low-resistance, high-flow rate conduit by bypassing the distal circulation. Efficient dialysis treatment depends on sufficient blood flow delivery in the haemodialysis machine. The time required for VA maturation varies among patients, but in general, allowing an AVF to mature for 6 to 8 weeks and an AVG for 3 weeks, is appropriate [1]. In general, a working access must have all the following characteristics: blood flow adequate to support dialysis, which usually equates to a blood flow greater than 600 mL/min; a diameter greater than 0.6 cm, with location accessible for cannulation and discernible margins to allow for repetitive cannulation; and a depth of approximately 0.6 cm (ideally, between 0.5 to 1.0 cm from the skin surface). This combination of characteristics is known as "the rule of 6s" [1].

There is general consensus in the literature on the superiority of AVF over AVG and CVC regarding patient's survival and complications such as thrombosis, infection, access-related hospitalization and quality of life. Guidelines of the National Kidney Foundation Kidney Disease Outcomes Quality Initiative (NKF-KDOQI) [1], [2] and the United States "Fistula First Breakthrough Initiative" (FFBI) program advocate the implementation of an all-autogenous policy to maximize the use of AVF over the AVG. Only if the patient has inadequate or unavailable veins to construct a native VA, surgeons may rely on grafts made by synthetic bio-compatible materials to create an AVG.

Consequently, the studies presented in the following chapters of this thesis deal with AVF, and we only may speculate that similar findings might be expected in AVG.

Native AVF can be constructed with different surgical techniques to create the anastomosis between vein and artery: (i) side artery to side vein (*side-to-side*), (ii) side artery to end vein (*side-to-end*), and (iii) end artery to end vein anastomosis (*end-to-end*) as presented in Figure 1.2. Naming rules for the fistula take into account the blood vessels involved and its location, e.g., distal radial-cephalic, proximal brachial-cephalic.

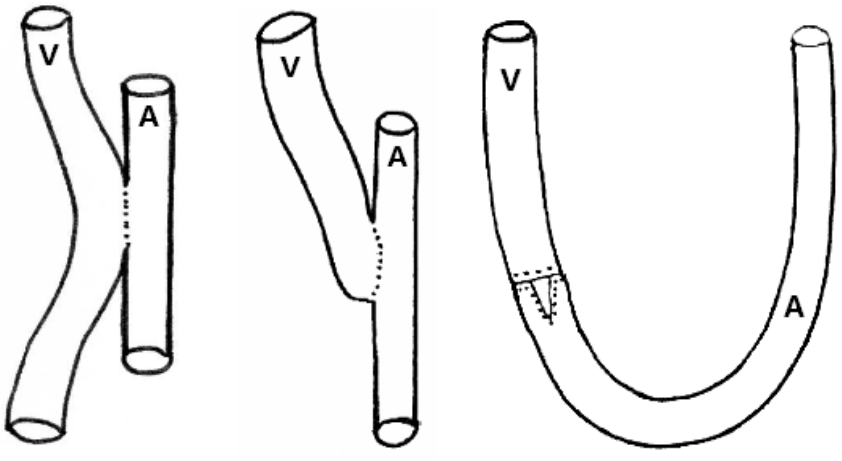


**Figure 1.2. Anastomosis techniques to create native AVF. From the left to right: *side-to-side*, *side-to-end* and *end-to-end*. In *end-to-end* case, both artery and vein are resected and the radial artery is curved at 180° to form an U-shaped bend before suturing the anastomosis. From Konner K, *Semin Dial*, 2003 [13].**

Arteriovenous fistulae for haemodialyis will be created preferentially in the most distal available site in the upper extremity because of the lower rate of complications and to preserve the more proximal vessels for possible future VA, in case of first access failure.

### 1.2.2.2. Haemodynamics of vascular access

Arteriovenous fistulae used for VA involve complex haemodynamic conditions. Firstly, constructing an arteriovenous shunt between arterial and venous circulation leads to very high blood volume flow in the VA feeding arteries and draining veins. Secondly, the non-uniform geometry of the anastomosis forces blood to change direction rapidly. Reversal of blood flow in the distal artery (sometimes referred as steal) occur in many cases of s*ide-to-end* AVF, but its presence has no pathophysiological significance related to hand ischaemia, at least in case of distal AVF [14]. Therefore, blood flow conditions in these VA blood vessels are very different from the physiological state and can cause changes in the vascular wall responsible for local remodeling, narrowing (stenosis) but also dilatation (aneurysm) of the internal lumen.

Assessment of haemodynamics in the AVF can be made by direct measurements (*in vivo*) or computer simulations (*in silico*). *In vivo* studies made by using Doppler ultrasound measurements are now also recommended by the guidelines for the surveillance of VA dysfunction [1]. In the last decades, numerical simulations of blood flow were widely employed for the study of haemodynamic parameters known to correlate well with the pathogenesis of vascular wall diseases, like atherosclerosis and intimal hyperplasia.

### 1.2.2.3. Complications of vascular access

The maturation process or fistula patency may be harmed by complications that might occur in AVF and AVG: thrombosis, stenosis, steal syndrome with hand ischemia and heart failure.

***Thrombosis*.** Thrombosis is the major cause of failure of all types of arteriovenous fistulae. The average incidence of thrombosis is estimated to be 0.2 occlusion/patient/year [15]. The occlusion results from initial deterioration of vessel wall due to intimal hyperplasia lesions that induce stenosis and subsequent thrombus formation. Thrombosis at a later lifetime of the VA is mostly preceded by stenoses.

***Stenosis*.** Stenosis is usually the underlying cause for thrombosis. Stenoses in AVF develop mainly in the anastomosis and in the draining vein and rarely in the feeding artery in all VA types [17]. Sivanesan et al. [18] found stenosis sites in radio-cephalic *side-to-end* AVF and classified them in three types. Type I and type II occurred at the anastomosis floor and at the inner wall of the juxatanastomosis vein and were not progressive. Type III stenoses occurred in the zone where the cephalic vein straightens out and were found to be progressive. As a stenosis often leads to thrombosis, it is important to detect stenosis formation at early stage. The risk for thrombosis increases with increasing stenosis degree. The NKF-KDOQI guidelines for VA define significant stenosis as a 50% or greater reduction in normal vessel diameter accompanied by a haemodynamic, functional, or clinical abnormality [1]. Several hypotheses have been put forward to explain the formation of AVF stenoses, of which the foremost is the mechanism of underlying intimal hyperplasia development [19]. The blood flow dynamics within the VA conduit is thought to have great influence on the initiation and development of intimal hyperplasia [20], [21]. Wall shear stress, the frictional force exerted by flowing blood on the inner vessel wall, is an important determinant of endothelial cell function and gene expression as well as of its structure *in vivo* [35]. Especially the low wall shear stress, as present in artery bifurcations opposite to the flow divider, expresses mitogenic factors which might initiate intimal hyperplasia [22], [23].

***Distal ischemia***. VA causes changes in vascular blood flow that may result in impeded perfusion of the extremity. This may lead to ischemia distal to the arteriovenous anastomosis.

Symptoms of distal ischemia are pain, weakness, pallor, paresthesia and, in cases of severe ischemia, ulceration, necrosis and eventual loss of digits and even the entire hand. Severe distal ischemia, requiring intervention, occurs in approximately 5% of patients after VA placement [14]. Some categories of patients are more likely to develop distal ischemia. In particular, patients with previous VA procedures, patients suffering diabetes and/or peripheral arterial occlusions are at greater risk to develop this complication. In these patients the collateral blood supply provided by medium-sized vessels can be diminished and this condition further jeopardizes peripheral perfusion, leading to distal hypoperfusion. *Steal syndrome* defined as reversal of blood flow in the distal artery occur in many cases of s*ide-to-end* AVF following VA creation [14]. In this context, also the location of the VA anastomosis is an important factor since more proximally located VA anastomosis is associated with higher incidence of distal ischemia compared to VA located more distally. Finally, arterial inflow characteristics deriving from small dimension of collateral vessels and/or small vessels obstructions are associated with steal syndrome.

***Heart failure.*** Heart failure represents the primary cause of death in ESRD patients. After creation of an AVF, there is a 10-20% increase in cardiac output due to both decreased peripheral resistance and increase of the sympathetic nervous system activity. The consequence of long-term AVF use may induce left ventricular hypertrophy, high-output cardiac failure and myocardial ischemia. Arteriovenous fistula creation, besides inducing changes in neuro-hormonal systems and vasoactive hormones, may trigger important changes in the structure and function of the heart over time, with cardiac remodeling and worsening of function [24].

# 1.3. The role of haemodynamics in vascular remodeling and disease

## 1.3.1. Haemodynamic stimuli

The haemodynamic conditions play a fundamental role in regulating the vascular structure. Blood vessels are permanently subjected to mechanical stimuli in the form of pressure that acts normal to the vessel wall inducing circumferential and axial stress (e.g. average force per unit area) into the wall, and of tangential shear stress due to the frictional force of flowing blood. Moreover, due to the pulsatile nature of blood volume flow, these stimuli vary from a minimum to a maximum acting cyclically with the pulse beat.

### 1.3.1.1. Haemodynamic pressure

Internal blood pressure is the major determinant of vessel stretch. The haemodynamic pressure, acting normal to the vessel wall, induces in the wall circumferential (hoop) - $\sigma_\theta$ - and axial - $\sigma_z$ - stresses which will counteract the intraluminal pressure (see Figure 1.3).

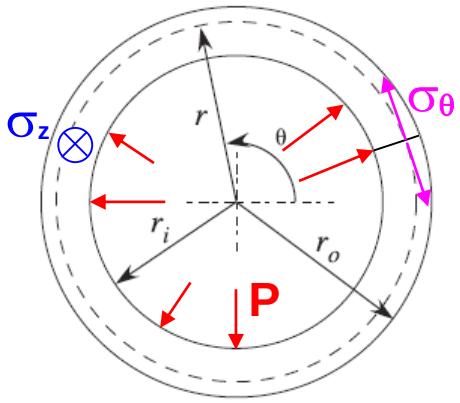


**Figure 1.3. Internal pressure load on blood vessel wall.**
**From Tsamis A, *J Biomech*, 2009 [25].**

It has been shown that chronic elevation of blood pressure affects the dimensions and properties of arterial walls [26]. One of the specific biomechanical manifestations to arterial wall adaptation in response to hypertension is wall hypertrophy that restores the circumferential wall stress at *in vivo* operating pressure to a normal value and changes arterial stiffness to an optimal level. The hypertension as a haemodynamic stimulus activates especially the vascular smooth cells in the vessel wall [26].

### 1.3.1.2. Haemodynamic shear stress

Wall shear stress (WSS or $\tau_s$) represents physically the stress vector exerted by flowing blood tangential to the endothelium, with a magnitude equal to the product between shear rate (the derivative of the blood velocity profile near the vessel wall) and blood viscosity (see Figure 1.4).

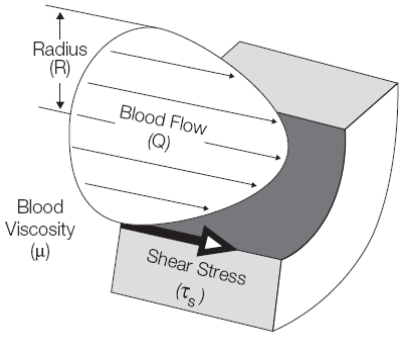


**Figure 1.4. Wall shear stress is the unit frictional force tangential to the endothelial cells layer. From Malek AM, *JAMA*, 1999 [37].**

Blood vessels respond to changes in wall shear stress, in the sense that increased shear leads to luminal dilatation and decreased shear stress leads to luminal reduction. It was demonstrated that blood vessels really sense the WSS, since keeping flow constant and increasing the blood viscosity also leads to dilatation [27]. Compared to pressure, shear stress acts tangential to the internal vessel surface. Accordingly, the WSS is sensed principally by endothelial cells (EC), located at the interface between blood and vessel wall. Hence, the endothelium acts as both sensor and effector of flow-dependent remodeling.

### 1.3.1.3. Mechanisms of blood vessel remodeling

Alterations of the haemodynamic stimuli invariably produce transformations in the vessel wall structure and lumen diameter that aim to accommodate the new conditions by restoring basal levels of tensile stress and shear stress. Blood volume flow and pressure *in vivo* vary simultaneously and it is likely that pressure- and flow-dependent responses interact. It seems that acute increases in blood volume are associated with a reduction in vascular resistance that offsets any increase in blood pressure [28], whereas the chronic increases in

circulating blood volume after AVF creation are associated with an increase in cardiac output, achieved by a reduction in peripheral resistance, an increase in sympathetic nervous system activity (increasing contractility and vascular tone), and an increase in stroke volume and heart rate [28].

Mechanisms at cell level within the blood vessel wall that enable vessels to respond to local changes in blood pressure and flow have been extensively studied. At macroscopic level, blood volume flow regulates arterial diameter through changes in ***wall shear stress*** (Q -> $\tau$) and intraluminal pressure regulates artery wall thickness through its effect on ***wall tension*** (P -> $\sigma$), as shown in Figure 1.5.

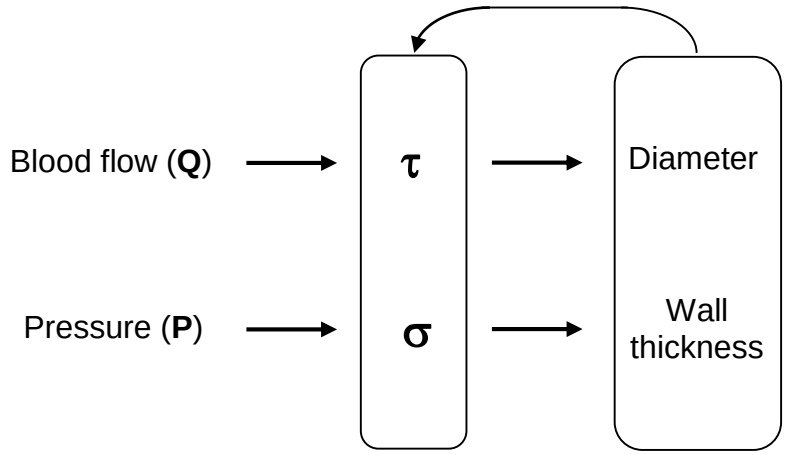


**Figure 1.5. Haemodynamic stimuli and structural responses of blood vessel. From Pries AR, *AJP*, 2005 [29].**

As perfusion pressure increases, the vascular smooth muscle contracts to elevate resistance and maintain a constant blood volume flow. Pressure-dependent autoregulation has been demonstrated in arteries, arterioles and veins in animals [30] and in humans [31]. In addition to responding to changes in pressure, blood vessels also respond to changes in blood flow. Increased blood volume flow leads to vasodilatation and elongation [23] and reduced vascular resistance [32] and chronic reduction in blood volume flow results in luminal diameter decrease [33].

## 1.3.2. The response of endothelium to shear forces

The endothelium is the primary sensor and regulator tissue of the vessel wall that releases substances to control vascular tone and structure in order to maintain homeostasis in response to changes in haemodynamic stimuli. In physiological state, the haemodynamic

stimuli act in beneficial way and protective against vessel wall disease. If different from the normal physiological range, namely in "disturbed flow" conditions, these haemodynamic factors are implicated in the etiology of the vascular wall disease.

*In vivo* data clearly show that at rest, time-averaged WSS is far from constant along the arterial tree, since it depends on the vascular territory [34], [35]. For example, WSS is substantially higher in the carotid artery than in the brachial and femoral arteries, and thus the anatomical location of the vascular bed is an important factor to take into account when doing *in vitro* studies on endothelial cells [36].

It was clearly shown that the WSS is pulsatile, and hence we should deal with peak, mean and minimum values and be aware that there is a range of physiologic values for each vascular bed [35]. In this direction, in a review article [37], Malek et al proposed a physiologic range of WSS for the whole vascular tree, considering that 10 to 70 dyne/cm$^2$ is normal, and that outside this range the WSS might trigger mechanisms leading to vascular pathology, as shown in Figure 1.6.

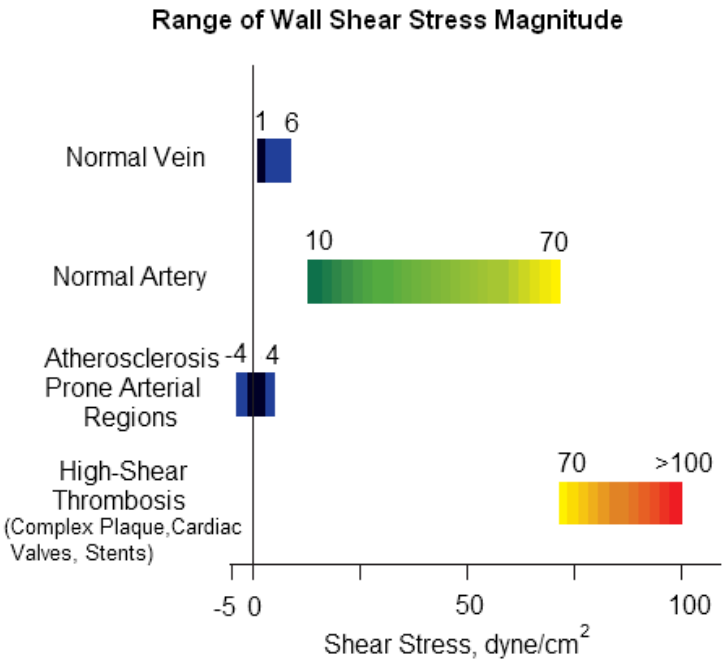


**Figure 1.6 Ranges of WSS encountered in arteries, veins and in low- and high-shear pathologic states. From Malek AM, *JAMA*, 1999 [37].**

Lower values of WSS may induce atherosclerotic plaques formation and therefore are considered "atherosclerosis prone" while WSS higher than this range may provoke endothelial cells cleavage and consequently "high-shear" induced thrombosis [37]. More recently, it was

clarified that "disturbed flow" is a condition of endothelium exposed to low averaged shear stress, constantly changing gradients of shear stress, oscillatory shear stress and multidirectional secondary flows. These haemodynamic conditions occur at specific sites of the arterial tree where there is blood flow separation or stagnation points like arterial branches, at stenosed sites or around stent struts [38].

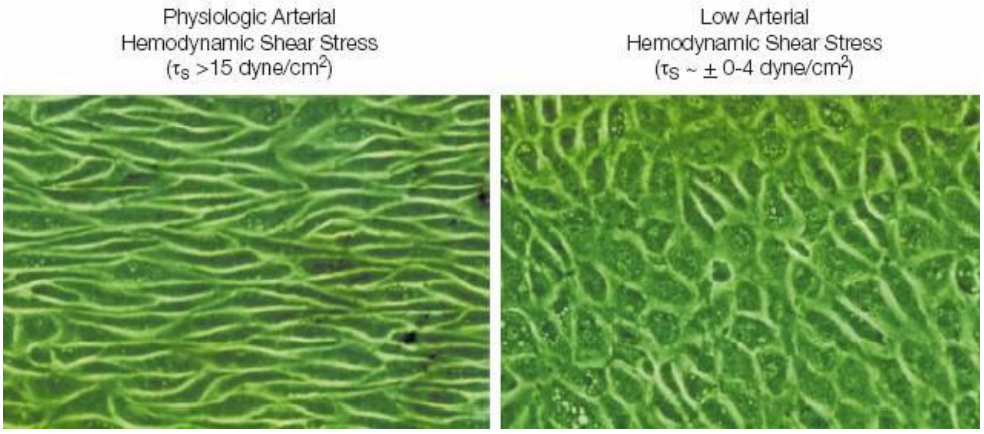


**Figure 1.7. Endothelial cells morphology is different according to the fluid shear. From Malek AM, *JAMA*, 1999 [37].**

Experimentally it was observed that the nature of flow, and therefore of the resulting fluid shear stress is sensed by the EC. There are differences in the endothelial cell morphology and biochemical substances that are released in pulsatile and oscillating flow versus the laminar flow [39], [40]. *In vivo* the flow pattern in the straight part of the arterial tree is pulsatile with a marked forward flow, whereas at the branch points it has a much lesser forward component and is similar to the reciprocating shearing in the reattachment zones (like for example on the outer wall of the sinus at the carotid bifurcation). It was demonstrated *in vitro*, that in this latter condition, haemodynamic stimuli on EC cause sustained molecular signaling of pro-inflammatory (monocyte adhesion, EC turnover and LDL permeability) and proliferative pathways (upregulation of inflammatory genes and genes that raise intracellular lipids) that are athero-prone. In experiments resembling the straight part of arterial tree, all these mechanisms are opposite and their effects are athero-protective [41].

## 1.3.3. Intimal hyperplasia

Intimal hyperplasia (IH) is a fibro-muscular thickening of the vessel wall. In the IH process, vascular smooth muscle cells migrate from media to the intima layer. Intimal hyperplasia is not really a disease, but rather a physiologic healing response to the injury of the

blood vessel wall. When the endothelium is injured, endothelial cells release inflammatory mediators that trigger platelet aggregation, fibrin deposition and recruitment of leukocytes to this area. These cells express growth factors that promote smooth muscle cells migration from the media to the intima. The smooth muscle cells proliferate in the intima and deposit extracellular matrix, in a process analogous to scar formation [42]. The result is formation of a neo-intima over the site of injury. An exuberant healing response leads to intimal thickening that encroaches on the vessel lumen and may cause stenosis, and subsequent thrombosis [19].

Also in intimal hyperplasia the haemodynamic shear stress seems to be the trigger factor, especially the low (mean) WSS at stagnation points [42]. Morinaga and colleagues [43] demonstrated in an *in-vivo* study in dogs already in 1985 that the low WSS is the major determinant of IH. They clearly showed that the change in WSS, but not the rate of blood volume flow, is the essential haemodynamic factor related to IH in autogenous vein grafts. A direct relation between low WSS profiles and pattern of IH was demonstrated recently *in-vivo* in a pig model of AVF [44]. Histology of neointimal hyperplasia and its relation with WSS has been characterized in subjects with AVF for haemodialysis that experienced early failure [45]. As seen in Figure 1.8, the luminal shape at site of stenoses were in the majority of cases off-centered, leading these authors to hypothesize that shear stress profiles were distributed non-uniformly along the circumference of the vein.

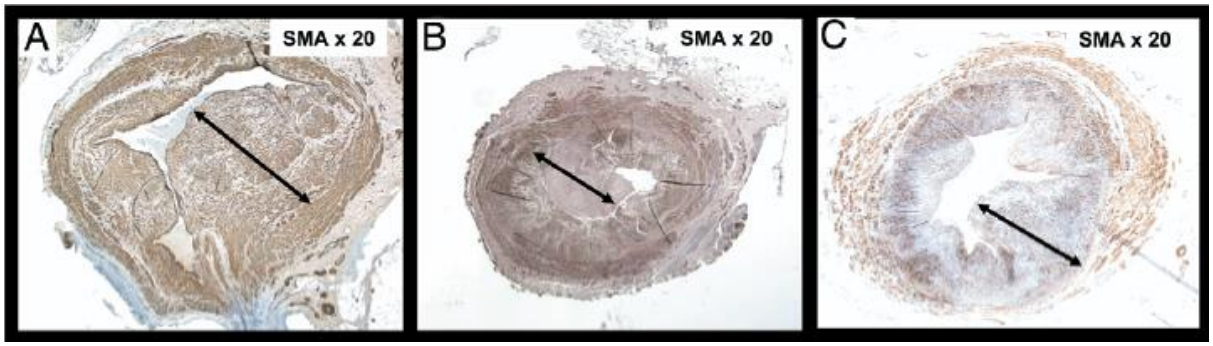


**Figure 1.8. Neointimal hyperplasia in representative sections from 3 patients with early AVF failure. From Roy-Chaudhury P et al, *AJKD*, 2007 [45].**

Morphological abnormalities of blood vessel wall, in particular intimal hyperplasia, should be carefully investigated in ESRD and haemodialysis patients because VA patency is strongly influenced by the lesions that induce luminal stenosis and subsequent decrease of the blood volume flow rate. Factors like aging, underlying diabetes and cardiovascular disease lead to arteriosclerotic change of blood vessels in ESRD patients. It follows that preexisting conditions of VA vessels, like for example the preexisting IH in radial artery or cephalic vein,

may influence the VA outcome. Indeed, in patients undergoing AVF creation for haemodialysis, preexisting radial artery IH [46] and also increased radial artery intima plus media thickness [47] were found to be closely correlated with early failure of radiocephalic AVF. Moreover, there is preexisting IH on the cephalic veins of ESRD patients before AVF construction [48] and this condition may influence the outcome of VA in terms of future stenosis and failure.

## 1.4. Study objectives

### 1.4.1. Unmet questions in AVF

The VA is a pervasive problem for the haemodialysis patients and still needs investigations after fifty years from the first fstula creation [49] to understand the reasons and to prevent short and long-term failure of the shunt. Considerable evidence exists about the role of ***disturbed flow*** in the pathogenesis of atherosclerosis [41]. Overall, the VA is a very high-blood flow rate conduit with respect to the physiological condition, but whether disturbed flow develops on the AVF walls was not studied yet.

In this context, new computational tools such as three-dimensional CFD may help in characterizing the blood flow inside the AVF, unraveling the mechanisms responsible for VA failure, with obvious implications in the improvement of clinical outcome of uremic patient management. The better understanding of haemodynamic conditions that develop after the surgical creation of the AVF, on one hand, should conduct us to deeper insights into the mechanisms that lead to intimal hyperplasia of the vascular wall and subsequent closure of the VA due to stenosis. On the other hand, understanding of vascular adaptation and local remodeling could help in optimizing the surgical management of VA placement, directed at increasing short and long term patency of the AVF for haemodialysis patients.

### 1.4.2. Aim of the dissertation

The aim of the present dissertation was to investigate with computational modeling methods the haemodynamics inside the VA. More specifically, two main classes of numerical methods were used in this thesis. The first class of numerical methods is three-dimensional, transient CFD simulations, applied either to idealized or to patient-specific models of the AVF

anastomoses. The second one is based on Womersley's theory for pulsatile flow starting from boundary conditions derived by echo-Doppler examination of the radial artery in wrist fistulae in patients starting dialysis therapy.

The following main research questions were addressed in this dissertation:

1°. Is CFD useful when studying blood flow dynamics in idealized geometry of VA anastomoses ? How could the results obtained in such numerical studies be helpful in basic research of AVF complications ? Does disturbed flow develop in idealized models of AVF ?

2°. As AVF are exposed to high blood volume flow rates, is CFD functional when studying blood flow dynamics in patient-specific models of VA anastomoses ? Is CFD adequate for obtaining a reliable map of WSS patterns ? Does disturbed flow develop in real geometries of AVF ?

3°. Is a more accurate calculation of WSS as a function of time useful in the clinical research ? Are there differences between classic (Poiseuille) estimation and such a method relevant to the understanding of adaptation processes occuring post-surgery in the AVF limbs ?

### 1.4.3. Thesis outline

Given the considerations presented above, the following research topics were addressed in specific chapters of this thesis:

- **Chapter 1** summarizes concepts considered necessary for the understanding of research topics, providing an introduction of the clinical problem and the aim of the dissertation.

- **Chapter 2** presents a numerical study by means of CFD of blood flow in idealized *side-to-end* and *end-to-end* anastomoses with real boundary conditions (in terms of dimensions and blood volume flow rate) resembling early post-surgery condition of AVF. The main focus was on the haemodynamic conditions, especially on the WSS

patterns that develop in the AVF after the fistula creation. The most important finding was that disturbed flow, i.e. low and reciprocating WSS, developed in the same sites where stenosis was documented in previous AVF experimental studies.

- The study presented in **Chapter 3** is a continuation of the previous work. Given that disturbed flow was found to develop in specific sites, the question was whether the anastomotic angle of *side-to-end* radial-cephalic AVF might have an impact on the local disturbed flow patterns, and hence on intimal hyperplasia development. To this end, a parametric CFD study of the AVF having anastomotic angles of 30°, 45°, 60° and 90° was performed.

- **Chapter 4** was an image-based CFD study in a realistic AVF geometry aimed mainly at corroborating the hypothesis made in Chapter 2 regarding the development of disturbed flow. The study was performed on a *side-to-end* anastomosis case of a patient from the ARCH clinical study [6]. The numerical analysis revealed laminar flow within the arterial limbs and a complex flow field in the swing segment, featuring turbulent eddies leading to high frequency oscillation of the WSS vectors. Multidirectional disturbed flow developed on the anastomosis floor and overall swing segment. Reciprocating disturbed flow zones were found on the distal artery near the floor and on the inner wall of the swing segment. This has obvious implications for elucidating the haemodynamic forces involved in the initiation of venous wall thickening in vascular access.

- The study in **Chapter 5** was focused on an *end-to-end* anastomosis case of a patient already in haemodialyis treatment in the Nephrology and Dialysis Unit of Bergamo Hospital. A three-dimensional patient-specific model of the AVF was reconstructed from digital subtraction angiography images of the fistula. As boundary conditions for CFD simulations we used blood volume flow measurements obtained by echo-color Doppler assessment of the radial artery. This study is an example of how CFD can be applied to study the flow field and WSS patterns in a patient-specific case of native fistula.

- **Chapter 6** reports the results of an observational pilot study on 28 patients that underwent *end-to-end* native fistula for haemodialysis and then were followed-up for

more than 3 months. For calculation of pulsatile blood volume flow and WSS, we used a numericalal model based on Womersley theory for unsteady flow in tubes. This model was applied to the radial artery of all patients, 1 day before surgery, and then, within 10, 40, and 100 days after. The results confirmed that the radial artery diameter increases in response to a chronic increase in blood flow in uremic patients. Moreover, it seems that the radial artery dilates in such a way as to maintain the peak wall shear stress constant, suggesting that endothelial cells sense the maximum rather than the time-averaged WSS.

- **Chapter 7** is a general discussion, including the achievements, future research considerations, study limitations and the take home messages of this thesis.

# 1.5. References


[1] NKF/KDOQI Vasclar Access Work Group. Clinical practice guidelines for VA. *Am J Kidney Dis*, 2006; 48 Suppl 1:S176-S247.

[2] NKF/KDOQI Vascular Access Work Group. Clinical practice guidelines for VA. *Am J Kidney Dis*, 2006;48 Suppl 1:S248-S273.

[3] Tordoir JHM, Canaud B, Haage P, Konner K, Basci A, Fouque D, Kooman J, Martin-Malo A, Pedrini L, Pizzarelli F, Tattersall J, Vennegoor M, Wanner C, ter Wee P, Vanholder R. EBPG on VA. *Nephrol Dial Transplant*, 2007;22 Suppl 2:ii88-117.

[4] Allon M, Robbin ML. Increasing arteriovenous fistulas in hemodialysis patients: problems and solutions. *Kidney Int*. 2002 Oct;62(4):1109-24. Review.

[5] Clinical study protocol for the ARCH project - computational modeling for improvement of outcome after VA creation. Bode A, Caroli A, Huberts W, Planken N, Antiga L, Bosboom M, Remuzzi A, Tordoir J; ARCH project consortium. *J Vasc Access*, 2011; 12(4):369-76.

[6] Caroli A, Manini S, Antiga L, Passera K, Ene-Iordache B, Rota S, Remuzzi G, Bode A, Leermakers J, van de Vosse F, Vanholder R, Malovrh M, Tordoir J and Remuzzi A on behalf of the ARCH project Consortium. Validation of patient specific hemodynamic computational model for surgical planning of VA in hemodialysis patients. *Kidney Int*, 2013;84(6):1237-45.

[7] Huberts W, Bode AS, Kroon W, Planken RN, Tordoir JH, van de Vosse FN, Bosboom EM. A pulse wave propagation model to support decision-making in VA planning in the clinic. *Med Eng Phys*, 2012; 34(2):233-48.

[8] Manini S, Passera K, Huberts W, Botti L, Antiga L, Remuzzi A. Computational model for simulation of vascular adaptation following VA surgery in haemodialysis patients. *Comput Methods Biomech Biomed Engin*, 2014;17(12):1358-67.

[9] Konner K, Lomonte C, Basile C. Placing a primary arteriovenous fistula that works - more or less known aspects, new ideas. *Nephrol Dial Transplant*, 2013; 28(4):781-4.

[10] Passera K, Manini S, Antiga L, Remuzzi A. Patient-specific model of arterial circulation for surgical planning of VA. *J Vasc Access*, 2013;14(2):180-9.

[11] Dirks J, Remuzzi G, Horton S, Schieppati A and Rizvi SAH. in *Disease Control Priorities in Developing Countries* (eds Jamison, D. T. et al.) 695–706 (Oxford University Press and The World Bank, New York, 2006).

[12] Xue J, Ma J, Louis T, Collins A. Forecast of the number of patients with end-stage renal disease in the United States to the year 2010. *J Am Soc Nephrol* 2001; 12: 2753–8.

[13] Konner K. The initial creation of native arteriovenous fistulas: surgical aspects and their impact on the practice of nephrology. *Semin Dial* 2003; 16: 291–298.

[14] Scheltinga MR, Bruijninckx CMA. Haemodialysis access-induced distal ischaemia (HAIDI) is caused by loco-regional hypotension but not by steal. *Eur J Vasc Endovasc Surg* 2012; 43:218-223.

[15] Tordoir JH, Van Der Sande FM, De Haan MW. Current topics on VA for hemodialysis. *Minerva Urol Nefrol* 2004 Sep;56(3):223-35.

[16] Asif A, Roy-Chaudhury P, Beathard GA: Early arteriovenous fistula failure: a logical proposal for when and how to intervene. *Clin J Am Soc Nephrol* 2006, 1(2):332-339.

[17] Badero OJ, Salifu MO, Wasse H, Work J: Frequency of swing-segment stenosis in referred dialysis patients with angiographically documented lesions. *Am J Kidney Dis* 2008, 51(1):93-98.

[18] Sivanesan S, How TV, Bakran A. Sites of stenosis in AV fistulae for haemodialysis access. *Nephrol Dial Transpl* 1999, 14(1):118-120.

[19] Roy-Chaudhury P, Spergel LM, Besarab A, Asif A, Ravani P. Biology of arteriovenous fistula failure. *J Nephrol* 2007, 20(2):150-163.

[20] Bassiouny HS, White S, Glagov S, Choi E, Giddens DP, Zarins CK. Anastomotic intimal hyperplasia: mechanical injury or flow induced. *J Vasc Surg* 1992 Apr;15(4):708-16.

[21] Zarins CK, Giddens DP. Relationship between anastomotic hemodynamics and intimal thickening. *J Vasc Surg* 1991 May;13(5):738-40.

[22] Nanjo H, Sho E, Komatsu M, Sho M, Zarins CK, Masuda H. Intermittent short-duration exposure to low wall shear stress induces intimal thickening in arteries exposed to chronic high shear stress. *Exp Mol Pathol* 2006 Feb;80(1):38-45.

[23] Sho E, Nanjo H, Sho M, Kobayashi M, Komatsu M, Kawamura K et al: Arterial enlargement, tortuosity, and intimal thickening in response to sequential exposure to high and low wall shear stress. *J Vasc Surg* 2004, 39(3):601-612.

[24] MacRae JM, Levin A, Belenkie I. The cardiovascular effects of arteriovenous fistulas in chronic kidney disease: a cause for concern? *Semin Dial* 2006 Sep-Oct;19(5):349-52.

[25] Tsamis A and Stergiopulos. Arterial remodeling in response to increased blood flow using a constituent-based model. *J Biomech* 2009, 42: 531-536.

[26] Hayashi K, Naiki T. Adaptation and remodeling of vascular wall; biomechanical response to hypertension. *J Mech Beh Biomed Mat* 2009, 2:3-19.

[27] Melkumyants AM, Balashov SA, Khayutin VM. Endothelium dependent control of arterial diameter by blood viscosity. *Cardiovasc Res* 1989; 23: 741-747.

[28] MacAllister RJ and Vallance P. Systemic vascular adaptation to increases in blood volume: the role of the blood vessel wall. *Nephrol Dial Tranpl* 1996, 11: 231-240.

[29] Pries AR and Secomb TW. Control of blood vessel structure: insights from theoretical models. *Am J Physiol Heart Circ Physiol* 2005, 288:H1010-H1015.

[30] Cowley AW. Long-term control of arterial blood pressure. *Physiol Rev* 1992, 72: 213-300.

[31] Berczi V, Green AS, Dorney G at al. Venous mytogenic tone: studies in human and canine vessels. *Am J Physio*l 1992, 263:H315-H659.

[32] Kamiya A, Togawa T. Adaptive regulation of wall shear stress to flow change in the canine carotid artery. *Am J Physiol* 1980, 239:H14-H21.

[33] Sho E, Sho M, Singh TM, Xu C, Zarins CK, Masuda H. Blood flow decrease induces apoptosis of endothelial cells in previously dilated arteries resulting from chronic high blood flow. *Arterioscler Thromb Vasc Biol*. 2001, 21(7):1139-1145.

[34] Dammers R, Stifft F, Tordoir JHM, Hameleers JM, Hoeks APG, Kitslaar P. Shear stress depends on vascular territory: comparison between common carotid and brachial artery. *J Appl Physiol* 2003, 94:485-489.

[35] Reneman RS, Arts T, Hoeks AP. Wall shear stress--an important determinant of endothelial cell function and structure--in the arterial system in vivo. Discrepancies with theory. *J Vasc Res* 2006, 43(3):251-269.

[36] Reneman RS and Hoeks APG. Wall shear stress as measured in vivo: consequences for the design of the arterial system. *Med Biol Eng Comput* 2008, 46:499-507.

[37] Malek AM, Alper SL, Izumo S. Hemodynamic shear stress and its role in atherosclerosis. *JAMA* 1999, 282(21):2035-2042.

[38] Davies PF. Hemodynamic shear stress and the endothelium in cardiovascular pathophysiology. *Nat Clin Pract Cardiovasc Med* 2009, 6(1):16-26.

[39] Conway DE, Williams MR, Eskin SG, McIntire LV: Endothelial cell responses to atheroprone flow are driven by two separate flow components: low time-average shear stress and fluid flow reversal. *Am J Physiol Heart Circ Physiol* 2010, 298(2):H367-37.

[40] Guo D, Chien S, Shyy JY: Regulation of endothelial cell cycle by laminar versus oscillatory flow: distinct modes of interactions of AMP-activated protein kinase and AKT pathways. *Circ Res* 2007, 100(4):564-571.

[41] Chien S. Mechanotransduction and endothelial cell homeostasis: the wisdom of the cell. *Am J Physiol Heart Circ Physiol* 2007, 292: H1209-H1224.

[42] Haruguchi H, Teraoka S: Intimal hyperplasia and hemodynamic factors in arterial bypass and arteriovenous grafts: a review. *J Artif Organs* 2003, 6(4):227-235.

[43] Morinaga K, Okadome K, Kuroki M, Miyazaki T, Muto Y, Onokuchi K. Effect of wall shear stress on intimal thickening of arterially transplanted autogenous veins in dogs. *J Vasc Surg* 1985, 2(3): 430-433.

[44] Krishnamoorthy MK, Banerjee RK, Wang Y, Zhang J, Roy AS, Khoury SF et al. Hemodynamic wall shear stress profiles influence the magnitude and pattern of stenosis in a pig AV fistula. *Kidney Int* 2008, 74(11):1410-1419.

[45] Roy-Chaudhury P, Arend L, Jianhua Zhang, Krishnamoorthy M, Wang Y, Banerjee R, Samaha A and Munda R. Neointimal Hyperplasia in Early Arteriovenous Fistula Failure. *Am J Kid Dis* 2007, 50(5): 782-790.

[46] Kim YO, Song HC, Yoon SA, Yang CW, Kim NI, Choi YJ, Lee EJ, Kim WY, Chang YS, Bang BK. Preexisting intimal hyperplasia of radial artery is associated with early failure of radiocephalic arteriovenous fistula in hemodialysis patients. *Am J Kidney Dis*. 2003 Feb;41(2):422-8.

[47] Kim YO, Choi YJ, Kim JI, Kim YS, Kim BS, Park CW, Song HC, Yoon SA, Chang YS, Bang BK The impact of intima-media thickness of radial artery on early failure of radiocephalic arteriovenous fistula in hemodialysis patients. *J Korean Med Sci*. 2006 Apr;21(2):284-9.

[48] Wali MA, Eid RA, Dewan M, Al-Homrany MA. Pre-existing histopathological changes in the cephalic vein of renal failure patients before arterio-venous fistula (AVF) construction. *Ann Thorac Cardiovasc Surg*. 2006 Oct;12(5):341-8.

[49] Brescia MJ, Cimino JE, Appel K, Hurwich BJ. Chronic hemodialysis using venipuncture and a surgically created arteriovenous fistula. *N Engl J Med* 1966; 275: 1089–1092.

# CHAPTER 2

# Disturbed flow in radial-cephalic arteriovenous fistulae for haemodialysis

This chapter is based on:

Ene-Iordache B and Remuzzi A.

**Disturbed flow in radial-cephalic arteriovenous fistulae for haemodialysis: low and oscillating shear stress locates the sites of stenosis**

***Nephrology Dialysis Transplantation*, 27(1): 358–368, 2012**

## 2.1. Abstract

Despite recent clinical and technological advancement the vascular access for haemodialysis still has important early failure rates after arteriovenous fistula creation. Vascular access failure is mainly related to the haemodynamic conditions that trigger phenomena of vascular wall disease such as intimal hyperplasia or atherosclerosis.

We performed transient computational fluid dynamics simulations within idealized three-dimensional models of *side-to-end* and *end-to-end* radio-cephalic anastomosis, using non-Newtonian blood, and previously measured flows and division ratio in subjects requiring primary access procedure as boundary conditions.

The numerical simulations allowed full characterization of blood flow inside the arterio-venous fistula (AVF) and of patterns of haemodynamic shear stress, known to be the major determinant of vascular remodeling and disease. Wall shear stress was low and oscillating in zones where flow stagnation occurs on the artery floor and on the inner wall of the juxta-anastomotic vein.

Zones of low and oscillatory shear stress were located at the same sites where luminal reduction was documented in previous experimental studies on sites stenosis distribution in AVF. We conclude that even exposed at high flow rates, there are spot regions along the AVF exposed to athero-prone shear stress that favor vessel stenosis by triggering intimal hyperplasia.

## 2.2. Introduction

Forty-five years after the first radio-cephalic arteriovenous fistula (AVF) performed by Dr. Appell in New York [1], maintenance of adequate vascular access (VA) at long term for chronic haemodialysis in patients needing renal replacement therapy is one of the most difficult problems vascular surgeons or nephrologists face. A newly created fistula must mature in order to be used for dialysis, that is, the artery and vein must remodel to accommodate the markedly increased blood volume flow that results from creating the arteriovenous anastomosis. Then, lifetime of a VA can range between months or several years until the fistula will stop function for adequate haemodialysis, requiring surgical revision.

Mechanisms underlying fistula early maturation failure have been studied for years. Anatomic factors such as diameter or intimal thickness of feeding artery and draining vein were shown to be important predictors for AVF maturation, while non-anatomic factors that are involved in maturation failure include the haemodynamic stresses (altered shear stress and venous hypertension) that result from creating a VA anastomosis, or underlying vascular pathology like impaired endothelial function associated with chronic kidney disease or diabetes [2]. Measures for problem resolution were proposed [3], [4] but the VA failure rate continues to remain high [5].To have an idea of the actual VA problems, it is worth knowing that in Dr. Appell's first series of surgically created fistulas there were only two failures out of fourteen, that is an early failure rate which would be difficult to achieve even today [6].

The haemodynamic conditions play a fundamental role in regulating the vascular structure. Blood flow regulates arterial diameter through changes in wall shear stress (WSS), and intraluminal pressure regulates artery wall thickness through its effect on wall tension. If different from the normal physiological range, namely in "disturbed flow" conditions, these haemodynamic factors are implicated in the etiology of the vascular wall disease. The physiologic magnitude of WSS is ranging from 10 to 70 dyne/cm$^2$ in normal arteries, while outside this range WSS can trigger mechanisms that lead to vascular pathology. Lower values of WSS may induce atherosclerotic plaques formation and therefore are considered "atherosclerosis prone" while WSS higher than this range may provoke endothelial cells cleavage and consequently "high-shear" induced thrombosis [7]. More recently, it was clarified that "disturbed flow" is a condition of endothelium exposed to low average shear stress, constantly changing gradients of shear stress, oscillatory shear stress and multidirectional secondary flows. These haemodynamic conditions occur at specific sites of the arterial tree

where there is blood flow separation or stagnation points like arterial branches, at stenosed sites or around stent struts [8].

The main cause of VA failure is thrombosis secondary to the development of stenosis, which in turn is caused by intimal hyperplasia (IH), a fibro-muscular thickening of the vessel wall [9], [10]. Previous studies have shown that in AVF for haemodialysis the stenoses occur at specific sites. In *side-to-end* AVF, Sivaneasn et al. [11] classified the stenoses developed at the anastomosis floor as Type 1, on the inner wall of the swing segment (the vein part mobilized in the creation of the anastomosis) as Type 2, and after the curved region when the vein straightens out as Type 3. Badero et al. [12] have found that the stenoses occur most on the swing segment, with the juxta-anastomotic as the most predominant site.

Also in IH the haemodynamic shear stress seem to be the trigger factor, especially the low WSS at stagnation points [13]. Wall shear stress is difficult to assess because it represents physically the stress (e.g. average force per unit area) vector exerted by flowing blood tangential to the endothelium, with a magnitude equal to the product between shear rate (the derivative of the blood velocity profile near the vessel wall) and blood viscosity. Previous studies on AVF maturation failure that have addressed the issue of haemodynamic forces that develop inside the AVF often used a simplified model (e.g. Poiseuille) for shear stress calculation [14], [15] yielding only a rough estimation of the averaged WSS. Computational fluid dynamics (CFD) are numerical techniques that allow proper calculation of the spatial distribution of WSS among other haemodynamic variables of interest like for example velocity field and pressure. Since the 90s numerical modeling on idealized geometries was intensively used to assess WSS in studying the link between haemodynamics and cardiovascular disease, like stenosis development in the carotid bifurcation [16], [17] the aortic arch [18], [19] or bypass anastomoses [20], [21]. Such computational studies allowed to better understand the haemodynamic phenomena on simplified models and introduced new concepts like the role of low WSS in triggering atherosclerosis [22], oscillatory shear index [16], [23], that overthrown the study of vascular diseases and were further transferred in patient-specific studies [24]. Despite its clinical relevance, this type of investigational method was less used for the study of VA complications. With respect to the literature on carotid and coronary arteries, there were relatively few papers that addressed this task by means of numerical modeling and all were published after the 2000s [25-32]. Beside haemodynamics evaluation, the CFD has been validated against particle image velocimetry (PIV) [30] and with in-vitro flow measurements [31] confirming the validity of these techniques in VA setting as well.

Overall, the VA access is a very high blood volume flow rate conduit respect to the physiological condition, but whether in these areas the low and/or oscillatory WSS develops is not well elucidated. Similar to the above mentioned studies [16-21] in other vascular segments affected by stenosis development, numerical studies on idealized models can characterize the general flow and WSS patterns that develop after the surgical creation of AVF if proper dimensional modeling and boundary conditions are employed. To this aim, we have used pulsatile CFD simulations in idealized models of the AVF created at the wrist as VA for haemodialyis patients.

## 2.3. Methods

### 2.3.1 Three-dimensional models of the AVF

There is now widespread agreement in the scientific community that the native subcutaneous arteriovenous fistula is the best choice with which we are acquainted for achieving VA for haemodialysis [33], [34]. The side-artery-to-end-vein (*side-to-end*) anastomosis at the wrist between the cephalic vein and radial artery is the most common technique performed in VA, although some groups prefer the *end-to-end* technique. The original Brescia-Cimino anastomoses of type side-to-side [1] are less used today, even though they are well indicated in case of patients with stiffer arm vessels [5]. For this reason in the present study we only considered the *side-to-end* and *end-to-end* connections between the cephalic vein and the radial artery performed at the wrist. *Side-to-end* fistulas are created by suturing the transected end of the cephalic vein to the side of the radial artery. In case of *end-to-end* AVF both artery and vein are resected and the radial artery is curved at 180° to form a U-shaped bend before suturing the anastomosis [5]. In designing idealized models of *side-to-end* and *end-to-end* AVF we were inspired by the drawings of surgical anastomoses presented by Konner [35], [5] as shown in Figure 2.1a and 2.1b.

For the *side-to-end* AVF model we have considered the geometrical parameters measured by Sivanesan et al [11] at 1 day post-operatively. Vessel lumen diameters were 3.1 and 4.1 mm for the radial artery and cephalic vein, respectively, and the anastomotic angle was 49°. The extent of the proximal (PA) and distal artery (DA) and of the vein was assumed twelve times the vein diameter in order to have enough hydraulic length to allow fully developed flow. The bend zone of the cephalic vein was generated with a curvature radius that is twofold the vessel diameter. For the *end-to-end* AVF we have used data from our previous study [36] where vessel diameters were measured pre- and then up to three months post-operatively. The radial artery diameter was 3.7 mm and that of the vein was 5.0 mm corresponding to 7 days post-operatively condition. The length of artery was fourteen and of the vein ten vein diameters, and the 180° bending zone was realized with a curvature radius equal to two artery diameters. For both AVF models, tapering of the juxta-anastomosis vein for a length equal to two diameters was created to ensure smooth transition between artery (smaller) to vein (greater) section.

Three-dimensional grids of AVF made of 8-node hexahedral elements, with a boundary layer of thinner elements near the wall, were created using a pre-processor meshing program

(GAMBIT, Fluent.Inc, NH). The schematic models of AVF and corresponding three-dimensional meshes for CFD are presented in Figure 2.1.

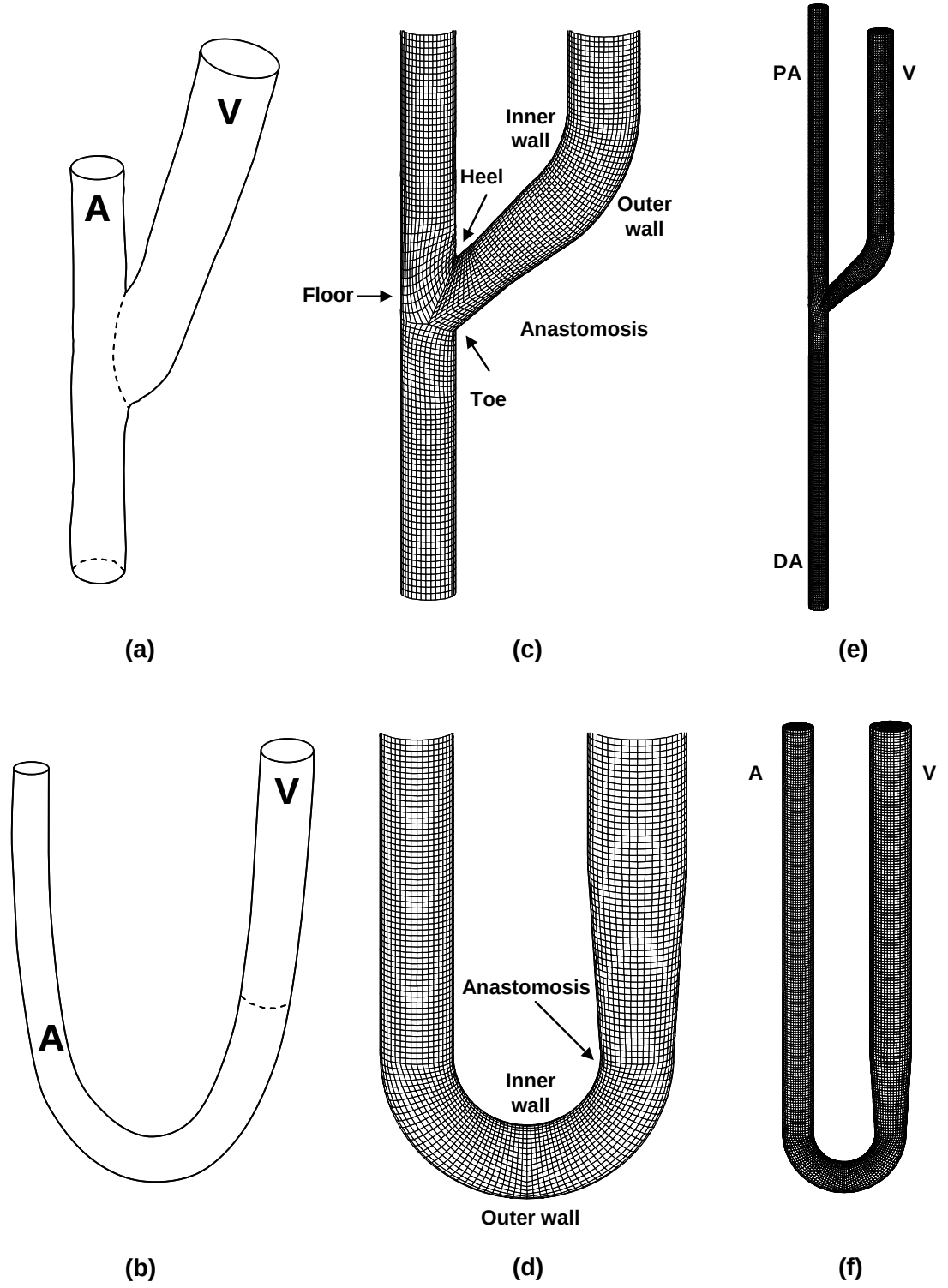


**Figure 2.1.** ***Side-to-end*** **(top row) and** ***end-to-end*** **model of anastomosis (bottom row), zoom on 3-D meshes near anastomotic area (middle) and 3-D meshes for numerical simulations (right). Schematic drawings of AVF were adapted from [5]. Legend: PA, proximal artery; DA, distal artery; V, vein.**

## 2.3.2. Numerical simulations of blood flow in the AVF

For the *side-to-end* fistula two types of flow may exist in the DA: retrograde, when blood flows towards the anastomosis, and antegrade, when blood flows towards the hand. For the unsteady simulations we have used the cephalic vein flow rate waveform provided in [37], opportunely scaled to yield a time-averaged flow rate of 432 mL/min for retrograde and 342 mL/min for antegrade flow in DA, as measured by the same authors in their previous study [38] aimed at characterizing AVF flow distribution at 1 day post-operatively.

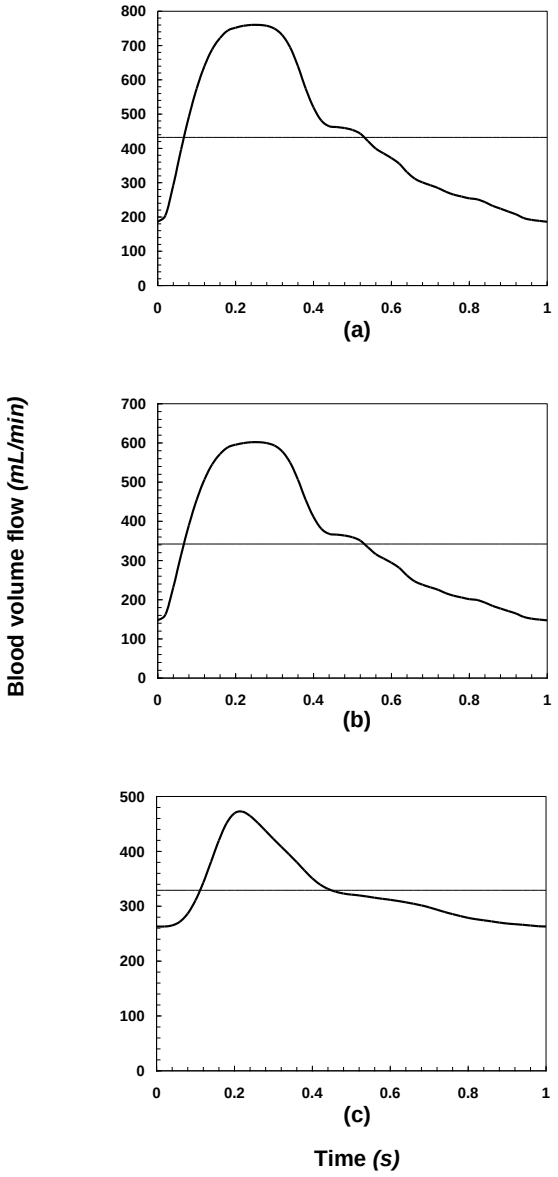


**Figure 2.2. Blood volume flow waveforms used in pulsatile CFD simulations. The horizontal line indicates the time-averaged blood volume flow rate over the cardiac cycle. (a) Venous outflow waveform used for the *side-to-end* AVF with retrograde flow in the DA (mean 432 mL/min). (b) Venous outflow waveform used for the *side-to-end* AVF with antegrade flow in the DA (mean 342 mL/min). (c) Arterial inflow waveform used for the *end-to-end* AVF (mean 329 mL/min).**

Blood volume flow waveform in the radial artery for the *end-to-end* AVF simulation was taken from [36] for the 7 days post-operatively condition which yields a time-averaged flow rate of 329 mL/min. The three pulse cycle waveforms are presented in Figure 2.2 and the flow characteristics together with the geometrical parameters of the AVF mesh models are summarized in Table 2.1.

**Table 2.1. Geometrical parameters and blood volume flow conditions used in the CFD simulations.**

| | | Diameter *(mm)* | Flow division ratio | Flow rate *(mL/min)* | Re # |
|---|---|---|---|---|---|
| ***Side-to-end AVF*** | | | | | |
| **Retrograde flow in DA** | V | 4.1 | 74%PA:26%DA:100%V | 432 (760 - 186) | 670 (1196 - 278) |
| | PA | 3.1 | | | |
| | DA | 3.1 | | | |
| **Antegrade flow in DA** | V | 4.1 | 100%PA:19%DA:81%V | 342 (602 - 147) | 526 (941 - 217) |
| | PA | 3.1 | | | |
| | DA | 3.1 | | | |
| ***End-to-end AVF*** | A | 3.7 | 100%A:100%V | 329 (472 - 263) | 563 (820 - 448) |
| | V | 5.0 | | | |

**Legend**: V, vein (cephalic); PA, proximal artery (radial); DA, distal artery (radial); Re, Reynolds number. Blood volume flow are expressed as time-averaged and (maximum – minimum) of the flow waveforms presented in Figure 2.2.

Three-dimensional pulsatile flow simulations in the AVF models were computed using a multipurpose CFD package (FIDAP, Fluent.Inc, NH) based on the finite element method. As boundary conditions, fully developed parabolic velocities at the vein outlet and at PA inlet (V and PA in Figure 2.1) were prescribed for *side-to-end* AVF, and at the artery inlet only for *end-to-end* AVF, with centerline velocities derived from the flow waveforms previously reported. Traction-free boundary condition was applied at the DA outlet for *side-to-end* and to vein outlet for *end-to-end* AVF to ensure conservation of mass and no-slip condition (i.e., zero velocity) was applied at the walls, which were considered rigid. We employed an implicit time integration scheme (backward Euler) with 50 fixed time steps for each pulse cycle to solve the time-dependent Navier-Stokes equations, assuming that cardiac cycle period is one second. Three complete flow cycles were solved in order to damp the initial transients of the fluid and only the third cycle was considered for the final results. Blood density was assumed constant (1.045 g/cm$^3$) and blood viscosity was considered non-Newtonian by using the Carreau rheological model implemented in the CFD package as described previously [25]. Since blood

viscosity depends on the shear rate, Reynolds number cannot be calculated directly, but a good approximation can be made by rescaling the Newtonian viscosity to a value corresponding to a characteristic shear rate [39]. For the outlet vein of *side-to-end* and the inlet artery of *end-to-end* AVF we have calculated the Reynolds number as described in [25] and the resulting mean and ranges are provided in Table 2.1.

The oscillatory shear index (OSI), originally introduced by Ku et al. [16], is aimed at quantifying the degree of deviation of the WSS from its average direction during the heart beat cycle due to either secondary and reverse flow velocity components occurring in pulsatile flow. In order to estimate whether oscillatory shear might occur on the AVF wall, for each point on the surface we calculated the OSI as proposed in [23]:

$$OSI = \frac{1}{2}\left(1 - \frac{\left|\int_0^T \tau_w dt\right|}{\int_0^T |\tau_w| dt}\right)$$

where $\tau_w(t)$ is the instantaneous wall shear stress vector and $T$ is the period of the cardiac cycle. The index is non-dimensional and can take values between 0 and 0.5, higher OSI indicating larger shear stress direction variations.

Himburg et al. [40] introduced another indicator of the "disturbed" shear environment, namely the relative residence time (RRT) of non-adherent particles in the blood flow moving adjacent to the vascular wall. They showed that RRT of a fully entrained particle at a small distance from the wall is inversely proportional with the distance the particle travels during a cardiac cycle, that may be expressed as a combination of OSI and time-averaged WSS (TAWSS) over the cardiac cycle. For each node on the AVF mesh surface we have calculated the RRT with the formula [40]:

$$RRT \sim [(1 - 2 \cdot OSI) \cdot TAWSS]^{-1}$$

In this formulation OSI acts to modify the effect of TAWSS on the relative residence of particles near the wall and thus RRT incorporates information on both low and oscillating shear [40]. The RRT must be normalized by a reference value [24], which we chose to be the RRT calculated for fully developed, time-averaged, blood volume flow in the straight part of the vein for each AVF. After this transformation, an RRT value near 1 indicates a condition of shear environment similar to the reference RRT, while RRT below 1 indicates high shear zones and RRT higher than 1 locates the sites with both low and oscillating shear stress or areas with only low WSS.

# 2.4. Results

## 2.4.1. Flow patterns in the AVF

Velocity contours of blood in the symmetry section of the *side-to-end* for the retrograde and antegrade flow in DA cases are shown in Figure 2.3 a, b for the peak systolic, and d, e for the minimum diastolic blood volume flow.

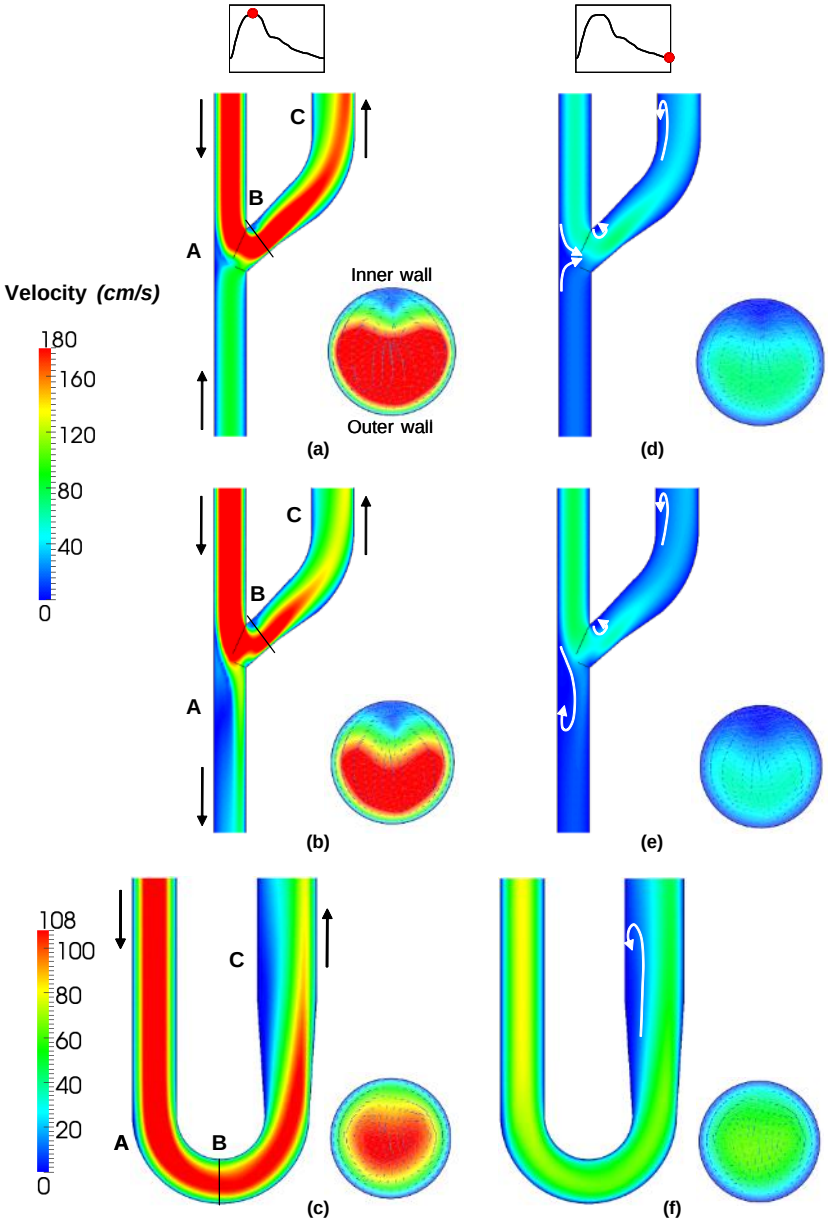


**Figure 2.3. Velocity magnitude contours of blood in the symmetry plane of the AVF and in a cross-section (B) of the bending vessel. Left and right columns illustrate velocity maps for the maximum and for the minimum blood volume flow, respectively. (a and d) *Side-to-end* AVF case with retrograde flow in the DA. (b and e) *Side-to-end* AVF case with antegrade flow in the DA. (c and f) *End-to-end* AVF. Black arrows indicate the direction of blood flow and white arrows indicate flow separation areas. In the cross-sections the velocity vectors show formation of Dean type vortices. Inner and outer wall position for all cases are as indicated on the cross-section (a) and in Figure 2.1c and 2.1d.**

In retrograde flow in DA (Figure 2.3a and 2.3d), blood that comes mostly (74% of flow) from the PA and in a smaller fraction (26%) from the DA enters through the anastomosis into the cephalic vein. This type of blood distribution between the proximal and DA creates a flow stagnation zone (A) on the anastomosis floor as depicted by the white arrows. A region of flow recirculation forms near the heel in the juxta-anastomosis vein, when the flow hits on the outer wall of the vein forming a counter clockwise vortex on the opposite inner wall (B). In antegrade flow in DA (Figure 2.3b and 2.3e) blood flows from the PA towards the anastomosis where it divides: the greater part of the flow enters into the vein (81%) and only a smaller part flows through the DA (19%) towards the palmary arch. When blood reaches the anastomosis the flow directed towards the DA changes direction suddenly creating a wider area of recirculation and low velocity on the floor, starting from the anastomosis down to the DA (A). The flow entering the vein collides against the outer wall near the anastomosis creating an area of recirculation flow on the inner wall near the heel (B). Flow patterns in retrograde and antegrade flow seem similar, except for the position A where a different shape of the flow recirculation region can be observed.

The sudden curvature of the vein limb of AVF near the anastomosis leads to formation of Dean vortices characteristic for curved tubes. These can be well observed in the cross-sections normal to the vessel axis in position B, as shown in Figure 2.3a and 2.3b. The Dean flow type is well developed immediately near the anastomosis and vanishes gradually after the vein bend.

Velocity magnitude plots of blood in the *end-to-end* AVF for peak systolic and minimum diastolic blood volume flow are shown in Figure 2.3c and 2.3f. In this case the whole blood coming from the radial artery flows through the cephalic vein in an U-shape tube. After the anastomosis the flow impacts on the outer wall and a recirculation zone (C) develops on the inner wall of the juxta-anastomosis vein. Also in this case the curvature of the artery induces Dean type flow in the bending tract of the AVF, as shown in the cross-section normal to the vessel axis in position B.

## 2.4.2. WSS patterns in the AVF

To assess how WSS patterns are distributed over the AVF surface we represented the wall shear stress magnitude with a cutoff value of 70 dyne/cm$^2$ representing the maximum value in normal arteries [7] and eight levels of WSS patterns as shown in Figure 2.4.

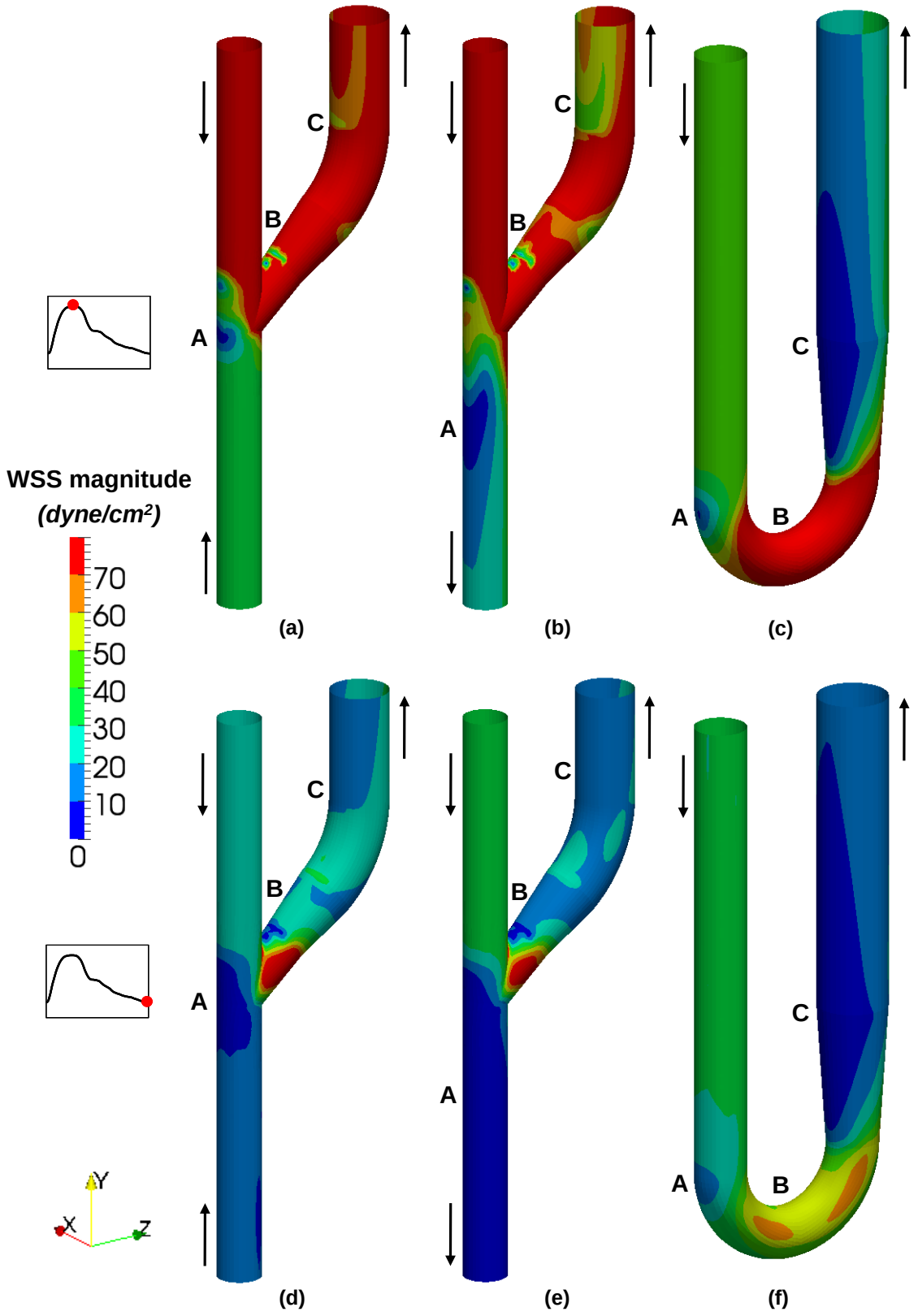


**Figure 2.4. Wall shear stress patterns on the AVF surface. Top and bottom rows illustrate WSS maps for maximum and minimum blood volume flow, respectively. (a and d) *Side-to-end* AVF with retrograde flow in the DA. (b and e) *Side-to-end* AVF with antegrade flow in the DA. (c and f) *End-to-end* AVF. High WSS zones are in red (> 70 dyne/cm$^2$) and low WSS zones in dark blue (< 10 dyne/cm$^2$).**

In this way low WSS zones are plotted in dark blue (<10 dyne/cm$^2$) and high WSS (> 70 dyne/cm$^2$) zones are in red. As shown, low WSS match well the sites of flow recirculation and stagnation presented in Figure 2.3. In particular, for *side-to-end* AVF, areas of low WSS are found along the wall of the anastomotic floor (A), near the anastomosis heel on the inner wall of the vein (B) and in a lesser extent on the inner wall (C) after the curvature of the vein. When the flow rate is maximum the high WSS covers all surface of the PA as well as of the cephalic vein, except for the small focal sites on the inner side in point B and C on *side-to-end* AVF. When the flow rate is minimum high WSS areas covering is only on the outer and lateral wall of the swing segment (see Figure 2.4a to 2.4e). WSS patterns on the PA and on the vein are very similar, but rather dissimilar on the DA, where area of low WSS (A) is wider in the antegrade flow in DA case respect to the retrograde case. As the AVF geometries are identical, this diversity is due to the different flow distributions between the two cases. For *end-to-end* AVF, low WSS regions are presented on the inner wall of the cephalic vein (position C) whereas high WSS develops on the inner and lateral walls of the bending artery in the peak systolic flow condition as shown in Figure 2.4c. These patterns are maintained at minimum diastolic blood volume flow but the highest WSS does not reach the limit of 70 dyne/cm$^2$ (Figure 2.4f).

It is worth noting from the shear stress patterns in Figure 2.4 that low and high WSS regions are present with different extent on the AVF surface in both maximum and minimum flow instances. We should imagine how these areas continue to fluctuate cyclically, from systole to diastole, with the heart frequency. It can also be observed that in all AVF, the Dean flow that develops in the curved tracts contributes to higher WSS on the lateral walls and lower WSS on the inner and outer walls that are normal respect to the radius of curvature of the bend. This type of pattern can be well observed in the minimum diastolic blood volume flow condition in Figure 2.4d to 2.4f.

### 2.4.3. OSI and RRT in the AVF

Surface maps of OSI are presented in Figure 2.5a to 2.5c. Zones of non-null OSI were found on the anastomosis floor (A) and near the heel on the inner wall (B) of the swing segment in *side-to-end* AVF (Figure 2.5a and 2.5b) and on the inner wall of the vein after the anastomosis (C) in *end-to-end* AVF (Figure 2.5c). In particular, the highest OSI were 0.31 in position A and 0.075 in position B of Figure 2.5a, 0.45 in position A and 0.077 in position B of Figure 5b and 0.29 in position C of Figure 2.5c. The RRT contours mapped over the AVF

model surface are presented in Figure 2.5d to 2.5f. As shown, the location of RRT on the wall is consistent with the distribution of OSI, but RRT patterns are more extended as they are caused either by elevated OSI or low TAWSS.

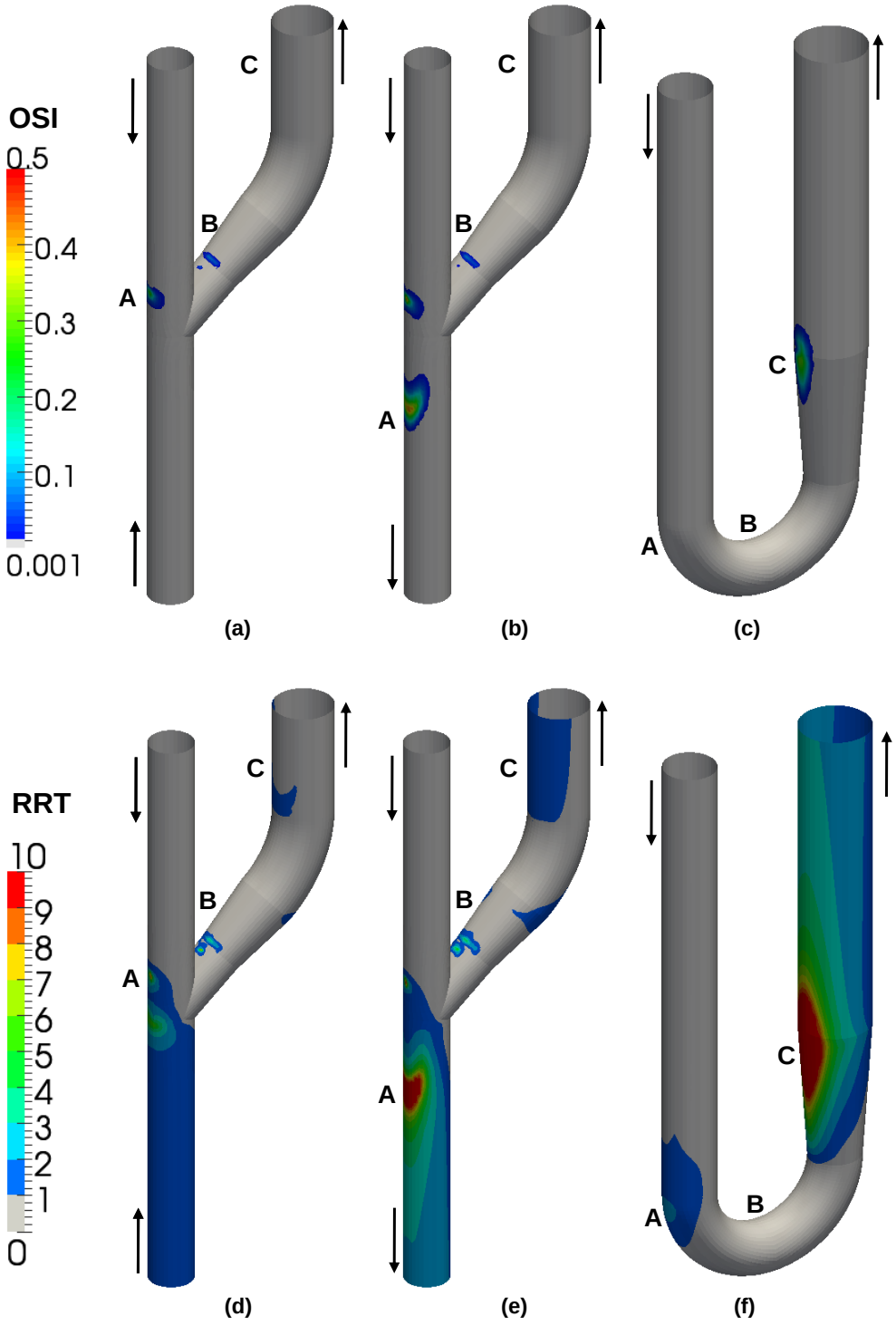


**Figure 2.5. Plot of OSI (a, b, and c) and RRT (d, e and f) on the AVF surface. (a and d) *Side-to-end* AVF with retrograde flow in the DA. (b and e) *Side-to-end* AVF with antegrade flow in the DA. (c and f) *End-to-end* AVF. OSI values below 0.001 were represented in light grey to give emphasis on sites with higher OSI. RRT values below 1, representing the mean of the 75% quintiles of its distributions over the mapped AVF surfaces, were represented in light grey.**

Median values of RRT distributions were 0.67, 0.64 and 0.42, respectively from Figure 2.5d to 2.5f. Since RRT does not have a well defined range, for the visualization map scale we chose the averaged 75% quintile of RRT distributions as lower limit and set the upper limit to the lowest maximum RRT, which is in Figure 2.5d. The peak RRT were 10.4 in position A and 9.7 in position B of Figure 2.5d, 54.6 in position A and 4.6 in position B of Figure 2.5e and 30.7 in position C of *end-to-end* AVF in Figure 2.5f.

## 2.5. Discussion

In the present work, by employing pulsatile CFD simulations in idealized models with realistic blood volume flow conditions, we have studied the shear environment in order to investigate whether "disturbed flow" occurs on the AVF territory. In particular, in idealized AVF we have found that low WSS (<10 dyne/cm$^2$) occurs at the anastomotic floor, on the inner wall of the swing segment and after the vein curvature in *side-to-end* and on the inner wall of the juxta-anastomotic vein in *end-to-end* AVF, in line with previous patient-specific CFD studies [25], [30], [32]. In all these sites, except for the venous outflow, we have found not only low, but also oscillating WSS. Niemann et al. have found similar findings on the draining veins in a side-to-side AVF model [31]. Our results demonstrate that also in *side-to-end* and *end-to-end* AVF for haemodialysis, exposed to post-operative sudden increase in blood volume flow and decrease of waveform pulsatility, there are regions of flow reversal producing oscillations in shear direction. Few authors reported oscillating WSS in the AVF for haemodialysis. Using OSI calculation based on axially directed WSS in cross-sections as defined in [18], we have shown non-null OSI on one perimeter slicing the swing segment [25] while a similar study [30] reported null OSI on several cross-sections considered, but none of these perimeters was encompassing the flow separation zone on the inner side of the swing segment. Recently, in [31] OSI levels were calculated and visualized on the model surface of a side-to-side AVF. Therefore, a recommendation to future CFD studies is to perform calculation of haemodynamic wall parameters and visualization on the full surface of the AVF.

We have presented maps of OSI and RRT as indicators of disturbed flow in the three models of AVF for haemodialysis. On the inner side of the juxta-anastomosis vein in *end-to-end* AVF the OSI was high (0.3), in line with the high incidence of stenosis on the swing segment [12], whereas in *side-to-end* AVF the relatively low OSI (0.075) is somewhat contradictory with this evidence. Even though OSI can identify regions of flow reversal, it is insensitive to the shear stress magnitude and it seems unlikely that endothelial cells sense OSI per se [40]. Instead, the RRT patterns, more extended on the swing segments due to the contribution of both oscillatory and low WSS, locate a larger portion of the sites of stenosis in *side-to-end* AVF. This confirms also that in the AVF territory low shear stress per se promotes intimal hyperplasia while the oscillatory shear may exacerbate the development of stenosis [8]. At the same time, OSI and RRT were higher on the anastomosis floor and on the lateral wall of DA, indicating that in *side-to-end* AVF the DA limb is at risk for stenosis. This is somewhat

conflicting with the current consideration that the occurrence of stenoses in this artery is low. The frequency of arterial stenoses is lower than those on venous limb, about 1.1% of all cases that rises up to 16.6% considering also the arterial anastomosis [12]. However, other studies [11], [41] reported even higher incidence, up to 35%. The anastomotic floor is known as a site with high IH development in by-pass grafts anastomosis [13]. Moreover, it was shown that even if thickening of the vessel wall occurs on the arterial limb of the AVF, the stenoses are non-progressive [11] and hence rarely lead to impairment of blood flow. Our finding regarding highly oscillating shear on the artery and the cited evidences indicate that the mechanism of stenosis formation on the arterial side might be different from that on the venous side in AVF for haemodialysis.

On the inner wall of the outflow vein of *side-to-end* AVF, also known as a site at risk for IH development, OSI resulted null and also RRT was relatively low, indicating only slight influence of low WSS. Our CFD simulation in idealized AVF model did not show oscillating shear at this level of the vein. However, in real AVF the enlargement and elongation of the vessels during the phase of the arterial remodeling may create outflow veins with sharp curvature and in that case oscillating WSS might occur.

Further studies are needed to decide the optimal haemodynamic wall parameters that better predict the sites of stenosis formation in AVF for haemodialysis. Beside OSI and RRT, that incorporates both OSI and TAWSS, other parameters that were previously proposed to quantify the haemodynamic disturbances as predictors of arterial wall sites at risk, like the WSS spatial gradient (WSSG) [42], the WSS temporal gradient (WSST) [43] or the WSS angle gradient (WSSAG) [44] are worth investigating in AVF patient-specific studies. Our results on the swing segment of idealized *side-to-end* AVF, showing that RRT located a higher portion of the site of stenosis than OSI, support well the work of Lee at al. on the normal carotid bifurcation [24], who proposed RRT as a robust, single metric of low and oscillating shear. Also, in line with our observations, it was already shown in the human coronary artery that OSI predicts well the actual site of plaque initiation while RRT locates better the entire plaque region [63].

On the basis of our actual findings and previous experimental studies on sites of stenosis in native AVF for haemodialysis we may speculate on the mechanisms of AVF remodeling, as illustrated in Figure 2.6. The VA as a whole remodels itself and matures due to the rise in blood volume flow rate and the augmentation of intraluminal pressure in the venous limb. The high flow rate induces vessel diameter enlargement through the increase in WSS and the higher pressure leads to thickening of the vessel wall to compensate for the rise of wall circumferential

stress. Local wall remodeling occurs at specific sites determined by the geometry of the AVF (points A, B, and C in Figure 2.6a), where the low and oscillating WSS trigger formation of neointima, growing of intima-media thickness and successive stenosis development (Figure 2.6b).

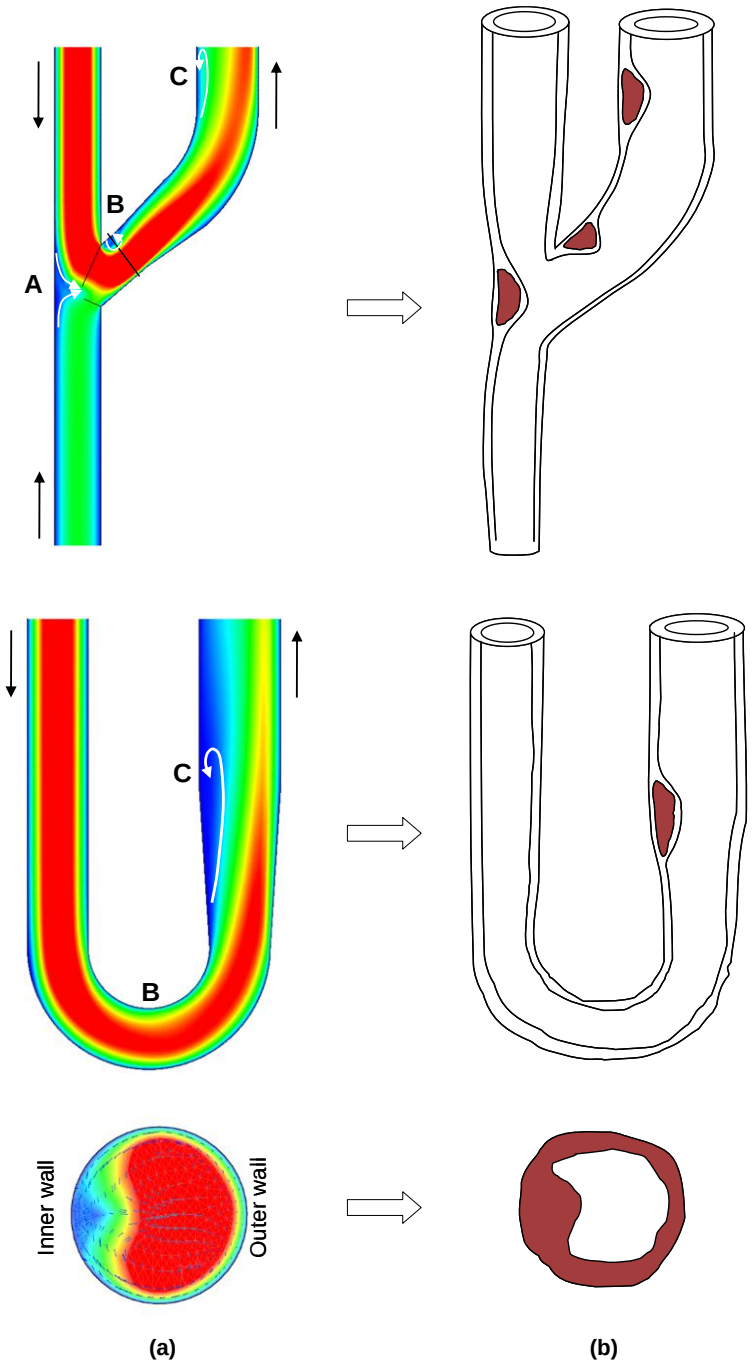


**Figure 2.6. Cartoon illustrating the mechanism of local AVF remodeling. (a) In focal sites determined by the geometry of the AVF athero-prone haemodynamic conditions may develop. (b) In these areas, low and oscillating shear stresses trigger formation of neointima with subsequent increase of wall thickness and stenosis development.**

The mechanism of AVF vessel thickening on the arterial limb is very likely that of IH observed in animal models of AVF [45] or in bypassed arteries [46]. It may not be excluded that atherosclerotic plaque-like formation may occur in parallel with intimal thickening even if no putative inflammatory effects from cholesterol or LDL accumulation are present [47], especially at the anastomosis floor (point A in Figure 6) that has WSS patterns resembling those developed at the carotid bifurcation sinus [7].

On the venous limb the mechanism responsible of luminal occlusion is the intimal hyperplasia at sites of low and oscillating WSS. We have shown that among blood distribution and impact on the vessel wall, the Dean flow that develops in the curved tracts of the AVF contribute to non-uniformity of WSS as well, since resulting WSS is higher on lateral and lower on inner and outer wall, normal to the radius of curvature of the vessel. This undoubtedly demonstrates existence of vein sections where WSS is not uniform circumferentially even in an idealized geometry of AVF. The non-uniform WSS along the circumference of the vein wall should result in non-constant intimal thickness and thus in development of eccentric stenoses. One limitation of our study is the lack of histopathology images that could directly demonstrate this hypothesis. We may, however, rely on data available in the literature on this topic. Histology of neointimal hyperplasia and its relation with WSS in stenotic AV grafts has been characterized in previous studies in animals [9], [48] and in subjects with AVF creation for haemodialysis [49]. The luminal shape at site of stenoses in [49] were in many cases eccentric, consistent with the hypothesis that shear stress profiles are distributed non-uniformly along the circumference of the vein. Non-uniform WSS profiles have been previously found in patient-specific CFD studies by our [25] and other group [28] in *end-to-end* AVF for haemodialysis. A direct demonstration of this hypothesis was made in an experimental study of *side-to-end* pig AVF combined with CFD in real geometries that revealed zones with non-uniform shear stress profiles circumferentially along the vein wall which correlated to a more eccentric histological pattern of intima-media thickening [48].

We found that arterial and vein walls are subjected to a haemodynamic shear stress that is much higher than the physiological shear in arteries [50] and in veins [32]. Wall shear stress was shown to remain elevated even after maturation process on the arterial side in prospective studies in patients followed-up after creation of AVF for haemodialysis [36], [51], [52]. Similar findings were reported in previous CFD studies performed in idealized geometries [27], [29] and in patient-specific investigations [25], [28], [32]. In particular, the WSS was high on the PA as well as on the outer and lateral walls of swing segments on *side-to-end*, and on the arterial bend in *end-to-end* AVF. The role of chronic exposure at high WSS was on controversy

debate for years and is not yet clearly understood. Earlier studies [53], [54] considered that levels of high shear stress may lead to endothelial layer degeneration and erosion. On the contrary, more recent studies elucidated that chronic exposure to high levels of WSS with little temporal fluctuations has beneficial effects by promoting an athero-protective phenotype [55], [56], [57]. Overall, high shear stress resulting from the high flow and higher venous pressure stimuli will elicit arterial and vein remodeling by promoting cell proliferation [58]. Locally, on one hand high WSS is protecting against neointima formation, but on the other hand high WSS spatial gradients may alter the functional state of the endothelial layer and probably that of underlying smooth muscle cell layer [59], [60]. Furthermore, little is known about the vein endothelium that is subjected to even higher gradient regimes of WSS after AVF creation considering that in the pre-operative condition vein physiological range of WSS is about 1-6 dyne/cm$^2$ [7], [32].

In the present work we only took into account the radio-cephalic native fistula created at the wrist in an *side-to-end* and *end-to-end* manner. Other types of VA, like the upper arm fistulae or arteriovenous grafts should be treated in further studies considering their different geometry and flow conditions. We used an idealized geometry and imposed realistic pulsatile boundary conditions in order to catch the general flow features that develop in the AVF soon after the surgical creation. While in patient-specific studies the variability of the AVF geometry in terms of bends, torsion and luminal area variation will reflect the haemodynamic condition of the single subject, in our opinion the present study may well represent the general flow behavior and common shear stress patterns in these two types of radial-cephalic AVF. The computational modeling of AVF provides advantages such as the possibility to simulate different geometries and a variety of flow conditions. For example, it was shown that the geometry of an out-of-plane graft with respect to a planar graft strongly influences perianastomotic WSS patterns by breaking the Dean vortices symmetry [61]. Also, in helically sinuous vascular prostheses it was demonstrated that the curvature and torsion affect the flow field in terms of axial velocity, WSS and vorticity [62]. More importantly, the Dean vortices produced by the curvature are changed by the torsion to a predominantly single vortex, with consequent changes of WSS patterns. This type of CFD modeling should be employed in upcoming studies in idealized AVF to better understand how the anastomotic angle or vein torsion, that in part may be amenable by surgical manipulation, would impact on the local WSS patterns and targeted towards the lowering of RRT. At the next level, these studies may be performed in patient-specific, pilot studies, aimed at minimizing the AVF failure by reducing the venous development of neointimal hyperplasia.

In conclusion, by using unsteady CFD modeling in radial-cephalic AVF created at the wrist we have found that, as contributing factors of the pathogenesis of IH, the localization of low and oscillating haemodynamic shear in the post-operative flow condition may explain the preferential localization of the stenosis. Despite being exposed to a sudden increase in flow rate, sites of "disturbed flow" with low and oscillating WSS in AVF occur in focal sites driven by the vessel geometry and the blood volume flow distribution.

## 2.6. Acknowledgments

The study was partially funded by the 7th Framework Program of the European Commission (FP7-ICT-2007-2 ARCH Project, grant agreement nr. 224390).

## 2.7. References


[1] Brescia MJ, Cimino JE, Appel K, Hurwich BJ. Chronic hemodialysis using venipuncture and a surgically created arteriovenous fistula. *N Engl J Med* 1966; 275(20): 1089-1092.

[2] Besarab A, Ravani P, Spergel LM, Roy-Chaudhury P, Asif A. The native arteriovenous fistula in 2007. Research needs. *J Nephrol* 2007; 20(6): 668-673.

[3] Asif A, Roy-Chaudhury P, Beathard GA. Early arteriovenous fistula failure: a logical proposal for when and how to intervene. *Clin J Am Soc Nephrol* 2006; 1(2): 332-339.

[4] Roy-Chaudhury P, Spergel LM, Besarab A, Asif A, Ravani P. Biology of arteriovenous fistula failure. *J Nephrol* 2007; 20(2): 150-163.

[5] Konner K. The initial creation of native arteriovenous fistulas: surgical aspects and their impact on the practice of nephrology. *Semin Dial* 2003; 16(4): 291-298.

[6] Konner K. History of vascular access for haemodialysis. *Nephrol Dial Transplant* 2005; 20(12): 2629-2635.

[7] Malek AM, Alper SL, Izumo S. Hemodynamic shear stress and its role in atherosclerosis. *JAMA* 1999; 282(21): 2035-2042.

[8] Davies PF. Hemodynamic shear stress and the endothelium in cardiovascular pathophysiology. *Nat Clin Pract Cardiovasc Med* 2009; 6(1): 16-26.

[9] Sho E, Nanjo H, Sho M, Kobayashi M, Komatsu M, Kawamura K, Xu C, Zarins CK, Masuda H. Arterial enlargement, tortuosity, and intimal thickening in response to sequential exposure to high and low wall shear stress. *J Vasc Surg* 2004; 39(3): 601-612.

[10] Diskin CJ, Stokes TJ, Dansby LM, Radcliff L, Carter TB. Understanding the pathophysiology of hemodialysis access problems as a prelude to developing innovative therapies. *Nat Clin Pract Nephrol* 2008; 4(11): 628-638.

[11] Sivanesan S, How TV, Bakran A. Sites of stenosis in AV fistulae for haemodialysis access. *Nephrol Dial Transplant* 1999; 14(1): 118-120.

[12] Badero OJ, Salifu MO, Wasse H, Work J. Frequency of swing-segment stenosis in referred dialysis patients with angiographically documented lesions. *Am J Kidney Dis* 2008; 51(1): 93-98.

[13] Haruguchi H, Teraoka S. Intimal hyperplasia and hemodynamic factors in arterial bypass and arteriovenous grafts. a review. *J Artif Organs* 2003, 6(4):227-235.

[14] Girerd X, London G, Boutouyrie P, Mourad J, Safar M, Laurent S. Remodeling of the radial artery in response to a chronic increase in shear stress. *Hypertension* 1996; 27(3): 799-803.

[15] Corpataux JM, Haesler E, Silacci P, Ris HB, Hayoz D. Low-pressure environment and remodeling of the forearm vein in Brescia-Cimino haemodialysis access. *Nephrol Dial Transplant* 2002; 17(6): 1057-1062.

[16] Ku DN, Giddens DP, Zarins CK, Glagov S. Pulsatile flow and atherosclerosis in the human carotid bifurcation. *Arteriosclerosis* 1985; 5(3): 293-302.

[17] Perktold K, Nerem RM, Peter RO. A numerical calculation of flow in a curved tube model of the left main coronary artery. *J Biomech* 1991; 24: 175-189.

[18] Moore JEJ, Xu C, Glagov S, Zarins CK, Ku DN. Fluid wall shear stress measurements in a model of the human abdominal aorta: oscillatory behavior and relationship to atherosclerosis. *Atheroscl* 1994; 110: 225-240.

[19] Moore JEJ, Ku DN. Pulsatile velocity measurements in a model of the human abdominal aorta under resting conditions. *J Biomech Eng* 1994; 116(3): 337-346.

[20] Steinman DA, Vinh B, Ross Ethier C, Ojha M, Cobbold RSC, Johnston KW. A numerical simulation of flow in a two-dimensional end-to-side anstomosis model. *J Biomech Eng* 1993; 115: 112-118.

[21] Ethier CR, Steinman DA, Zhang X, Karpik SR, Ojha M. Flow waveform effects on end-to-side anastomotic flow patterns. *J Biomech* 1998; 31(7): 609-617.

[22] Zarins CK, Giddens DP, Bharadvaj BK. Carotid bifurcation atherosclerosis: quantitative correlation of

plaque localization with flow velocity profiles and wall shear stress. *Circ Res* 1983; 53: 502-514.

[23] He X, Ku DN. Pulsatile flow in the human left coronary artery bifurcation : average conditions. *J Biomech Eng* 1996; 118: 74-82.

[24] Lee SW, Antiga L, Steinman DA. Correlations among indicators of disturbed flow at the normal carotid bifurcation. *J Biomech Eng* 2009; 131(6): 061013.

[25] Ene-Iordache B, Mosconi L, Remuzzi G, Remuzzi A. Computational fluid dynamics of a vascular access case for hemodialysis. *J Biomech Eng* 2001; 123: 284-292.

[26] Krueger U, Zanow J, Scholz H. Computational fluid dynamics and vascular access. *Artif Organs* 2002; 26(7): 571-575.

[27] Van Tricht I, De Wachter D, Tordoir J, Verdonck P. Comparison of the hemodynamics in 6 mm and 4-7 mm hemodialysis grafts by means of CFD. *J Biomech* 2006; 39(2): 226-236.

[28] Kharboutly Z, Fenech M, Treutenaere JM, Claude I, Legallais C. Investigations into the relationship between hemodynamics and vascular alterations in an established arteriovenous fistula. *Med Eng Phys* 2007; 29(9): 999-1007.

[29] Van Canneyt K, Pourchez T, Eloot S, Guillame C, Bonnet A, Segers P, Verdonck P. Hemodynamic impact of anastomosis size and angle in side-to-end arteriovenous fistulae: a computer analysis. *J Vasc Access* 2010; 11(1): 52-8.

[30] Kharboutly Z, Deplano V, Bertrand E, Legallais C. Numerical and experimental study of blood flow through a patient-specific arteriovenous fistula used for hemodialysis. *Med Eng Phys* 2010; 32(2): 111-118.

[31] Niemann AK, Udesen J, Thrysoe S, Nygaard JV, Frund ET, Petersen SE, Hasenkam JM. Can sites prone to flow induced vascular complications in AV fistulae be assessed using computational fluid dynamics? *J Biomech* 2010; 43(10): 2002-2009.

[32] Carroll GT, McGloughlin TM, Burke PE, Egan M, Wallis F, Walsh MT. Wall shear stresses remain elevated in mature arteriovenous fistulas: a case study. *J Biomech Eng* 2011; 133(2): 021003.

[33] NKF-KDOQI. Clinical practice guidelines for vascular access, update 2000. *Am J Kidney Dis* 2001; 37(1): S137-S181.

[34] Berardinelli L. The endless history of vascular access: a surgeon's perspective. *J Vasc Access 2006*; 7(3): 103-111.

[35] Konner K. The anastomosis of the arteriovenous fistula--common errors and their avoidance. *Nephrol Dial Transplant* 2002; 17(3): 376-379.

[36] Ene-Iordache B, Mosconi L, Antiga L, Bruno S, Anghileri A, Remuzzi G, Remuzzi A. Radial artery remodeling in response to shear stress increase within arteriovenous fistula for hemodialysis access. *Endothelium* 2003; 10(2): 95-102.

[37] Sivanesan S, How TV, Black RA, Bakran A. Flow patterns in the radiocephalic arteriovenous fistula: an in vitro study. *J Biomech* 1999; 32(9): 915-925.

[38] Sivanesan S, How TV, Bakran A. Characterizing flow distributions in AV fistulae for haemodialysis access. *Nephrol Dial Transplant* 1998; 13(12): 3108-3110.

[39] Gijsen FJH, Brands PJ, van de Vosse FN, Janssen JD. Assessment of wall shear rate measurements with ultrasound. *J Vasc Invest* 1998; 4: 187-196.

[40] Himburg HA, Grzybowski DM, Hazel AL, LaMack JA, Li XM, Friedman MH. Spatial comparison between wall shear stress measures and porcine arterial endothelial permeability. *Am J Physiol Heart Circ Physiol* 2004; 286(5): H1916-1922.

[41] Asif A, Gadalean FN, Merrill D, Cherla G, Cipleu CD, Epstein DL, Roth D. Inflow stenosis in arteriovenous fistulas and grafts: a multicenter, prospective study. *Kidney Int* 2005; 67(5): 1986-1992.

[42] Lei M, Kleinstreuer C, Truskey GA. A focal stress gradient-dependent mass transfer mechanism for atherogenesis in branching arteries. *Med Eng Phys* 1996; 18(4): 326-332.

[43] Ojha M. Wall shear stress temporal gradient and anastomotic intimal hyperplasia. *Circ Res* 1994; 74(6): 1227-1231.

[44] Longest PW, Kleinstreuer C. Computational haemodynamics analysis and comparison study of arterio-

venous grafts. *J Med Eng Technol* 2000; 24(3): 102-110.

[45] Fan Y, Xu Z, Jiang W, Deng X, Wang K, Sun A. An S-type bypass can improve the hemodynamics in the bypassed arteries and suppress intimal hyperplasia along the host artery floor. *J Biomech* 2008; 41(11): 2498-2505.

[46] Migliavacca F, Dubini G. Computational modeling of vascular anastomoses. *Biomech Model Mechanobiol* 2005; 3(4): 235-250.

[47] Sloop GD, Fallon KB, Zieske AW. Atherosclerotic plaque-like lesions in synthetic arteriovenous grafts: implications for atherogenesis. *Atherosclerosis* 2002; 160(1): 133-139.

[48] Krishnamoorthy MK, Banerjee RK, Wang Y, Zhang J, Roy AS, Khoury SF, Arend LJ, Rudich S, Roy-Chaudhury P. Hemodynamic wall shear stress profiles influence the magnitude and pattern of stenosis in a pig AV fistula. *Kidney Int* 2008; 74(11): 1410-1419.

[49] Roy-Chaudhury P, Arend L, Zhang J, Krishnamoorthy M, Wang Y, Banerjee R, Samaha A, Munda R. Neointimal hyperplasia in early arteriovenous fistula failure. *Am J Kidney Dis* 2007; 50(5): 782-790.

[50] Dammers R, Stifft F, Tordoir JH, Hameleers JM, Hoeks AP, Kitslaar PJ. Shear stress depends on vascular territory: comparison between common carotid and brachial artery. *J Appl Physiol* 2003; 94(2): 485-489.

[51] Dammers R, Tordoir JH, Welten RJ, Kitslaar PJ, Hoeks AP. The effect of chronic flow changes on brachial artery diameter and shear stress in arteriovenous fistulas for hemodialysis. *Int J Artif Organs* 2002; 25(2): 124-128.

[52] Dammers R, Tordoir JH, Kooman JP, Welten RJ, Hameleers JM, Kitslaar PJ, Hoeks AP. The effect of flow changes on the arterial system proximal to an arteriovenous fistula for hemodialysis. *Ultrasound Med Biol* 2005; 31(10): 1327-1333.

[53] Fry DL. Acute vascular endothelial changes associated with increased blood velocity gradients. *Circ Res* 1968; 22(2): 165-197.

[54] Langille BL, Reidy MA, Kline RL. Injury and repair of endothelium at sites of flow disturbances near abdominal aortic coarctations in rabbits. *Arteriosclerosis* 1986; 6(2): 146-154.

[55] Caro CG, Fitz-Gerald JM, Schroter RC. Atheroma and arterial wall shear. Observation, correlation and proposal of a shear dependent mass transfer mechanism for atherogenesis. *Proc Roy Soc Lond* 1971; 177: 109-159.

[56] Davies PF. Flow-mediated endothelial mechanotransduction. *Physiol Rev* 1995; 75(3): 519-560.

[57] Traub O, Berk BC. Laminar shear stress: mechanisms by which endothelial cells transduce an atheroprotective force. *Arterioscler Thromb Vasc Biol* 1998; 18(5): 677-685.

[58] Sho E, Komatsu M, Sho M, Nanjo H, Singh TM, Xu C, Masuda H, Zarins CK. High flow drives vascular endothelial cell proliferation during flow-induced arterial remodeling associated with the expression of vascular endothelial growth factor. *Exp Mol Pathol* 2003; 75(1): 1-11.

[59] DePaola N, Gimbrone Jr. MA, Davies PF, Dewey Jr. CF. Vascular endothelium responds to fluid shear stress gradients. *Arteriosclerosis and Thrombosis* 1992; 12(11): 1254-1257.

[60] DePaola N, Davies PF, Pritchard WFJ, Florez L, Harbeck N, Polacek DC. Spatial and temporal regulation of gap junction connexin43 in vascular endothelial cells exposed to controlled disturbed flows in vitro. *Proc Nat Acad Sci USA* 1999; 96(6): 3154-3159.

[61] Papaharilaou Y, Doorly DJ, Sherwin SJ. The influence of out-of-plane geometry on pulsatile flow within a distal end-to-side anastomosis. *J Biomech* 2002; 35(9): 1225-1239.

[62] Lee KE, Lee JS, Yoo JY. A numerical study on steady flow in helically sinuous vascular prostheses. *Med Eng Phys* 2010; 33(1): 38-46.

[63] Knight J, Olgac U, Saur CS, Poulikakos D, Marshall W, Cattin PC, Alkhadi H, Kurtcuoglu V. Chosing the optimal wall shear parameter for the prediction of plaque location - A patient-specific computational study in human right coronary arteries. *Atherosclerosis* 2010; 211: 445-450.

# CHAPTER 3

# The anastomosis angle does change disturbed flow patterns in *side-to-end* fistulae for haemodialysis

This chapter is based on:

Ene-Iordache B, Cattaneo L, Dubini G, Remuzzi A.

**Effect of anastomosis angle on the localization of disturbed flow in *side-to-end* fistulae for haemodialysis access**

***Nephrology Dialysis Transplantation*, 28(4):995-1005, 2013**

## 3.1. Abstract

Early failure of vascular access for haemodialysis after the surgery of radial-cephalic arteriovenuos fistula (AVF) occurs mainly due to a juxta-anastomotic stenosis. Even if the elevated blood flow induces high wall shear stresses, we have recently shown that disturbed flow, characterized by low and reciprocating flow, may develop in zones of the AVF that locate well the sites of future stenosis. Our present study was aimed at investigating whether the anastomosis angle influences the localization of disturbed flow in radial-cephalic *side-to-end* AVF.

By means of a parametric AVF model we created 4 equivalent meshes, having the anastomotic angle of 30°, 45°, 60° and 90°, respectively. We then performed transient, non-Newtonian computational fluid dynamics simulations using previously measured blood flow and division ratio in subjects requiring primary access as boundary conditions. The relative residence time (RRT), a robust indicator of disturbed flow, was calculated for the overall wall surface and disturbed flow was localized by areas having RRT > 1. Quantitative characterization and statistical tests were employed to assess the difference in RRT medians between the four anastomosis angle cases.

Disturbed flow was located in all AVF models in the same areas where flow recirculation and stagnation occurs, on the inner wall of the swing segment (SS) and on the arterial wall on the anastomosis floor. Smaller angle AVF had smaller disturbed flow areas with lower RRT peak values, either on the vein or the arterial limb. There were significant differences in the RRT medians on the swing segment and on the anastomosis floor between sharper (30° and 45°) and wider (60° or 90°) angles.

We have found that in *side-to-end* radial-cephalic AVF for haemodialysis the anastomosis angle does impact on the local disturbed flow patterns. Among the four geometries we considered in this study, the smaller angle (30°) would be the preferred choice that minimizes development of neointima. Clinicians should consider this at the time of AVF creation because anastomosis angle is in part amenable to surgical manipulation.

## 3.2. Introduction

Distal radial-cephalic arteriovenous fistula (AVF) is the best choice with which we are acquainted for achieving vascular access (VA) for haemodialysis (HD), but even this type of AVF has relatively high rates of early failure [1]. Early failure of radial-cephalic AVF is defined as the impossibility to use the VA for dialysis or total failure within the first 3 months [2] and is usually due to a juxta-anastomotic stenosis [3], [4] while late AVF failure is due to stenosis that may occur anywhere within the venous segment [1].

Maturation of the AVF or its early failure are closely related to the response of both feeding artery and draining vein to the increase in hemodynamic forces that occurs after the surgical creation of the anastomosis. The flow patterns and haemodynamic forces that act on the luminal layer of endothelial cells (EC) modulating vascular biology and EC functions, are not constant [5], [6] and also not uniform along the arterial tree [7]. In the straight parts of the arterial tree, blood flow is generally laminar and the wall shear stress (WSS) is relatively high and unidirectional. In branches and curvatures, blood flow is disturbed with non-uniform and irregular distribution of low WSS. It was shown that sustained laminar flow with high WSS upregulates expressions of EC genes and proteins that are protective against atherosclerosis, whereas disturbed flow with associated reciprocating, low shear stress generally upregulates the EC genes and proteins that promote atherogenesis [8]. These findings have led to the concept that the disturbed flow pattern in branch points and curvatures causes the preferential localization of stenotic lesions. In the venous system, disturbed flow resulting from reflux, outflow obstruction, and/or stasis leads to venous inflammation and thrombosis, and hence the development of chronic venous diseases [9]. Disturbed flow also results in postsurgical neointimal hyperplasia and contributes to pathophysiology of clinical conditions such as VA failure due to thrombosis secondary to stenosis formation [10] as well as VA re-occlusion after percutaneous interventions [2], [11].

That anastomosis angle influences the blood flow field and pathologic response of the vessel wall was already observed in *end-to-side* arterial bypass anastomoses. Experimental studies have shown that the angle of anastomosis does change the flow field at vascular anastomoses in pig aorta [12] and that different branch angles result in different pathologic changes to the vessel wall in anastomoses of right to left carotid arteries in rabbits [13]. Similar results were obtained in computational fluid dynamics (CFD) studies in models of left interior mammary artery [14] and of a typical stenotic coronary artery bypass grafting [15]. These findings would indicate an influence of the angle on the disturbed flow patterns also in *side-*

*to-end* anastomoses used as VA in HD treated subjects. Sivanesan et al. have shown that in AVF for HD access the flow in the distal artery (DA) is retrograde in about 75% of well-functioning fistulae, whereas in 25% the DA flow is antegrade, and this does not seem to threaten satisfactory fistula function [16]. It follows that, even very similar geometrically to the bypass grafts, the *side-to-end* anastomoses used in VA, having different blood volume flow and blood pathways (see Figure 3.1 for a schematic illustration), might have similar or diverse WSS levels and spatial distribution, but this effect of the anastomosis angle on the disturbed flow patterns has not been investigated yet. As changes in fistula anastomosis angle are amenable to surgical manipulation, the goal would be to inform clinicians what angle minimizes the development of intimal hyperplasia as a response of the endothelium to disturbed haemodyamic shear condition.

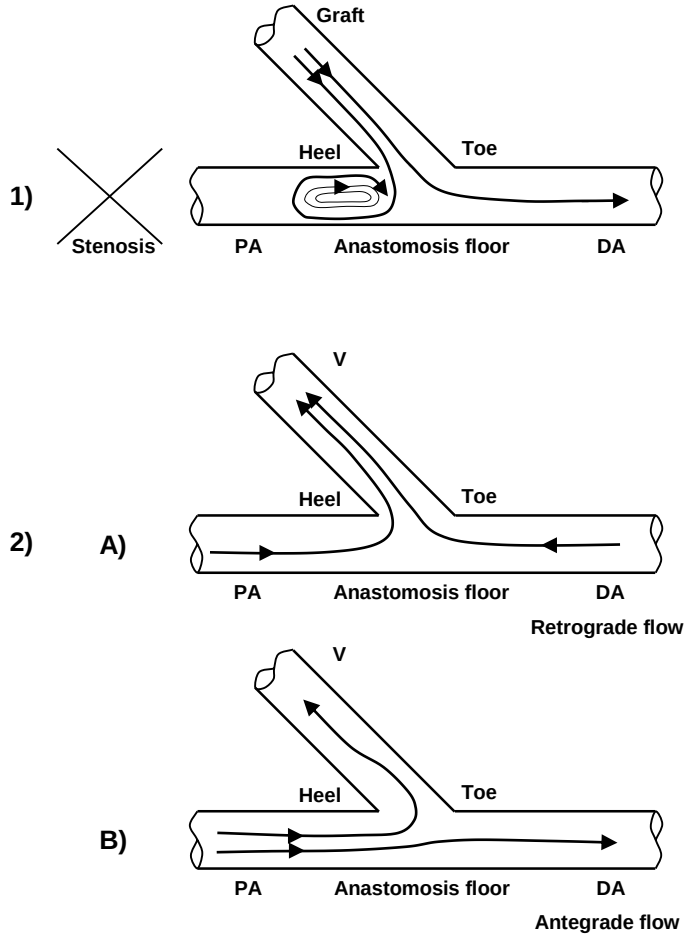


**Figure 3.1. Illustration of typical anastomoses and blood flow pathways. The correct description of the anastomosis (e.g. *end-to-side* or *side-to-end*) is by following the direction of blood flow [17].**
**1) *End-to-side* (distal) anastomosis of a bypass graft with a stenosed host artery. 2) Radial-cephalic *side-to-end* AVF used as VA for HD: A) AVF with retrograde blood flow in the DA; B) AVF with antegrade flow in the DA. Legend: V, vein ; PA, proximal artery; DA, distal artery.**

By using computational modeling we have recently shown that disturbed flow develops at focal sites of radial-cephalic AVF for HD access, either in an *side-to-end* or *end-to-end* anastomosis configuration [21]. One of the major benefits of developing these type of numerical studies is to facilitate simulations on multiple geometries and blood flow distributions for a better understanding of how changes in fistula geometry would impact on local WSS and thus on the future development of intimal hyperplasia [18]. To this purpose, in the present work we have studied the effect of anastomosis angle on the local distribution of disturbed flow in *side-to-end* radial-cephalic AVF used as primary access in HD treated subjects.

## 3.3. Methods

***3D meshes of AVF***. In order to simulate multiple anastomotic angles we employed a parametric model of the *side-to-end* radial-cephalic AVF as presented in Figure 3.2A.

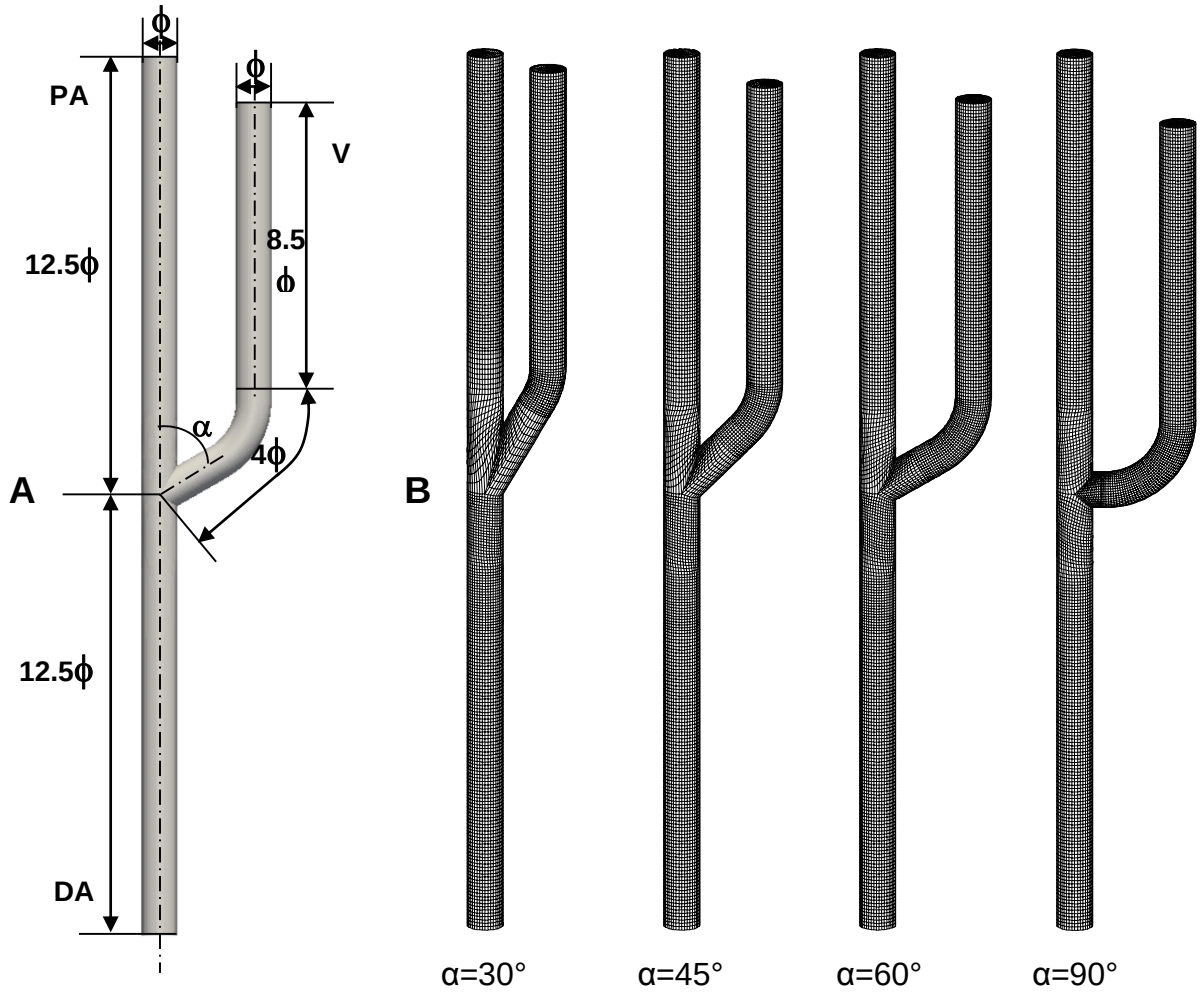


**Figure 3.2. A) Parametric model of side-to-end radial-cephalic anastomosis used for the generation of numerical meshes. B) The 3-D meshes created with an anastoomosis angle of 30°, 45°, 60° and 90°, respectively. Legend: V, vein (cephalic); PA, proximal artery; DA, distal artery; α, anastomotic angle; ϕ, diameter.**

Model's main parameters are the anastomosis angle (α) and vessel diameter (ϕ). In deciding the values of these parameters, we assumed an intra-operative condition of a newly created fistula. The value of ϕ was taken from existing literature, namely 2.4 mm either for radial artery as found in our previous study [19], or for cephalic vein as measured by Corpataux et al. [20]. The extent of the proximal (PA) and distal artery (DA) and of the vein (V) was assumed 12.5 times the diameter in order to have enough hydraulic length to allow fully developed flow. Also, we assumed the length of the swing segment, the part of vein mobilized

in the creation of the anastomosis, equal to 4 diameters and its bending zone was generated with a curvature radius that is 2-fold the diameter (see Figure 3.2A).

Four three-dimensional (3D) meshes of an AVF anastomosis, made of 8-node hexahedral elements, were generated by means of a script run with a pre-processor meshing program for different values of $\alpha$ (30°, 45°, 60° and 90°, respectively). Within the mesh, a boundary layer was generated near the wall so that the elements on the outer surface of the meshwork are about 1/3 in thickness of the internal elements. Regardless of anastomotic angle, the meshes obtained with this procedure have same diameter and length, maintaining thus similar fluid dynamics features like hydraulic length and mesh grid size in terms of number of elements. The 3D mesh grids generated with different bifurcation angles of 30°, 45°, 60° and 90° are presented in Figure 3.2B.

***CFD simulations of blood flow in AVF***. Numerical transient simulations of non-Newtonian blood reproducing both retrograde and antegrade flow in DA in the 4 AVF models were performed. Detailed numerical settings and blood rheological model of the CFD simulations were as previously described [20]. Briefly, we employed an implicit time integration scheme (backward Euler) with 50 fixed time steps for each pulse cycle to solve the time-dependent Navier-Stokes equations. For the unsteady simulations we have used the cephalic vein blood flow rate waveform provided in [21], scaled to yield a time-averaged flow rate of 215 mL/min corresponding to the intra-operative fistula condition measured by same authors in patients requiring primary access for HD [16]. It is worth mentioning that by this assumption we imposed the same blood volume flow and Reynolds number in the vein in both retrograde and antegrade flow in the DA simulations. As boundary conditions, fully developed parabolic velocities at PA and DA inlet were prescribed. Three complete cardiac pulse cycles were solved in order to damp the initial transients of the fluid and only the third cycle was considered for the final results. Geometrical parameters and blood volume flow and division ratio used in the CFD simulations are provided in Table 3.1.

**Table 3.1. Geometrical parameters and blood volume flow used in the CFD simulations.**

| | Diameter *(mm)* | Flow division ratio | V flow rate *(mL/min)* | V Re # |
|---|---|---|---|---|
| ***Retrograde flow in DA*** | 2.4 | 70%PA : 30%DA : 100%V | 215 (378 - 92) | 583 (1034 - 245) |
| ***Antegrade flow in DA*** | 2.4 | 100%PA : 20%DA : 80%V | 215 (378 - 92) | 583 (1034 - 245) |

***Legend***:V, (cephalic) vein; PA, proximal (radial) artery; DA, distal (radial) artery; Re, Reynolds number
***Note***: Flow rates and Reynolds numbers are for the cephalic vein and are expressed as time-averged and (maximum - minimum) values over the pulse cycle.

***Data post-processing.*** For the third cardiac cycle we calculated the relative residence time (RRT) on the overall AVF wall surface, a robust indicator of disturbed flow introduced by Himburg et al. [22]. To calculate the RRT we employed an in-house developed program in python language using the library for scientific computation *numpy* [23]. RRT was calculated with the formula [22]

$$RRT \sim [(1-2\cdot OSI)\cdot TAWSS]^{-1}$$

where OSI is the oscillatory shear index computed with the formula [24]

$$OSI = \frac{1}{2}\left(1 - \frac{\left|\int_0^T \tau_w dt\right|}{\int_0^T |\tau_w| dt}\right)$$

and TAWSS represents the time-averaged WSS calculated as

$$TAWSS = \frac{1}{T}\int_0^T |\tau_w| dt$$

where $\tau_w(t)$ is the instantaneous WSS vector and $T$ is the period of the cardiac cycle.

In this formulation, RRT is a strong indicator of disturbed flow because it incorporates information on both oscillating and low shear stress [22]. The RRT must be normalized by a reference value, which we chose to be the RRT calculated for fully-developed (Poiseuille) flow in the vein [20]. In this way, disturbed flow sites, meaning wall surface areas exposed to low and oscillating WSS, are localized by zones with RRT > 1, while the remaining AVF surface wall areas subjected to high shear stresses, higher or equal to the Poiseuille laminar flow equivalent for the time-averaged blood volume flow over a cardiac cycle condition, are localized by RRT $\leq$ 1.

RRT was post-processed graphically using the program for parallel, interactive, scientific visualization Paraview [26]. The RRT values of surface grid points inside the areas of disturbed flow were exported for further quantitative and statistical analyses. Normality of these RRT samples was assess by Shapiro-Wilk test and the homogeneity of their variances was evaluated with the Bartlett test. Since RRT samples were not normally distributed and the variances were non-homogeneous, we employed the non-parametric Kruskal-Wallis test followed by a pairwise Mann-Whitney test with Holm correction [27] to assess the difference in RRT medians between the four angled *side-to-end* AVF. All statistical analyses were performed using the R environment for statistical computing and graphics [28].

## 3.4. Results

The numerical CFD simulations allowed complete characterization of the haemodynamic field in the different angled AVF models. General blood flow velocity and WSS patterns in retrograde as well as in antegrade flow in DA were as previously described in detail in *side-to-end* radial-cephalic AVF for HD access [21].

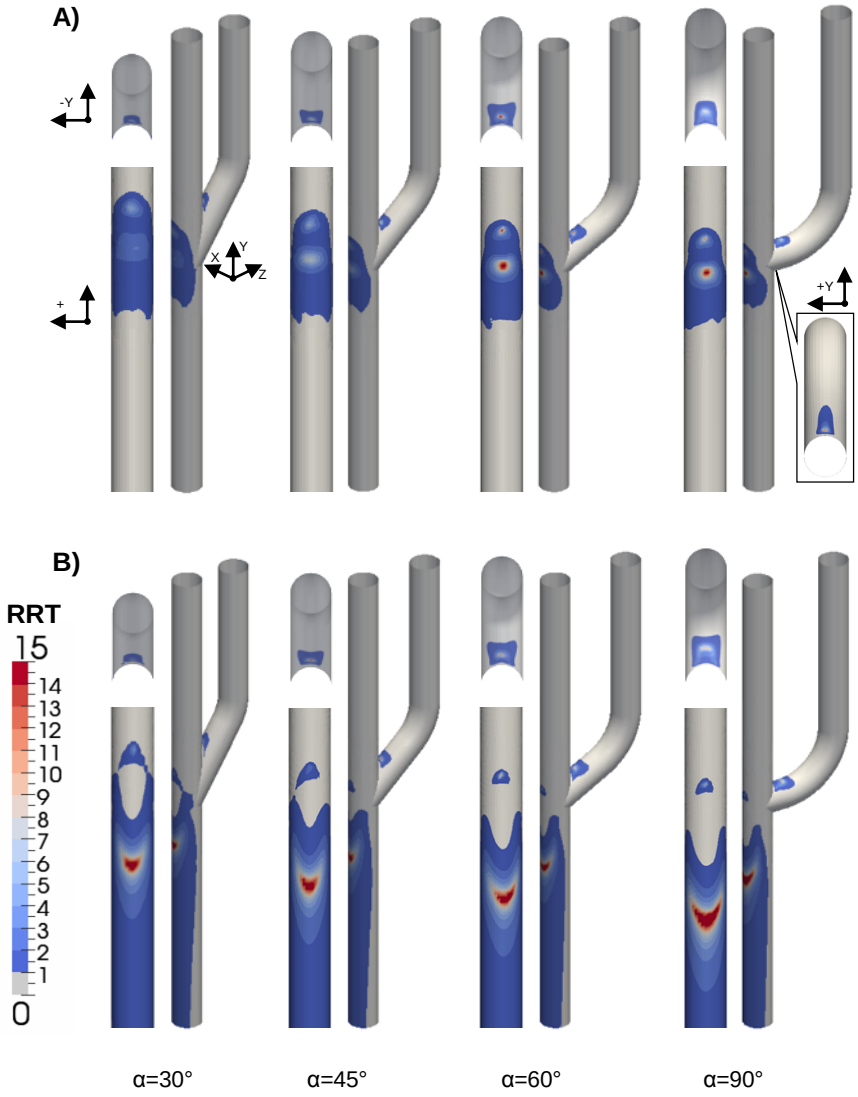


**Figure 3.3. Surface plot of disturbed flow areas on the AVF wall, 2 cm proximal and distal to the anastomosis. From left to right the anastomosis angle is 30°, 45° 60° and 90°, respectively. For each case, the top left image represents RRT patterns on the inner wall of the SS (-Y view), the bottom left image represents RRT patterns on the AF (+Z view), and the right image shows a 3D view of overall anastomosis model (XYZ view). A) Simulations performed assuming retrograde blood flow in DA. B) Simulations performed assuming antegrade flow in DA (see text for boundary conditions). Inset image (+Y view): only in the 90° case with retrograde flow in DA disturbed flow develops also on the outer wall of the SS.**

Therefore, disturbed flow was located in the same areas where flow recirculation and stagnation occurs, near the heel, on the inner wall of the SS and on the arterial wall at the anastomosis floor (AF). Surface maps of disturbed flow located as wall areas having RRT > 1 are presented in Figure 3.3A for retrograde flow and in Figure 3.3B for antegrade flow in the DA simulations.

The disturbed flow zones on the SS are shown in the top left image (–Y view) for each case. It is worth noting on the inner wall of SS how minor angled AVF have smaller disturbed flow areas and also lower RRT absolute peak values, either in retrograde or antegrade flow in DA. Only for the 90° anastomosis angle case in retrograde flow in DA, disturbed flow develops also on the outer wall of the SS (see the inset image in Figure 3.3). The disturbed flow sites on the AF and down to the DA are larger than those on the SS as shown in the bottom-left images (+Z view) of the artery. Also, it can be observed that these sites are larger in antegrade with respect to retrograde flow in DA, owing to opposite blood flow direction in this tract of AVF (see Figure 3.1).

Characterization of disturbed flow zones localized by RRT > 1 in terms of surface area, peak value, and median and interquartile range are presented in Table 3.2. There exists a tendency of disturbed flow sites on the inner wall of the SS to enlarge with the anastomotic angle. In fact, the area of these sites is 0.92, 1.97, 3.39 and 2.42 $mm^2$ in retrograde and 1.21, 2.27, 3.38 and 3.84 $mm^2$ in antegrade flow in DA, as the bifurcation angle increases from minimum to maximum value. The augment of RRT in such sites is not only in area, but also in absolute peak value, that is 7.22, 8.87, 18.27 and 8.11 for retrograde and 4.63, 19.77, 18.27 and 10.19 for antegrade flow in DA, for the AVF angle of 30°, 45°, 60 and 90, respectively. The only site of disturbed flow on the outer wall of the SS, found for the 90 case with retrograde flow in DA as shown in the inset image of Figure 3.3, has an area of 1.95 $mm^2$ and a peak RRT of 11.91 (data not shown in Table 3.2). There was no increase in the area of disturbed flow sites on the AF in both flow settings in DA, but in retrograde flow there is an evident RRT peak increase as the anastomosis angle increases from 30° to 90° (5.66, 7.64, 29.01 and 21.82) while in the antegrade flow in DA cases this tendency is not observed (61.42, 33.28, 43.75 and 67.07).

**Table 3.2. Characterization of disturbed flow sites on the swing segment and on the anastomosis floor in different angled AVF.**

| | | α | | 30° | 45° | 60° | 90° |
|---|---|---|---|---|---|---|---|
| **SS** | ***Retrograde*** | **$RRT_{AREA}$** | *($mm^2$)* | 0.92 | 1.97 | 3.39 | 2.42 |
| | ***flow in DA*** | **$RRT_{PEAK}$** | *(-)* | 7.22 | 8.87 | 18.27 | 8.11 |
| | | **RRT** | *(-)* | 1.28 (1.13 - 1.36)* | 1.27 (1.07 - 1.74)§ | 1.48 (1.13 - 2.03)^ | 1.81 (1.19 - 2.65) |
| | ***Antegrade*** | **$RRT_{AREA}$** | *($mm^2$)* | 1.21 | 2.27 | 3.38 | 3.84 |
| | ***flow in DA*** | **$RRT_{PEAK}$** | *(-)* | 4.63 | 19.77 | 18.27 | 10.19 |
| | | **RRT** | *(-)* | 1.36 (1.03 - 1.54)* | 1.32 (1.12 - 1.65)§ | 1.48 (1.13 - 2.03)^ | 1.75 (1.22 - 2.62) |
| **AF** | ***Retrograde*** | **$RRT_{AREA}$** | *($mm^2$)* | 30.09 | 27.85 | 27.31 | 26.12 |
| | ***flow in DA*** | **$RRT_{PEAK}$** | *(-)* | 5.66 | 7.64 | 29.01 | 21.82 |
| | | **RRT** | *(-)* | 1.13 (1.03 - 1.51)** | 1.21 (1.04 - 1.71)§§ | 1.23 (1.05 - 1.77) | 1.30 (1.08 - 1.80) |
| | ***Antegrade*** | **$RRT_{AREA}$** | *($mm^2$)* | 128.73 | 129.02 | 131.84 | 134.79 |
| | ***flow in DA*** | **$RRT_{PEAK}$** | *(-)* | 61.42 | 33.28 | 43.75 | 67.07 |
| | | **RRT** | *(-)* | 1.21 (1.08 - 1.58)** | 1.24 (1.09 - 1.68)§§ | 1.25 (1.11 - 1.68)^^ | 1.31 (1.14 - 1.86) |

**Legend:** Data are expressed as value or median and ($1^{st}$ - $3^{rd}$ ) quartile range; RRT, relative residence time; SS, swing segment; AF, anastomosis floor; DA, distal artery. Results refer to AVF wall surface areas localized by RRT > 1 as shown in Figure 3.

**Subscripts:** AREA, wall surface area; PEAK, peak (maximum) value.

$P < 0.05$: * vs. 90°; § vs. 90°; ^ vs. 90°.
** vs. 45°, 60° and 90°; §§ vs. 90°; ^^ vs. 90°.

Regarding the sites of disturbed flow on the SS, the Kruskal-Wallis test revealed an effect of anastomosis angle on RRT medians, confirmed also by the post-hoc analyses that showed significant differences between acute angles and the 90° case. Medians of RRT on the inner side of the SS for the retrograde blood flow in DA were 1.28, 1.27, 1.48 and 1.81 for the 30°, 45°, 60° and 90° anastomosis angle, respectively. There were significant differences for 30° vs. 90° ($P = 0.011$), 45° vs. 90° ($P = 0.001$) and 60° vs. 90° ($P = 0.022$). Similarly, for the antegrade flow in DA, the medians of RRT on the inner wall of the SS were 1.36, 1.32, 1.48 and 1.75 and there were significant differences for 30° vs. 90° ($P = 0.003$), 45° vs. 90° ($P = 0.003$) and 60° vs. 90° ($P = 0.043$) cases.

On the arterial limb at AF and down to the DA, the medians of RRT for the retrograde flow were 1.13, 1.21, 1.23 and 1.30 for the 30°, 45°, 60° and 90° anastomosis angle, respectively. There was a significant effect of angle between the RRT medians of cases 30° vs. 45° ($P = 0.002$), 30° vs. 60° ($P = 0.001$), 30° vs. 90° ($P = 0.001$) and 45° vs. 90° ($P = 0.019$).

Likewise, for the antegrade flow in DA cases, RRT medians on the AF were 1.21, 1.24, 1.25 and 1.31, whereas significant differences resulted for 30° vs. 45° ($P$ = 0.004), 30° vs. 60° ($P$ = 0.001), 30°vs. 90° ($P$ = 0.001), 45° vs. 90° ($P$ = 0.001) and 60° vs. 90° ($P$ = 0.001).

## 3.5. Discussion

The development of areas of disturbed flow in the arterial tree is strongly dependent on blood vessel's geometry and on haemodynamic conditions. For the *side-to-end* AVF, disturbed flow is preponderant on the inner wall of the SS and on the arterial limb on the AF and down to the distal artery [21]. The predilection of the disturbed flow to form at these sites was confirmed in the present study for all four anastomotic geometries. The main goal of our study was, however, to assess whether and how the anastomosis angle affects the patterns of disturbed flow in idealized models of *side-to-end* anastomoses and the blood volume flow in a newly created VA. Regarding the anastomotic angle, we found an angle-dependence of areas with disturbed flow in radial-cephalic AVF. This finding is sustained by the RRT area and peak absolute value increment as the angle increases and enforced by the significant differences in RRT medians between acute and the 90° angle case for SS and between lower to higher angles for AF. As smaller angle anastomoses develop lower areas covered by low and oscillating WSS for the same haemodynamic condition, in terms of blood volume flow, will tend to develop less intima in proximity of these sites. Hence, an acute angle (~ 30°) represents the solution which most minimizes the disturbed flow zones in *side-to-end* radial-cephalic AVF.

Our simulations were performed in models of wrist radial-cephalic *side-to-end* AVF representing the intra-operative haemaodynamic conditions of a newly created VA. In the following days the PA, DA and vein will remodel and mature to accommodate the new haemodynamic condition, by changing their luminal diameter [29], [19] and length according to the chronic rise in blood volume flow and intraluminal pressure increase in the venous limb. Local wall remodeling will occur at the specific sites of disturbed flow that triggers formation of neointima, growing of intima-media thickness and successive stenosis development. The higher area and peak value of RRT in the DA in antegrade flow correlated with the lower blood flow rate in this limb and suggests that DA might clot more likely in these type of VA. This fact, however, might not preclude the functioning of VA that will transform in an *end-to-end* fistula. Also, the two areas of RRT on the inner and on the outer wall of SS for 90° with retrograde flow would indicate that this type of geometry might clot with higher frequency.

Our results achieved by computational modeling are in the same direction of analogous studies performed in by-pass anastomoses so far, using numerical methods [30], [14], [15]. All these studies found that a smaller, acute angle, is the optimal geometry for the distal anastomosis for minimization of zones of disturbed flow or where less intima formation occurs.

Despite the similarity of *side-to-end* AVF and by-pass anastomoses, the direction of blood and the amount of blood flow (see Figure 1) distinguish them markedly so that the results obtained in by-pass studies cannot be extrapolated to AVF anastomoses. In such circumstances, to our knowledge, the originality of the present study is the first application of numerical techniques aimed at studying the influence of anastomosis angle on disturbed flow distribution in native AVF used as VA in HD.

Thus, we infer that smaller angle anastomoses will have less intima formation as suggested by the RRT, a robust indicator of disturbed flow. One important limitation of our study is the lack of histological images of tissue specimens of AVF that could directly demonstrate this hypothesis. We may, however, rely on data available in the literature on this topic. Jackson et al. [13] showed that different branch angles result in different pathologic changes to the vessel wall in anastomoses of right to left carotid arteries in rabbits. Also Staalsen et al. found that the anastomosis angle does change the flow fields at vascular *side-to-end* anastomoses in abdominal aorta in pigs [12]. To demonstrate this hypothesis in humans further patient-specific pilot studies should be performed and linked with histopathological studies on vein specimes. At the next level, studies targeted towards the lowering the areas of disturbed flow should be performed with the end-point of improving the maturation rates of VA by reducing the venous development of neointimal hyperplasia. With the present study we would like to introduce the concept of the effect of anastomois angle on the localization of disturbed flow in *side-to-end* fistulae for HD as a phenomenon markedly different than that in by-pass anastomoses and bring it to the attention of clinicians involved in management of VA.

Present study findings should be considered by nephrologists and/or vascular surgeon at the time of surgery of native AVF for HD. It seems that vascular surgeons already do 30° anastomosis AVF and about 89°-90° at the elbow and upper arm, but it is not clear whether guidelines recommending the angle size are in place. In fact, in the European Guidelines on vascular access [31], there are no guidelines specific for the angle creation in wrist radial-cephalic AVF, even if this type of access is the primary choice. Our study is in line with the recommendations of these guidelines for further research on the prevention of IH and into the development of novel non-thrombotic grafts. Moreover, only a few studies on the measurement of anastomosis angle were performed so far. Sivanesan et al. in their study on the sites of stenosis in AVF for HD access found a mean anastomotic angle of 49° for fistulae with progressive stenoses and 42° for fistulae with non-progressive stenosis [3]. While this reference suggests an angle of 45° for a radial-cephalic AVF, our study would suggest to perform the anastomosis with an angle of 30°.

In conclusion, in the present study we have studied with numerical methods the effects of anastomotic angle on the local patterns of low and oscillating WSS in *side-to-end* anastomoses used as VA for HD. Our results show that the anastomosis angle does really impact on the local disturbed flow patterns. Because changes in anastomosis angle is amenable to surgical manipulation, one important implication of our study is to inform clinicians about the optimal angle to minimize the development of intimal hyperplasia resulting from the response of the endothelium to disturbed haemodynamic shear.

## 3.6. Acknowledgments

Part of this study were presented at the 18th Congress of the European Society of Biomechanics (ESB) held in Lisbon in July 2012. The study was partially funded by the 7th Framework Program of the European Commission (FP7-ICT-2007-2 ARCH Project, grant agreement nr. 224390).

## 3.7. References


[1] Roy-Chaudhury P, Spergel LM, Besarab A, Asif A, Ravani P. Biology of arteriovenous fistula failure. *J Nephrol* 2007, 20(2):150-163.

[2] Beathard GA, Arnold P, Jackson J, Litchfield T. Aggressive treatment of early fistula failure. *Kidney Int* 2003, 64(4):1487-1494.

[3] Sivanesan S, How TV, Bakran A. Sites of stenosis in AV fistulae for haemodialysis access. *Nephrol Dial Transplant* 1999, 14(1):118-120.

[4] Badero OJ, Salifu MO, Wasse H, Work J. Frequency of swing-segment stenosis in referred dialysis patients with angiographically documented lesions. *Am J Kidney Dis* 2008, 51(1):93-98.

[5] Dammers R, Stifft F, Tordoir JH, Hameleers JM, Hoeks AP, Kitslaar PJ. Shear stress depends on vascular territory: comparison between common carotid and brachial artery. *J Appl Physiol* 2003, 94(2):485-489.

[6] Reneman RS, Hoeks AP: Wall shear stress as measured in vivo: consequences for the design of the arterial system. *Med Biol Eng Comput* 2008, 46(5):499-507.

[7] Davies PF: Hemodynamic shear stress and the endothelium in cardiovascular pathophysiology. *Nat Clin Pract Cardiovasc Med* 2009, 6(1):16-26.

[8] Chiu JJ, Chien S: Effects of disturbed flow on vascular endothelium: pathophysiological basis and clinical perspectives. *Physiol Rev* 2011, 91(1):327-387.

[9] Bergan JJ, Schmid-Schonbein GW, Smith PD, Nicolaides AN, Boisseau MR, Eklof B: Chronic venous disease. *N Engl J Med* 2006, 355(5):488-498.

[10] Roy-Chaudhury P, Wang Y, Krishnamoorthy M, Zhang J, Banerjee R, Munda R, Heffelfinger S, Arend L. Cellular phenotypes in human stenotic lesions from haemodialysis vascular access. *Nephrol Dial Transplant* 2009, 24(9):2786-2791.

[11] Asif A, Roy-Chaudhury P, Beathard GA: Early arteriovenous fistula failure: a logical proposal for when and how to intervene. *Clin J Am Soc Nephrol* 2006, 1(2):332-339.

[12] Staalsen NH, Ulrich M, Winther J, Pedersen EM, How T, Nygaard H. The anastomosis angle does change the flow fields at vascular end-to-side anastomoses in vivo. *J Vasc Surg* 1995, 21(3):460-471.

[13] Jackson ZS, Ishibashi H, Gotlieb AI, Langille BL. Effects of anastomotic angle on vascular tissue responses at end-to-side arterial grafts. *J Vasc Surg* 2001, 34(2):300-307.

[14] Freshwater IJ, Morsi YS, Lai T. The effect of angle on wall shear stresses in a LIMA to LAD anastomosis: numerical modelling of pulsatile flow. *Proc Inst Mech Eng H* 2006, 220(7):743-757.

[15] Do H, Owida AA, Yang W, Morsi YS. Numerical simulation of the haemodynamics in end-to-side anastomoses. *Int J Numer Meth Fluids* 2011, 67:638-650.

[16] Sivanesan S, How TV, Bakran A. Characterizing flow distributions in AV fistulae for haemodialysis access. *Nephrol Dial Transplant* 1998, 13(12):3108-3110.

[17] Konner K. The anastomosis of the arteriovenous fistula – common errors and their avoidance. *Nephrol Dial Transplant* 2002, 34:300-307.

[18] Brien TO, Walsh M, McGloughlin T. On reducing abnormal hemodynamics in the femoral end-to-side anastomosis: the influence of mechanical factors. *Ann Biomed Eng* 2005, 33(3):310-322.

[19] Ene-Iordache B, Mosconi L, Antiga L, Bruno S, Anghileri A, Remuzzi G, Remuzzi A. Radial artery remodeling in response to shear stress increase within arteriovenous fistula for hemodialysis access. *Endothelium* 2003, 10(2):95-102.

[20] Corpataux JM, Haesler E, Silacci P, Ris HB, Hayoz D. Low-pressure environment and remodeling of the forearm vein in Brescia-Cimino haemodialysis access. *Nephrol Dial Transplant* 2002, 17(6):1057-1062.

[21] Ene-Iordache B and Remuzzi A. Disturbed flow in radial-cephalic arteriovenous fistulae for haemodialysis: low and oscillating shear stress locates the sites of stenosis. *Nephrol Dial Transplant* 2012, 27:358-368.

[22] Sivanesan S, How TV, Black RA, Bakran A. Flow patterns in the radiocephalic arteriovenous fistula: an in vitro study. *J Biomech* 1999, 32(9):915-925.

[23] Himburg HA, Grzybowski DM, Hazel AL, LaMack JA, Li XM, Friedman M. Spatial comparison between wall shear stress measures and porcine arterial endothelial permeability. *Am J Physiol Heart Circ Physiol* 2004, 286(5):H1916-1922.

[24] Numpy - scientific computing tools for Pyhton. [http://numpy.scipy.org/].

[25] He X and Ku DN. Pulsatile flow in the human left coronary artery bifurcation: average conditions. *J Biomech Eng* 1996, 118:74-82.

[26] Paraview - open-source scientific visualization. [http://www.paraview.org/]

[27] Hart A. Mann-Whitney test is not just a test of medians: differences in spread can be important. *BMJ* 2001, 323(7309):391-393.

[28] R development core team. R: a language and environment for statistical computing. ISBN 3-900051-07-0, 2011. [http://www.R-project.org/]

[29] Dammers R, Tordoir JH, Welten RJ, Kitslaar PJ, Hoeks AP. The effect of chronic flow changes on brachial artery diameter and shear stress in arteriovenous fistulas for hemodialysis. *Int J Artif Organ*s 2002, 25(2):124-128.

[30] Fei D, Thomas JD, Rittgers SE. The effect of angle and flow rate upon hemodynamics in distal vascular graft anastomoses: a numerical model study. *J Biomech Eng* 1994, 116:331-336.

[31] Tordoir J, Canaud B, Haage P, Konner K, Basci A, Fouque D, Kooman J, Martin-Malo A, Pedrini L, Pizzarelli F et al. EBPG on Vascular Access. *Nephrol Dial Transplant* 2007, 22 Suppl 2:ii88-117.

# CHAPTER 4

# Multidirectional and reciprocating disturbed flow in a patient-specific case of *side-to-end* arteriovenous fistula for haemodialysis

This chapter is based on:

Ene-Iordache B, Semperboni C, Dubini G, Remuzzi A.

**Disturbed flow in a patient-specific arteriovenous fistula for haemodialysis: Multidirectional and reciprocating near-wall flow patterns**

***Journal of Biomechanics*, 48:2195-2200, 2015**

## 4.1. Abstract

Actual surgical creation of vascular access has unacceptable failure rates of which stenosis formation is a major cause. We have shown previously in idealized models of *side-to-end* arteriovenous fistula that disturbed flow, a near-wall haemodynamic condition characterized by low and oscillating fluid shear stress, develops in focal points that correspond closely to the sites of future stenosis. Our present study was aimed at investigating whether disturbed flow occurs in patient-specific fistulae, too.

We performed an image-based computational fluid dynamics study within a realistic model of wrist *side-to-end* anastomosis fistula at six weeks post-surgery, with subject-specific blood rheology and boundary conditions. We then categorized disturbed flow by means of established haemodynamic wall parameters.

The numerical analysis revealed laminar flow within the arterial limbs and a complex flow field in the swing segment, featuring turbulent eddies leading to high frequency oscillation of the wall shear stress vectors. Multidirectional disturbed flow developed on the anastomosis floor and on the whole swing segment. Reciprocating disturbed flow zones were found on the distal artery near the floor and on the inner wall of the swing segment.

We have found that both multidirectional and reciprocating disturbed flow develop on the inner side of the swing segment in a patient-specific *side-to-end* fistula used for vascular access six weeks post-operatively. This has obvious implications for elucidating the haemodynamic forces involved in the initiation of venous wall thickening in vascular access.

## 4.2. Introduction

A well-functioning vascular access (VA) serves as lifeline for the patients with end-stage renal disease on renal replacement therapy by haemodialysis. There is general consensus in the literature on the superiority of native arteriovenous fistulae (AVF) over arteriovenous grafts (AVG) and central venous catheters regarding VA survival, related complications and costs. Despite the existence of clinical guidelines [1],[2] recommending well-defined criteria to create native AVF, a high early failure rate (within 3 months post-operatively) is complained worldwide due to the formation of juxta-anastomosic stenoses. In studies performed between 1977 and 2002 where VA was provided by AVF placement [3], the mean early failure rate was 25% (range 2 - 53%) while the mean one-year patency rate was 70% (42 - 90%). Clinical results from the ARCH project trial performed in four experienced clinical sites in Europe [4] are in line with these observations by reporting an early failure rate of 21% and one-year primary patency rate of 66%.

Since the 1990s computational fluid dynamics (CFD) applied to blood vessels was intensively used to assess the wall shear stress (WSS) in the study of the link between haemodynamics and cardiovascular disease. Despite its clinical relevance, this type of investigational method was less used for the study of VA complications in the last decade, but more recently, studies performed in this research area [5],[6] are promising in reducing this gap. Beside characterization of the general flow field, many patient-specific CFD studies have focused on the assessment of the so-called "disturbed flow" acting near wall. The pattern of disturbed flow is irregular, it features secondary and recirculation eddies that may change in direction with time and space, and hence it exerts low and oscillating WSS on the endothelial layer [7]. Localization of atherosclerosis within specific sites in branch points or curvatures of the arterial tree, in humans and in experimental animals [26], led to the concept that the disturbed flow is related to the vascular lesions. Also in VA, recent findings about the localization of these sites matching areas of disturbed flow [25] may add new insights into the mechanism of pathogenesis of neointimal hyperplasia (NH) after the surgical creation of the anastomosis.

By using CFD we have recently shown that disturbed flow may develop in focal sites of radial-cephalic models of AVF, either in *side-to-end* or *end-to-end* configuration, at least in idealized geometry with flow conditions resembling the initial days after surgery [8]. In that study, we speculated on a local remodeling mechanism for neointima formation induced by the

local disturbed flow. The present study was aimed at investigating whether disturbed flow occurs also in a patient-specific AVF model, which would confirm the above hypothesis on the haemodynamics-related mechanism of local development of stenosis.

## 4.3. Methods

***Patient-specific data.*** The subject was a 48 year old male, who participated in a prospective clinical trial [4]. As per study protocol [9], the patient had blood sample, ultrasound (US) and magnetic resonance angiography (MRA) investigations of the left arm vessels, pre-operatively and six weeks post-operatively. In order to assess the volumetric flow rates in the AVF, pulsed Doppler velocity spectra images at six weeks were analysed with a general-purpose image analysis software (ImageJ v1.48, NIH, Bethesda, MD) and three cycles were averaged to obtain the final waveform [10]. Patient-specific flow rate waveforms derived from US in the arteries, namely the proximal artery (PA) and the distal artery (DA) are shown in Figure 4.1.

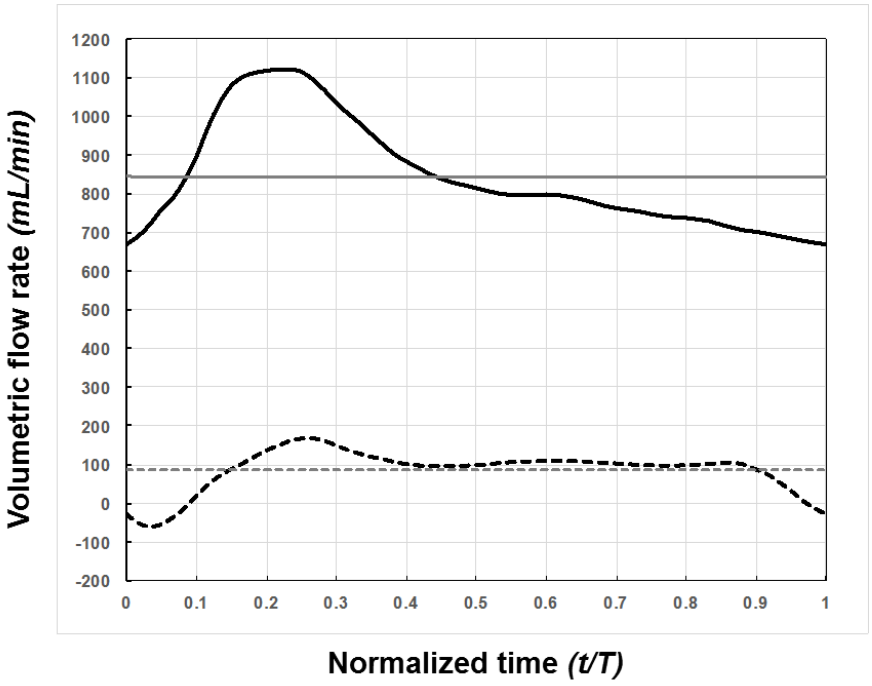


**Figure 4.1. Patient-specific blood volumetric flow rate waveforms derived from US pulsed-Doppler velocity spectra images. Continuous and dashed curves represent the blood flow in the PA and DA, respectively. Blood flow in the DA changes direction during the cardiac cycle, negative is antegrade (towards the hand) and positive is retrograde flow. Horizontal lines indicate the time-averaged blood flow rate over the cardiac cycle, 844 mL/min for PA and 86.5 mL/min for DA, respectively. Legend: PA, proximal artery; DA, distal artery; V, vein.**

The cycle-averaged blood flow rate in the PA was 844 mL/min, indicative for a well-matured radial-cephalic fistula. Time-averaged volumetric flow rate in the DA was 86 mL/min and was retrograde (i.e., directed from the hand towards the anastomosis), although in some portions of the cardiac cycle the flow was inverted (antegrade). Overall, in this case of *side-to-*

*end* patient-specific AVF model, cycle-averaged blood flow division ratio was 91%PA:9%DA:100%V. Patient's cardiac frequency was 62 strokes/min, so we assumed a cardiac cycle period of 1 s in the CFD simulation.

The MRA image acquisition protocol was already described in a previous study to evaluate the feasibility of non-contrast-enhanced MRA for the assessment of upper extremity vasculature as compared with contrast-enhanced MRA [12]. Briefly, the MRA image series of the lower arm used in our 3-D reconstruction were acquired with a voxel size of 0.75 x 1.38 x 1.68 mm usimg a 1.5 T scanner (Intera R9.1 Philips Healthcare, Best, The Netherlands).

Also at six weeks post-operatively, the patient had 29% blood haematocrit and 5.4 g/dL total plasma protein concentration. These values were used for the calculation of blood viscosity as previously reported [11], which yielded a whole blood viscosity ($\mu$) of 0.024 Poise.

***Three-dimensional reconstruction and meshing of the AVF model.*** Segmentation of AVF lumen from the MRA images was performed with the Vascular Modeling Tool Kit (*vmtk*), an open-source framework for patient-specific computational haemodynamics [13]. We generated a surface model consisting of the *side-to-end* anastomosis, the three main vessels of the anastomosis, namely the PA, the DA and the draining vein consisting of the swing segment (SS) and the vein curvature. Straight cylindrical flow extensions were added in order to allow fully development of the flow field inside the computational domain.

Since hexahedral meshes are known to reduce the computational costs respect to the tetrahedral ones [20], and to provide higher accuracy in the calculation of WSS [21], we decided to use hexahedral cells for the AVF mesh. The internal volume was discretized with the *foamyHexMesh* mesher which is part of *OpenFOAM* v. 2.3.1 suite [14]. Starting from the surface geometry, this mesher produced high quality hexahedral grids with regular shape cells. Two thin boundary layers of cells were generated near the wall in order to increase the accuracy of WSS calculation. A coarser mesh with more than 128,000 cells, and two refined, consisting of more than 300,000 and 780,000 cells were generated for the AVF model. After a steady CFD study for mesh-independence, which yielded a maximum difference in WSS lower than 5% relative to the finest grid, we concluded that the mesh with 300,000 cells resolves accurately the flow field and related WSS inside this type of AVF setting. Full and detailed view of the AVF grid, with highlighted the anastomosis floor and the swing segment (SS) of cephalic vein, are presented in Figure 4.2.

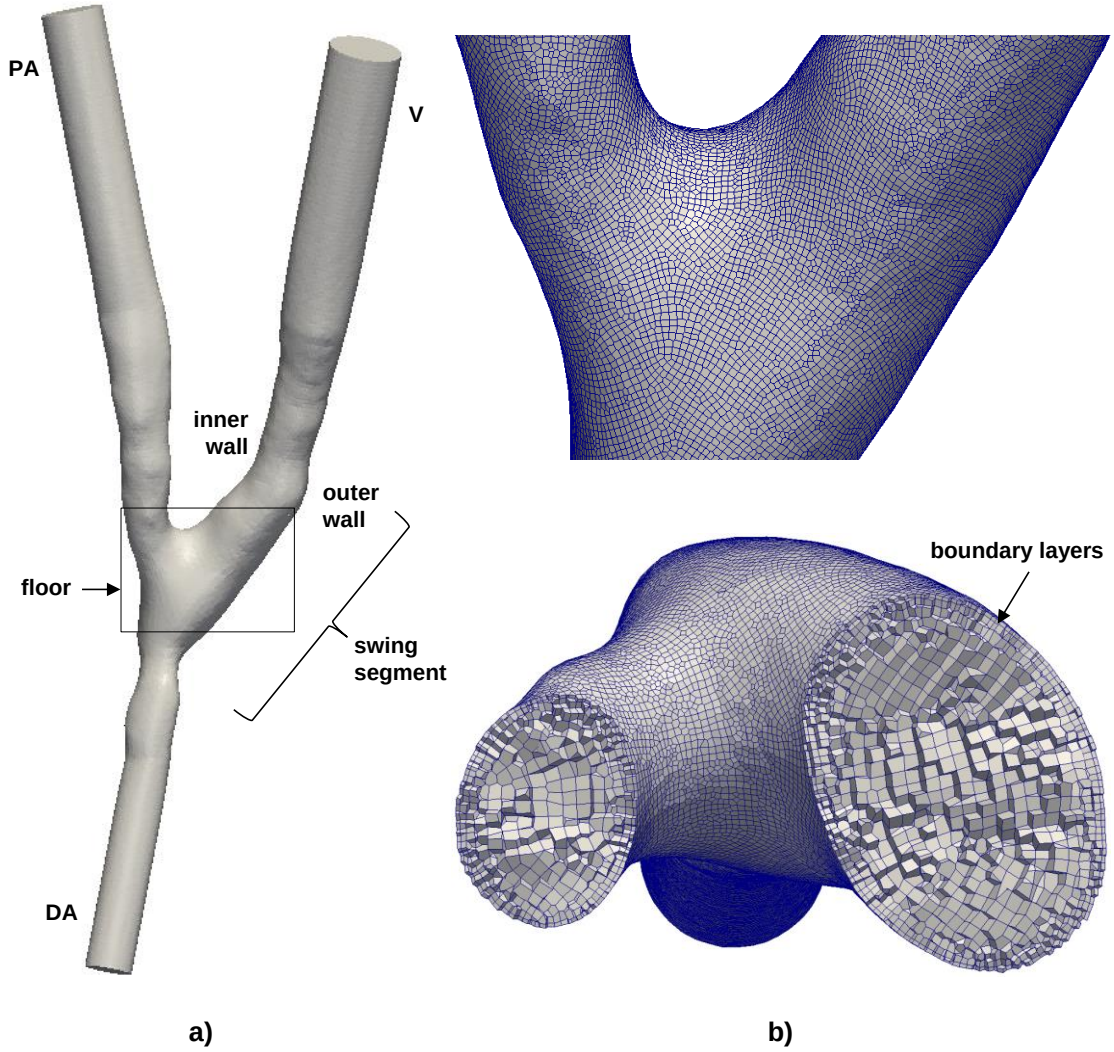


**Figure 4.2. Patient-specific model of the radial-cephalic, side-to-end AVF; a) 3-D surface of the model; b) detail of the surface and volume meshwork showing internal cells and the boundary layer near the wall. Legend: PA, proximal artery; DA, distal artery V, vein.**

***CFD simulations of blood flow in the AVF.*** Transient flow simulation was performed using the *OpenFOAM* code, a multipurpose and well validated CFD tool based on the finite volume method [14]. We considered the non-Newtonian behaviour of blood by employing the Bird-Carreau rheological model implemented in *OpenFOAM* in the form:

$$\mu = \mu_\infty + (\mu_0 - \mu_\infty)\,[1 + (k\,D)^2]^{(n-1)/2}$$

where $\mu_\infty$ is the limiting viscosity at infinite shear rate, $\mu_0$ is the limiting viscosity at zero shear rate, $k$ is a constant and $D$ is the second invariant of the strain rate tensor. We assumed $\mu_\infty$ = 0.024 Poise (previously calculated whole blood viscosity of the patient) and the other parameters of the equation were determined as described in [15], resulting in $\mu_0$ = 0.16 Poise, $k$ = 1 s and $n$ = 0.6. Blood density was assumed $\rho$ = 1.05 g/cm$^3$.

As boundary conditions we prescribed blood flow rates at the PA and DA inlets with the waveforms shown in Figure 4.1, traction-free at the vein outlet and no-slip at the walls. We used *pimpleFoam*, a transient solver for incompressible flows using the PIMPLE (merged PISO-SIMPLE) algorithm and first order Euler time integration scheme. This solver adjusts the time step based on a user-defined maximum Courant–Friedrichs–Lewy (CFL) number, which we set to 1. The numerical simulation ran in 19,940 variable time steps for a cycle, corresponding to a temporal resolution between 0.018 to 0.067 ms, and results were saved for post-processing in 1,000 equal time steps for each cycle. Three complete cardiac cycles were solved in order to damp the initial transients of the fluid and only the results of the third cycle were considered for data processing.

For the PA and DA inlets, and the vein outlet, we calculated the Reynolds and the Womersley numbers as described previously [15]. Geometric and haemodynamic features of the patient-specific AVF model are summarized in Table 4.1.

**Table 4.1. Geometric and haemodynamic features of the patient-specific AVF model**

| | Diameter *(mm)* | Volumetric flow rate *(mL/min)* | Re | Wo |
|---|---|---|---|---|
| **PA inlet** | 5 | 844 (1121; 669) | 1387 (1879; 1080) | 3.91 (3.95; 3.88) |
| **DA inlet** | 3.8 | 86 (168; -60) | 161 (338; 106) | 2.76 (2.87; 2.69) |
| **V outlet** | 5.9 | 930 (1283; 639) | 1263 (1788; 837) | 4.52 (4.58; 4.44) |

***Note***: Waveforms of the flow rate in the PA and DA are shown in Figure 4.1. The flow rate in V is obtained by their summation. Volumetric flow rates, Re and Wo numbers are calculated for the given diameters and are expressed as time-averaged and (maximum; minimum) values over the pulse cycle.

***Legend***: PA, proximal (radial) artery; DA, distal (radial) artery; V, (cephalic) vein; Re, Reynolds number; Wo, Womersley number.

***Data post-processing.*** We described the general flow field by means of velocity and shear stress plots, and localized disturbed flow zones on the AVF surface by means of specific defined haemodynamic wall parameters. In particular, we localized reciprocating disturbed flow by means of the oscillatory shear index (OSI) [16], and multidirectional near-wall disturbed flow by means of the transverse WSS (transWSS) metric [18]:

$$transWSS = \frac{1}{T}\int_0^T \left| \vec{\tau}_w \cdot \left( \vec{n} \times \frac{\vec{\tau}_{mean}}{|\vec{\tau}_{mean}|} \right) \right| dt$$

where $\vec{\tau}_w(t)$ is the instantaneous WSS vector, $\vec{n}$ the normal to arterial surface, $t$ the time and $T$ is the period of the cardiac cycle. This metric averages the magnitude of WSS components perpendicular to the mean shear vector on the vessel wall. Low transWSS areas indicate that the flow remains approximately parallel to a single direction throughout the cardiac cycle, while high transWSS indicate changes in near-wall flow direction.

Also, aimed at describing the nature of the haemodynamic shear, we generated plots of WSS magnitude in time in several feature points on the AVF surface, considering the WSS vector positive in the direction of the main flow.

Post-processing and visualization of the results were performed using *paraview* [19].

## 4.4. Results

Representative 3-D velocity profiles in the PA, DA, SS and more distally after the vein curvature, corresponding to peak-systolic and end-diastole time-points are shown in Figure 4.3. The profiles in both arteries have a parabolic shape, representative for laminar flow. At contrary, the velocity profiles in the vein have complex shapes with ridges inside the lumen and skewed towards the wall. These profiles reveal development of multiple vortexes and important secondary flows at peak-systole in the SS, which are damped more distally on the vein and in the diastolic phase of the cardiac cycle (see cross-section images in Figure 4.3).

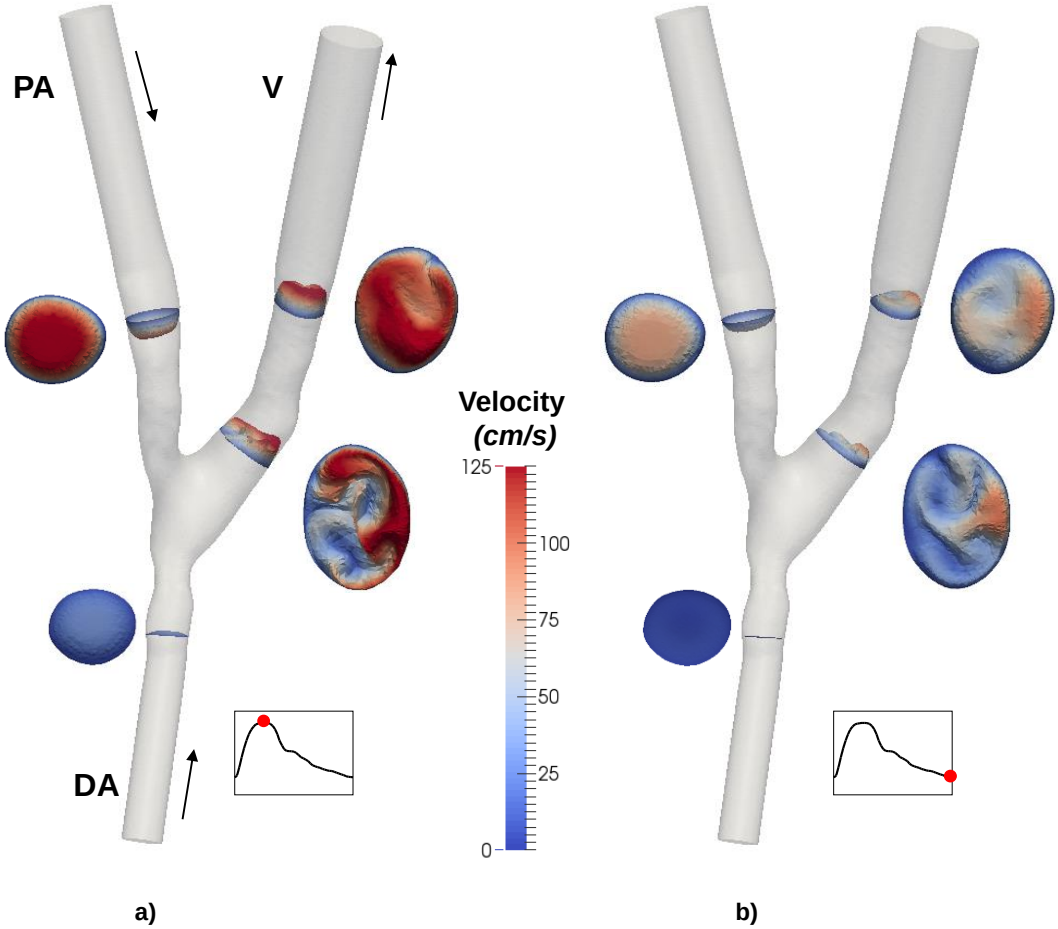


**Figure 4.3. 3-D velocity profiles of blood in four cross-sections on the PA, DA, SS and V for peak systolic a) and end-diastole b). The inset images are top-view of the velocity profile in the vein, showing development of multiple vortices. The arrows in the left panel indicate the direction of blood flow, inner wall position is as indicated on the bottom image.**
**Legend: PA, proximal artery; DA, distal artery; SS, swing segment; V, vein.**

The WSS distribution on the AVF at peak-systole and end-diastole are presented in Figure 4.4. A big portion of the AVF surface is subjected to very high WSS (in red colour, > 70 dyne/cm$^2$). However, areas of low WSS are found along the DA, on the anastomotic floor,

on the inner wall of the SS, and after the vein curvature. In particular, when the blood flow rate is at maximum, low WSS is still located in focal sites at the inner wall of the SS, as well as on the inner wall after the vein curvature (see Figure 4.4a).

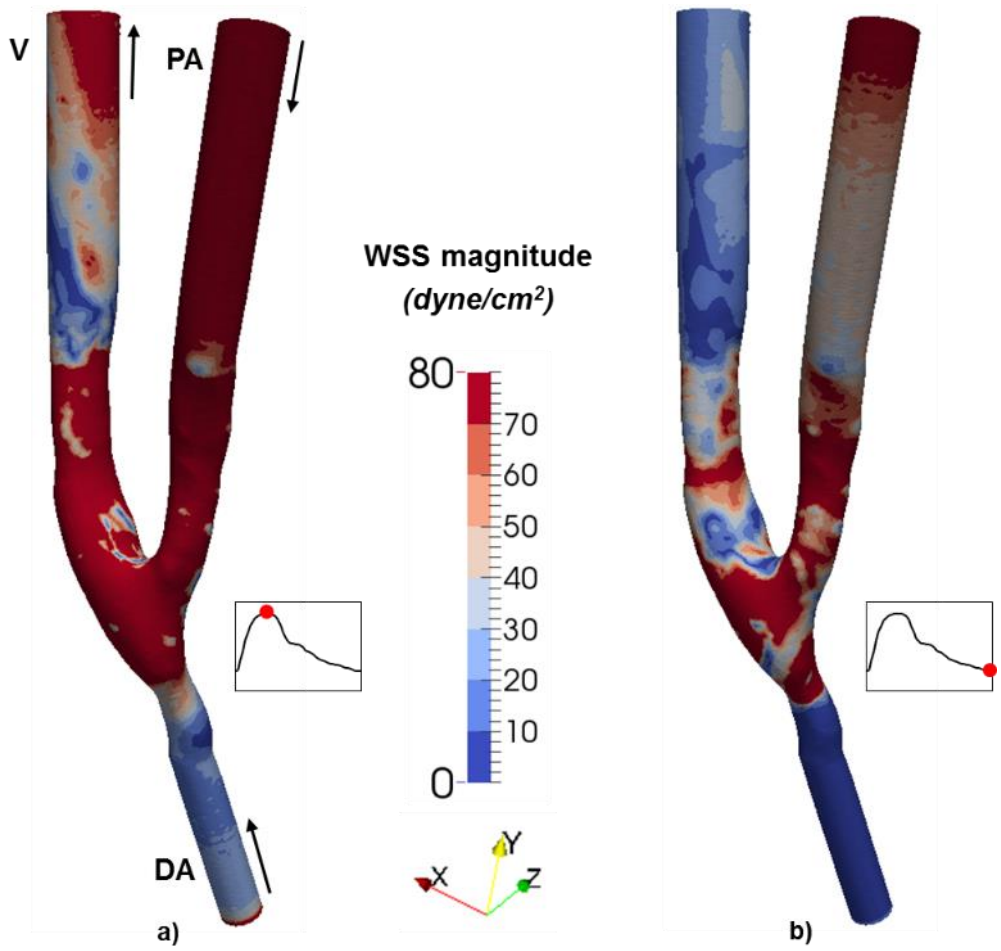


**Figure 4.4. Wall shear stress patterns on the AVF surface for peak systolic (a) and end-diastole (b). Color scale: high WSS zones are in red (> 70 dyne/cm2) and low WSS zones in dark blue (< 10 dyne/cm2). The arrows indicate the direction of blood flow. Legend: PA, proximal artery; DA, distal artery V, vein.**

The patterns of disturbed flow in this patient-specific AVF are presented in Figure 4.5. Reciprocating shear disturbed flow zones revealed by high OSI (Figure 4.5a), are located on the inner wall of the SS, after the vein curvature, and on the DA near the anastomosis floor. Multidirectional flow, as characterized by medium-to-high transWSS (> 10 dyne/cm$^2$, Figure 4.5b) is located on the anastomosis floor, the whole SS and, in a lesser extent more distally, after the vein curvature. Such patterns of transWSS indicate that shear vectors change direction throughout the cardiac cycle on the whole SS surface, while they remain approximately parallel to the main direction of flow on the PA and DA walls.

.

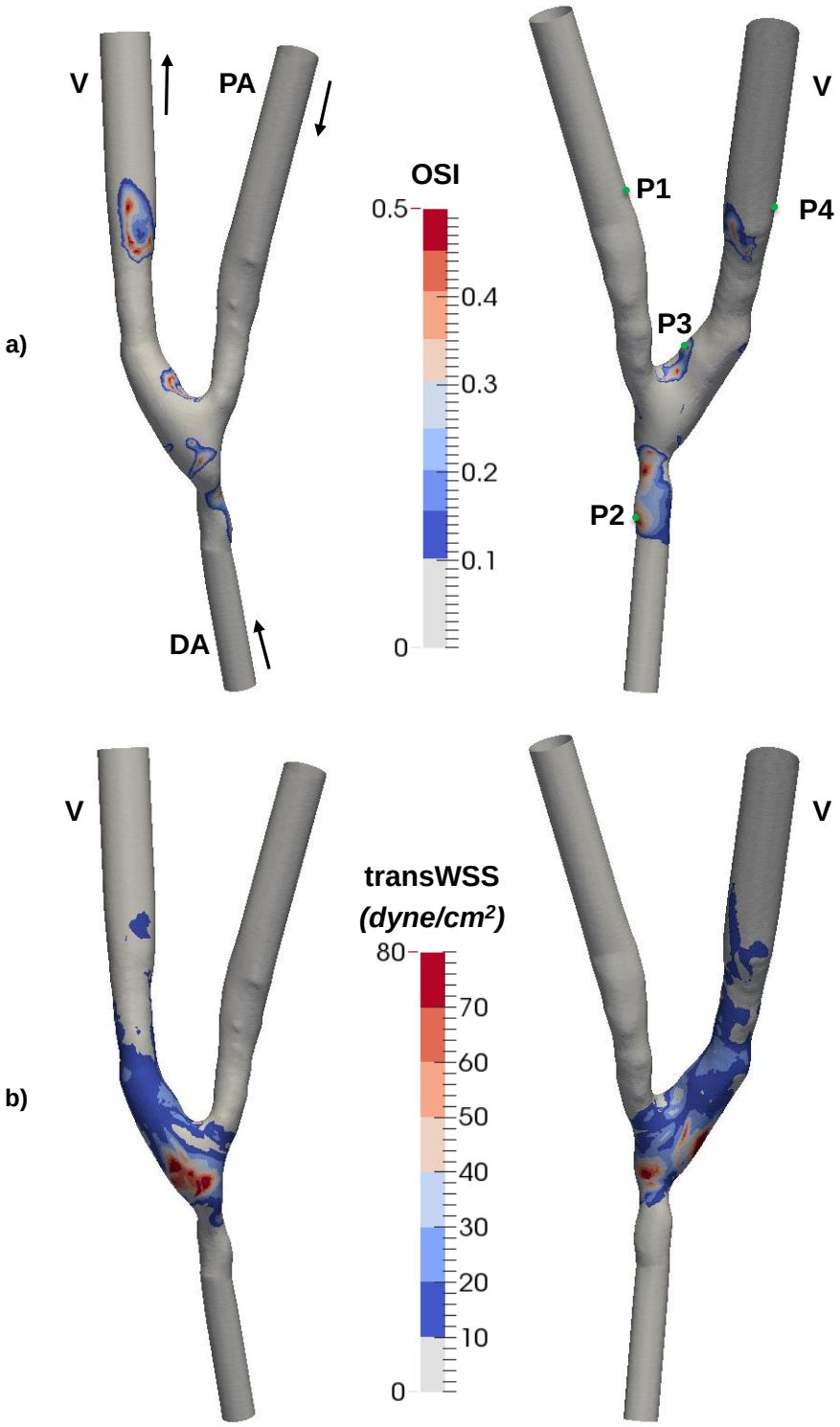


**Figure 4.5. Distribution of haemodynamic wall parameters on the AVF wall: a) plot of OSI; b) plot of tranWSS. Values of OSI below .1 and of transWSS below 10 dyne/cm2 were represented in light grey to emphasize the pattern of disturbed flow on the AVF surface.**
**Left, front view; right, rear view of the AVF. The arrows indicate the direction of blood flow.**
**Legend: PA, proximal artery; DA, distal artery V, vein.**

Of note, the transWSS is low (< 10 dynes/cm$^2$) in zones far from anastomosis, on the PA, the DA and on the vein after the curvature. Such patterns of transWSS indicate that the shear vectors remain approximately parallel to the main direction of flow on the wall of these limbs, while they change direction throughout the cardiac cycle on the whole anastomotic and SS surface.

The time-course of the WSS vector throughout the pulse cycle for four feature points on the AVF surface are presented in Figure 4.6 while their near-wall flow characteristics are summarized in Table 2. These points are shown in Figure 4.5a and were selected specifically to characterize the shear vector acting on the inner wall of PA (P1) corresponding to laminar bulk flow, matching the highest OSI on the DA and SS (P2 and P3) in disturbed flow zones, and on the outer wall of the vein (P4) after the SS curvature.

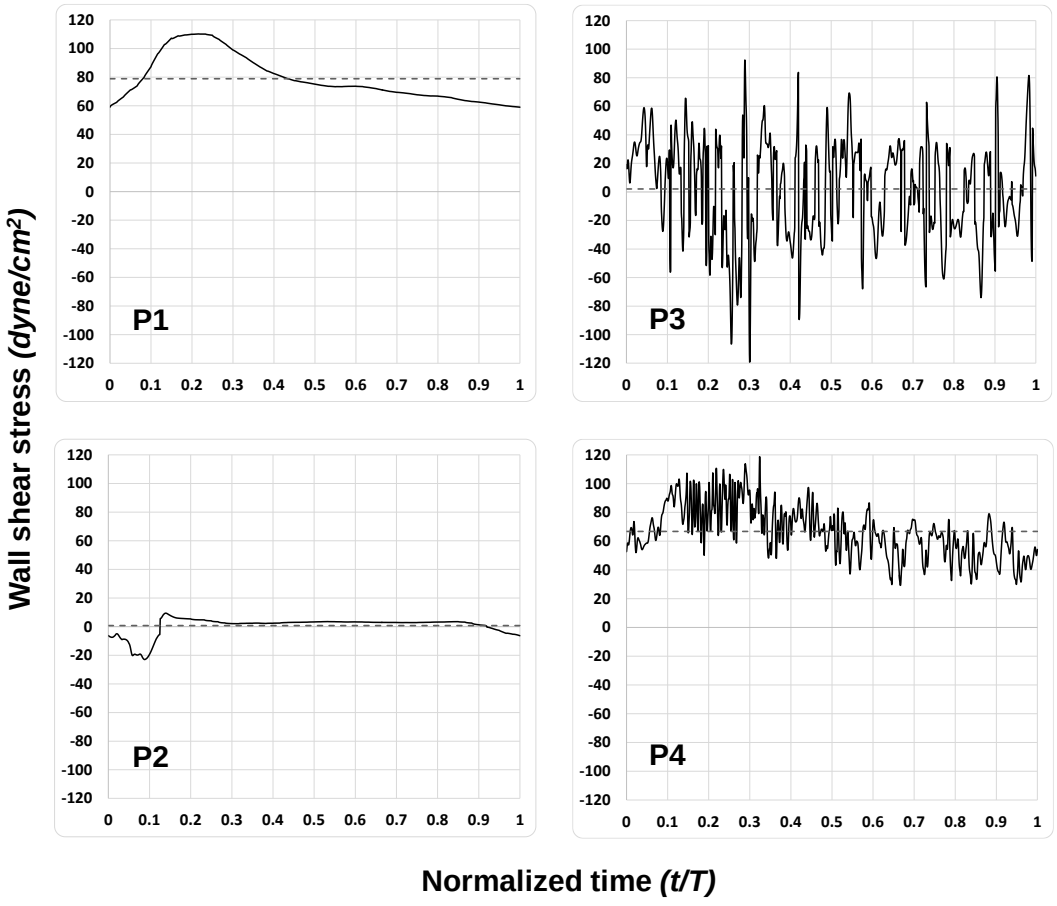


**Figure 4.6. Plot of the WSS vector variation throughout the cardiac cycle for four feature points on the AVF surface. The sign of the WSS vector was taken into account by considering positive the direction of the bulk flow. Position of the feature points (P1 to P4) on the AVF surface is as depicted in Figure 4.5a right. Continuous, WSS magnitude; dashed line, time-averaged WSS over the pulse cycle.**

The graphs reveal high WSS on the PA (P1, time-averaged 78.9 dyne/cm$^2$), specific for laminar and high blood flow. Pure reciprocating flow develops on the DA, oscillating with the

frequency of heart rate and having a low average (P2, OSI 0.42, time-averaged WSS 0.7 dyne/cm$^2$). High frequency, either multidirectional or reciprocating flow develops on the inner wall of the SS (P3, transWSS 22.7 dyne/cm$^2$, OSI 0.47 and time-averaged 2.1 dyne/cm$^2$). More distally on the outer vein, the WSS pattern is multidirectional lowered (P4, transWSS 6.1 dyne/cm$^2$) and oscillating with high frequency around a big value (time-averaged 66.7 dyne/cm$^2$).

Of note, respect to the point (P2) on DA where the WSS vector oscillates with low frequency (i.e., of the heart rate), the oscillations of the WSS vector at point (P3) on the inner side of SS have a very high frequency.

**Table 4.2. Characteristics of near-wall flow at four feature points on the AVF surface.**

| Point | Position | Type of bulk flow | Type of disturbed flow | OSI | transWSS *(dyne/cm$^2$)* | max WSS *(dyne/cm$^2$)* | min WSS *(dyne/cm$^2$)* | TAWSS *(dyne/cm$^2$)* |
|---|---|---|---|---|---|---|---|---|
| **P1** | PA (inner wall) | laminar | - | 0 | 0.7 | 110.2 | 59.0 | 78.9 |
| **P2** | DA | laminar | reciprocating | 0.42 | 1.2 | 9.4 | -23.0 | 0.7 |
| **P3** | SS (inner wall) | turbulent | reciprocating, multidirectional | 0.47 | 22.7 | 92.4 | -119.2 | 2.1 |
| **P4** | V (outer wall) | turbulent (damped) | multidirectional | 0.003 | 6.1 | 118.7 | 29.3 | 66.7 |

***Note***: The position of the four feature points is as shown in Figure 4.5a (right).

***Legend***: PA, proximal (radial) artery; DA, distal (radial) artery; SS, swing segment; V, vein (cephalic); WSS, wall shear stress; OSI, oscillatory shear index; transWSS, transverse wall shear stress.

## 4.5. Discussion

While the mechanism of vessel wall pathophysiology has been subject of considerable research, the idea of the link between disturbed flow and NH in VA is relatively new [25]. In the present study we employed image-based CFD in a realistic model of side-to-end radial-cephalic AVF, showing development of disturbed flow. The working hypothesis regarding existence of disturbed flow zones that may trigger the local remodeling mechanism [8], was corroborated also in this patient-specific AVF case. Our study is in agreement with previous idealized geometry [27],[28] and image-based CFD studies [7] that reported development of reciprocating disturbed flow (high OSI) on the AVF walls.

This is the first study to reveal the multi-directionality of WSS on the anastomosis floor and on the SS walls. The high values of transWSS in Figure 4.5b are indicative for development of complex vortices in the SS that rotate also the shear stress vectors at the vessel wall. At the same time, in some areas of the inner wall of the SS, reciprocating disturbed flow develops as shown in Figure 4.5a. Another novel finding was to show that the nature of reciprocating flow developed on DA and SS walls are different. While the DA experienced pure reciprocating flow at the frequency of the heart rate, the oscillations of the WSS on the SS wall were at high frequencies, induced by the turbulent bulk flow at this level.

Our results are confirmed by an in vivo study in canines [30] showing that NH develops more on the inner compared to the outer wall of SS, and compared with the proximal vein. Also, in a clinical study[31], serial AVF patients were showing development of turbulence only in the SS, while spiral laminar flow developed in the PA and distally in the draining vein. By solving the numerical solution with a very high temporal resolution we could catch the transition from laminar to turbulent flow that develops in the SS, in line with similar findings of other authors[22],[23].

Our study has obvious implications for elucidating the haemodynamic forces involved in the initiation of venous wall thickening in VA. The high frequency shear oscillations on the SS wall, having a low time-averaged WSS, may trigger or enhance venous NH. A similar conclusion was achieved by [17], showing that regions of porcine iliac arteries with increased endothelial permeability experience higher frequency oscillations in shear. While there is considerably evidence in vitro on laminar pulsatile vs. oscillatory shear, demonstrating clearly the atherogenic effect of pure reciprocating flow on the endothelium [26], few data exist in literature on the effect of multidirectional WSS.

Among the limits of the work, the study of only one patient-specific model with no longitudinal data is recognised, recalling the need of further larger studies. We also did not include the compliance of the wall in the AVF model. McGah et al. [24] studied the effects of wall distensibility, finding lower time-averaged WSS compared to the rigid-walled simulation in a side-to-end AVF, but whether this affects also the near-wall disturbed flow should be further investigated. However, the technologies available today allow to optimize anastomotic geometries [29] or to conduct longitudinal patient-specific studies for the follow-up of VA adaptation and local remodeling [5],[6].

In conclusion, in the present study we have studied the local patterns of WSS in a patient-specific side-to-end anastomosis, an AVF setting with high blood flow developed at six weeks post-operatively. We have found that the swing segment of the vein is a conduit subjected to multidirectional hemodynamic shear stress and simultaneously develops reciprocating disturbed flow in some focal points. This combination may boost the initiation of NH after the surgically creation of the AVF, leading to subsequent failure of VA.

## 4.6. Acknowledgments

Part of this study was presented at the 7th World Congress of Biomechanics held in Boston in July 2014. The authors acknowledge their collaborators from the ARCH-Consortium (Project FP7-ICT-2007-2-224390) for patient-data gathering.

# 4.7. References


[1] NKF/KDOQI Vascular Access Work Group. Clinical practice guidelines for vascular access. *Am J Kidney Dis*, 2006; 48 Suppl 1:S176-S247.

[2] Tordoir JHM, Canaud B, Haage P, Konner K, Basci A, Fouque D, Kooman J, Martin-Malo A, Pedrini L, Pizzarelli F, Tattersall J, Vennegoor M, Wanner C, ter Wee P, Vanholder R. EBPG on Vascular Access. *Nephrol Dial Transplant*, 2007;22 Suppl 2:ii88-117.

[3] Allon M, Robbin ML. Increasing arteriovenous fistulas in hemodialysis patients: problems and solutions. *Kidney Int*, 2002; 62(4):1109-24. Review.

[4] Caroli A, Manini S, Antiga L, et al. Validation of a patient-specific hemodynamic computational model for surgical planning of vascular access in hemodialysis patients. *Kidney Int* 2013;84(6):1237-1245.

[5] Sigovan M, Rayz V, Gasper W, et al. Vascular remodeling in autogenous arterio-venous fistulas by MRI and CFD. *Ann Biomed Eng* 2013;41(4):657-668.

[6] He Y, Terry CM, Nguyen C, et al. Serial analysis of lumen geometry and hemodynamics in human arteriovenous fistula for hemodialysis using magnetic resonance imaging and computational fluid dynamics. *J Biomech* 2013;46(1):165-169.

[7] Davies PF. Hemodynamic shear stress and the endothelium in cardiovascular pathophysiology. *Nat Clin Pract Cardiovasc Med* 2009; 6, 16-26.

[8] Ene-Iordache B, Remuzzi A. Disturbed flow in radial-cephalic arteriovenous fistulae for haemodialysis: low and oscillating shear stress locates the sites of stenosis. *Nephrol Dial Transplan*t 2012;27(1):358-368.

[9] Bode A, Caroli A, Huberts W, et al. Clinical study protocol for the ARCH project - computational modeling for improvement of outcome after vascular access creation. *J Vasc Access* 2011;12(4):369-376.

[10] Ene-Iordache B, Mosconi L, Antiga L, et al. Radial artery remodeling in response to shear stress increase within arteriovenous fistula for hemodialysis access. *Endothelium* 2003;10(2):95-102.

[11] Remuzzi A, Ene-Iordache B, Mosconi L, et al. Radial artery wall shear stress evaluation in patients with arteriovenous fistula for hemodialysis access. *Biorheology* 2003;40(1,2,3):423-430.

[12] Bode AS, Planken RN, Merkx MA, et al. Feasibility of non-contrast-enhanced magnetic resonance angiography for imaging upper extremity vasculature prior to vascular access creation. *Eur J Vasc Endovasc Surg* 2012;43(1):88-94.

[13] Antiga L, Piccinelli M, Botti L, et al. An image-based modeling framework for patient-specific computational hemodynamics. *Med Biol Eng Comput* 2008;46(11):1097-1112

[14] The OpenFOAM Foundation. OpenFOAM http://www.openfoam.org/.

[15] Ene-Iordache B, Mosconi L, Remuzzi G, et al. Computational fluid dynamics of a vascular access case for hemodialysis. *J Biomech Eng* 2001;123:284-292.

[16] He X, Ku DN. Pulsatile flow in the human left coronary artery bifurcation: average conditions. *J Biomech Eng* 1996;118:74-82.

[17] Himburg HA, Grzybowski DM, Hazel AL, et al. Spatial comparison between wall shear stress measures and porcine arterial endothelial permeability. *Am J Physiol Heart Circ Physiol* 2004;286(5):H1916-1922.

[18] Peiffer V, Sherwin SJ, Weinberg PD. Computation in the rabbit aorta of a new metric - the transverse wall shear stress - to quantify the multidirectional character of disturbed blood flow. *J Biomech* 2013;46(15):2651-2658.

[19] Paraview. http://www.paraview.org/.

[20] De Santis G, De Beule M, Van Canneyt K, et al. Full-hexahedral structured meshing for image-based computational vascular modeling. *Med Eng Phys* 2011.

[21] De Santis G, Mortier P, De Beule M, et al. Patient-specific computational fluid dynamics: structured mesh generation from coronary angiography. *Med Biol Eng Comput* 2010;48(4):371-380.

[22] Lee SW, Smith DS, Loth F, et al. Importance of flow division on transition to turbulence within an arteriovenous graft. *J Biomech* 2007;40(5):981-992.

[23] McGah PM, Leotta DF, Beach KW, et al. Incomplete restoration of homeostatic shear stress within arteriovenous fistulae. *J Biomech Eng* 2013;135(1):011005.

[24] McGah PM, Leotta DF, Beach KW, et al. Effects of wall distensibility in hemodynamic simulations of an arteriovenous fistula. *Biomech Model Mechanobiol* 2014;13, 679-695.

[25] Remuzzi A and Ene-Iordache B. Novel Paradigms for Dialysis Vascular Access: Upstream Hemodynamics and Vascular Remodeling in Dialysis Access Stenosis. *Clin J Am Soc Nephrol* 2013;8(12):2186-93.

[26] Chiu JJ, Chien S. Effects of disturbed flow on vascular endothelium: pathophysiological basis and clinical perspectives. *Physiol Rev* 2011;91(1):327-387.

[27] Niemann AK, Udesen J, Thrysoe S, et al. Can sites prone to flow induced vascular complications in a-v fistulas be assessed using computational fluid dynamics? *J Biomech* 2010;43, 2002-2009.

[28] Ene-Iordache B, Cattaneo L, Dubini G, et al. Effect of anastomosis angle on the localization of disturbed flow in 'side-to-end' fistulae for haemodialysis access. *Nephrol Dial Transplant* 2013;28(4):997-1005.

[29] Walsh MT, Kavanagh EG, O'Brien T, et al. On the existence of an optimum end-to-side junctional geometry in peripheral bypass surgery--a computer generated study. *Eur J Vasc Endovasc Surg* 2003;26, 649-656.

[30] Jia L, Wang L, Wei F, et al. Effects of wall shear stress in venous neointimal hyperplasia of arteriovenous fistulae. *Nephrology* 2015.

[31] Marie Y, Guy A, Tullett K, et al. Patterns of blood flow as a predictor of maturation of arteriovenous fistula for haemodialysis. *J Vasc Access* 2014;15, 169-174.

# CHAPTER 5

# Flow patterns and wall shear stress distribution in a patient-specific case of *end-to-end* arteriovenous fistula for haemodialysis

This chapter is based on:

Ene-Iordache B, Mosconi L, Remuzzi G, Remuzzi A.

**Computational fluid dynamics of a vascular access case for haemodialysis**

***Journal of Biomechanical Engineering* 123(3): 284-292, 2001**

## 5.1. Abstract

Vascular access (VA) for haemodialysis is provided mostly by surgically creation of a native or synthetic graft arteriovenous fistula in the arm. Maintaining patency of VA continues to be a major problem for patients with end-stage renal disease since in these vessels thrombosis and intimal hyperplasia often occur. These lesions are frequently associated with disturbed flow that develops near bifurcations or sharp curvatures.

We explored the possibility of investigating blood flow dynamics in a patient-specific model of *end-to-end* native AVF using computational fluid dynamics (CFD). Using digital subtraction angiographies of an AVF, we generated a 3-D meshwork for numerical analysis of blood flow. As input condition a time-dependent blood waveform in the radial artery was derived from centerline velocity obtained during echo-color-Doppler ultrasound examination. The finite element solution was calculated using a commercial fluid-dynamic software package.

In the straight, afferent side of the radial artery wall, shear stress ranged between 20 and 36 dynes/cm$^2$, while on the outer surface of the bending zone it increased up to 350 dynes/cm$^2$. On the venous side, proximal to the anastomosis, wall shear stress was oscillating between negative and positive values (from -12 dynes/cm$^2$ to 112 dynes/cm$^2$), while distal from the anastomosis, the wall shear stress returned within the physiologic range, ranging from 8 to 22 dynes/cm$^2$. Areas of the vessel wall with very high shear stress gradients were identified on the bending zone of the radial artery and on the venous side, after the arteriovenous shunt. Secondary blood flows were also observed in these regions.

CFD gave a detailed description of blood flow field and showed that this approach can be used for patient-specific analysis of blood vessels, to better understand the role of local hemodynamic conditions in the development of vascular lesions.

## 5.2. Introduction

A lasting functioning vascular access (VA) is essential for renal function replacement therapy by haemodialysis, but VA complications remain a leading cause of morbidity and hospitalization in these patients [1]. VA for haemodialysis is usually provided by native arteriovenous fistula (AVF) or synthetic grafts to allow adequate blood flow during dialysis session [2]. The most frequent complications of vascular accesses are stenosis and thrombosis, which occur mainly on the venous side of the fistula or synthetic graft [3]. With increasing recognition of the costs and morbidity associated with VA complications, there has been renewed interest in the early detection and treatment of VA failure. Potential risk factors, including sex, vessel size, surgical technique and underlying renal disease are believed to be important for the patency of VA, but no consensus has been achieved yet [1].

In the last decade, several studies have demonstrated that local hemodynamic factors play an important role in arterial remodeling and atherosclerotic disease. This consideration is based on the observation that blood vessels remodel themselves to keep wall shear stress, the tractive force induced by the flow of blood on endothelial cells, within a "physiologic range" [4]. In addition, it is common finding that clinically relevant plaque formation is most frequent in areas of complex flow, near branch points and bifurcations. It has been shown that in these regions vascular lesions localization correlates with low and oscillating wall shear stress [5-7]. Dobrin and coworkers [8] reported that also for autogenous vein grafts, intimal thickening was correlated with low blood velocity and resulting mean low wall shear stress. On the other hand, Fillinger [9] showed that on the venous side of arteriovenous grafts higher blood flow leads to flow disturbances and to intima-media thickening. The influence of wall shear stress on haemodialysis AVF was demonstrated in a study by Girerd et al. [10] who found that the radial artery remodeled in response to the chronic increase in wall shear stress. In this study, changes in the diameter of the radial artery were not a result of hypertrophy of the wall because its cross-section was not increased, thus pointing to a true remodeling of the arterial wall.

In order to investigate in more detail the relation between local blood flow velocities at the vessel wall and the development of arterial wall complications, estimations of the 3-D flow field of the vessel are required, since wall shear stress cannot be measured directly and has to be derived from the velocity profiles. These profiles can be directly measured in vivo using magnetic resonance (MR) or color-flow Doppler ultrasound (CDU), however both methods have limitations for the computation of shear stress from the flow field that develops in AVF.

MR has still low spatial resolution for vessels of this diameter (< 5 mm), as there are few voxels in the vessel cross-section, so that velocity gradients can be greatly affected by experimental error. On the other hand, CDU estimates velocity in spatially limited regions and does not allow to describe the entire flow field.

An alternative for the evaluation of wall shear stress is the use of computational fluid dynamics (CFD) software to simulate flowing fluid in a known geometry. In this study, we firstly set up a technique to derive the 3-D geometry of an AVF using two orthogonal images obtained during digital subtraction angiography (DSA) and then used this geometrical model to simulate blood flow dynamics in the fistula by CFD.

## 5.3. Methods

In a 60-year-old woman on chronic haemodialysis in the Nephrology Unit of the "Ospedali Riuniti di Bergamo", a native AVF was created by an *end-to-end* anastomosis between the radial artery and the cephalic vein, as schematically presented in Figure 5.1.

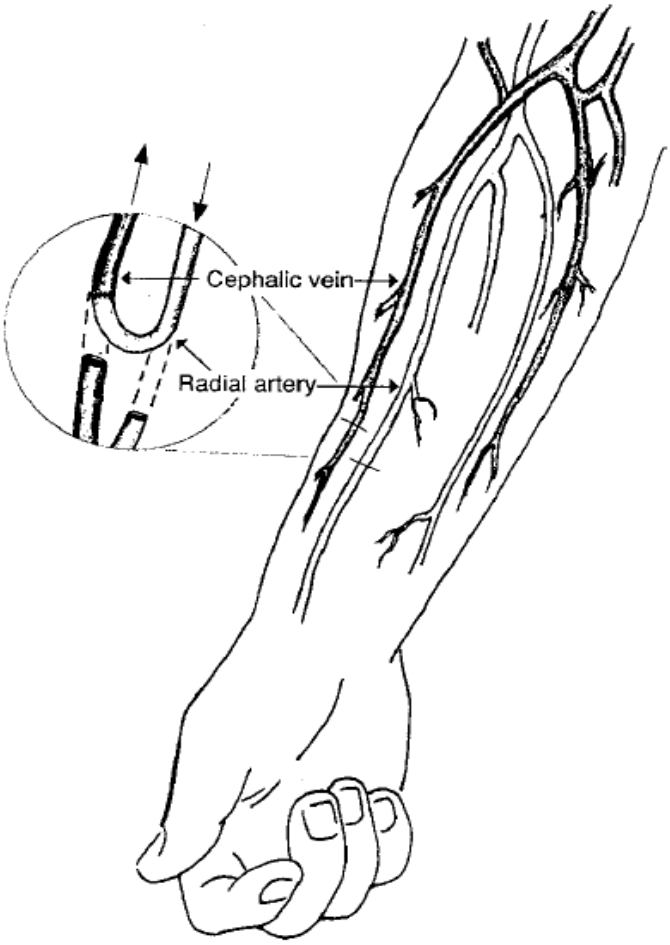


**Figure 5.1. Schematic drawing of the *end-to-end* arteriovenous fistula (AVF) created as a shunt between the radial artery and the cephalic vein.**

To assess the morphology of the AVF, digital subtraction angiography was performed 26 months after the surgery using an Integris C2000® angiograph (Philips, Eindhoven, NL). During image acquisition, the patient's arm was fixed in the center of rotation of the C-arm of the angiograph, and two orthogonal projections were acquired at –45° and +45° relatively to the vertical plane. We also acquired two DSA images of a spatial calibration grid placed on the surface of the intensifier immediately after examining the patient, keeping constant acquisition parameters, in order to correct the angiographic images for non-linear geometric distortion of

the intensifier [11]. The next day, an echo-Doppler examination of the AVF was done (HDI 5000, ATL Ultrasound, Bothell, WA) to measure the centerline blood flow velocity in the radial artery to be used as boundary condition for CFD. A blood collection from the contralateral arm was performed before the echo-Doppler study to determine the hematocrit ($H_t$) and total plasma protein concentration ($C_p$).

### 5.3.1. Three-Dimensional reconstruction of AVF

DSA images of the AVF and of the calibration grid were transferred from the angiograph into the memory of a PC for digital processing (see Figure 5.2).

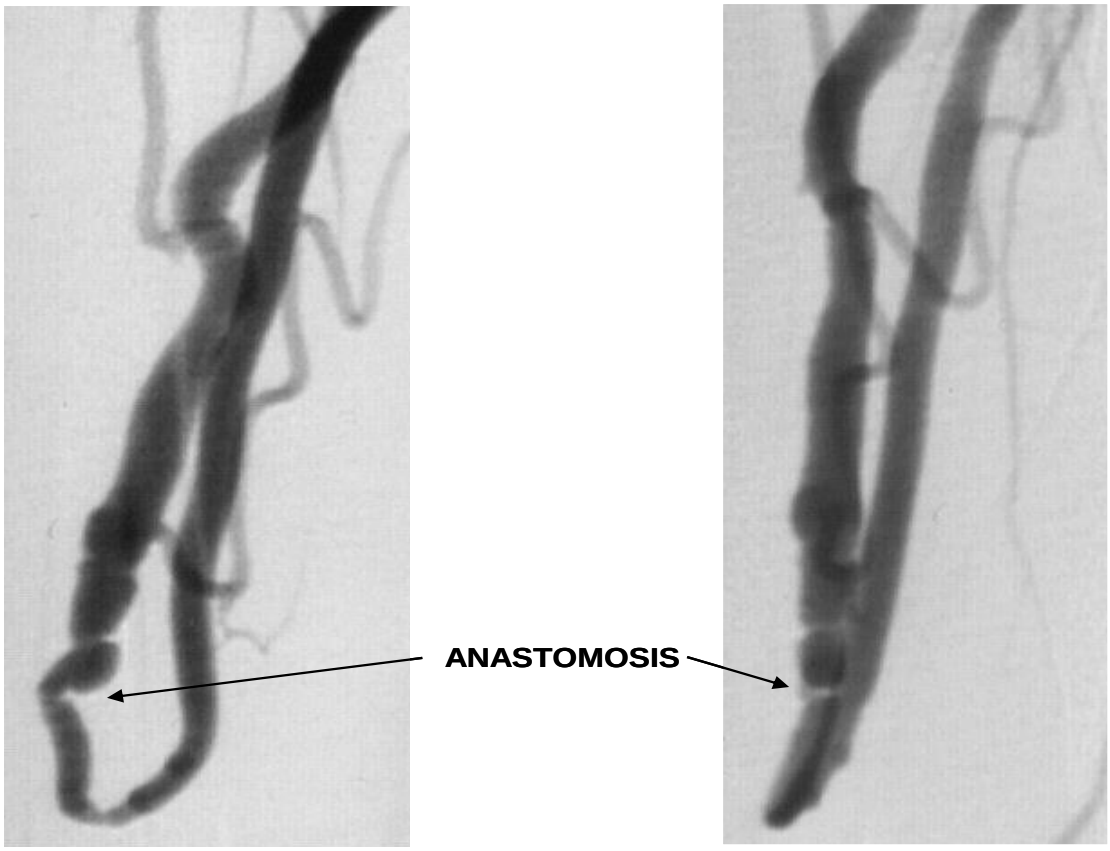


**Figure 5.2. Orthogonal views of DSA images used for the three-dimensional reconstruction of the AVF.**

Non-linear distortion was corrected using a method previously described [11]. This method uses bilinear interpolation of the four edges of each square in the grid to correct spatial distortion, and allows the generation of dimensionally corrected images with known enlargement (pixels/mm). To obtain a 3-D reconstruction of the AVF geometry, we developed a computer program based on the back-projection algorithm of the DSA images, as shown in Figure 5.3.

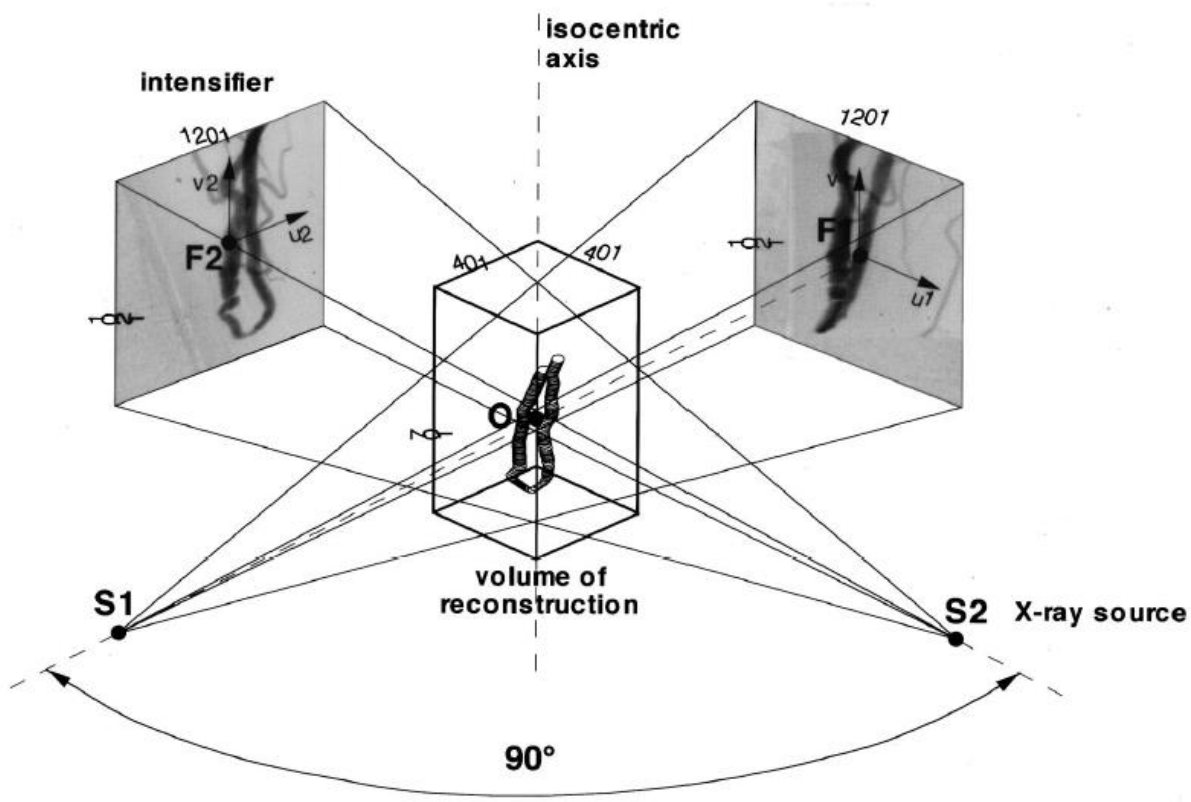


**Figure 5.3. Scheme of the back-projection method. Volume of reconstruction (401 x 401 x 701voxels) is symmetrically displaced around the center of rotation (O) of the C-arm of the angiograph.**

The reconstruction technique consists in calculating the gray intensity of the voxels contained in a defined geometry (later referred as the volume of reconstruction). DSA images (256 gray levels, 1201×1021 pixels) were initially segmented using a general-purpose image processing software (NIH Image, NIH, Bethesda), after manual tracing the vessel boundaries. Four gray levels were used, the lumen of the radial artery was set to 252, the lumen of the cephalic vein to 180, the intersection zone of the two vessels to 196, and the background and other small vessels to 0 (black). A volume of reconstruction of 401×401×701 voxels was assumed to be located around the isocentric axis of the angiograph. We then considered one angiographic image and assigned a gray level to each voxel equal to the gray level of the corresponding pixel in the angiographic image, according to the X-ray projection geometry. To identify pixel coordinates (u and v) in the angiographic image corresponding to a given voxel of the reconstruction volume, we used linear projection on the basis of the known distance between the isocenter (point O in Figure 5.3) and the X-ray source (S) and between the isocenter (O) and the plane of the reference grid (F). Once the gray level of each voxel was assigned using the first image, we repeated the assignment using the second image and considered the mean of the two previous levels as the final gray level of each voxel. The result

of this operation is reported in Figure 5.4, which represents a cross-section plane of the reconstruction volume.

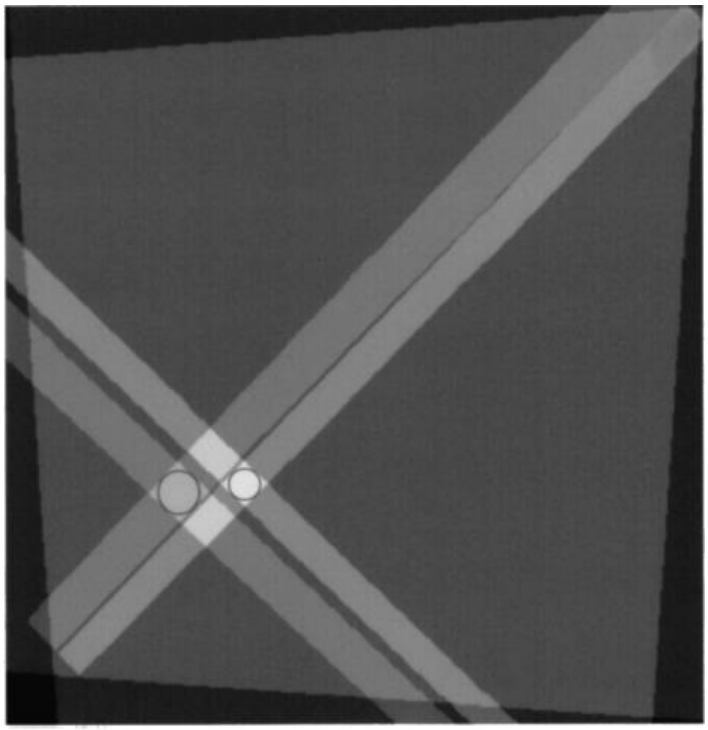

**Figure 5.4. Cross-sectional plane of the volume of reconstruction; ellipses represent the assumed vessel lumen profile.**

A threshold operation was then applied to identify voxels belonging to the 3-D geometry of the vessel. According to the different combinations of gray levels previously defined, different threshold levels were adopted to binarize the voxels contained in the volume of reconstruction (white if belonging to the vessel and black if belonging to the background). The resulting rectangular areas were then used to calculate the ellipses tangent to their boundaries that were assumed to indicate the vessel lumen (see Figure 5.4). The 3-D data set composed of serial cross-sections of the vessel lumen was used to generate a surface model of the AVF. To this purpose we used the VTK 2.0 library [12] and developed a C++ program based on the *marching cubes* algorithm [13], that creates triangles of constant density surfaces from 3-D data. The resulting polygonal structure was imported into GAMBIT (v 1.1, Fluent Inc., Lebanon, NH), a pre-processor program for building mesh models for CFD. A 3-D meshwork of the AVF was then generated for finite element solution of the blood flow problem.

## 5.3.2. Numerical simulation of blood flow

Fluid dynamics of viscous flow in tubes is based on the application of momentum (Navier-Stokes) and mass conservation equations [14]. We solved the Navier-Stokes and continuity equations using the software FIDAP (v 8.5, Fluent Inc., Lebanon, NH), a multipurpose CFD package based on Galerkin's finite element method [15]. The 3-D meshwork (see Figure 5.5) is made up of 8-node isoparametric brick-type elements and it has more than 38,000 nodes.

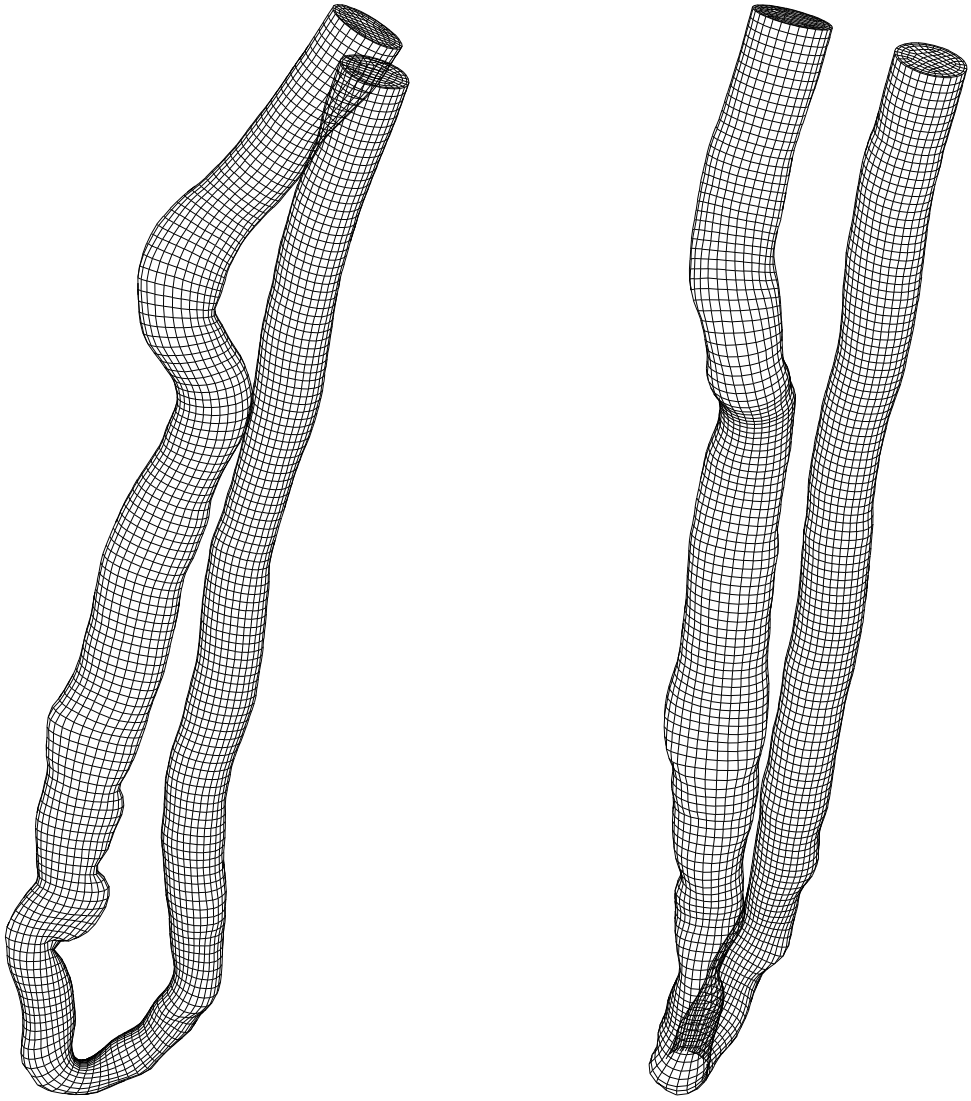

**Figure 5.5. Three-dimensional meshwork used for finite element analysis.**

Within the mesh, a boundary layer was generated near the wall so that the elements on the outer surface of the meshwork are about 1/3 in thickness of the internal elements and their average distance to the wall is 6.5 % of the radius. The size of outer cells is in average 0.18 mm, while the size of the central cells is in average 0.53 mm (18.7% of radius). To verify the

independence of numerical solution from the grid refinement, we performed steady calculations using the peak flow rate within a meshwork made up of more than 120,000 nodes. Using this new grid we calculated that axial velocities in four cross-sections of the AVF (see Figure 5.9 for the location of the four sections) varied, in average less than 3%, in respect to the 38,000 nodes grid. Wall shear stress in the same cross-sections varied in average 8.5% (median 3.7%) between the two meshes. Due to the large number of elements required for flow simulation, we considered that the mesh with 38,000 nodes resulted in acceptable grid independence for both velocity and wall shear stress, considering that the later parameter is very sensitive because it is based on numerical differentiation.

Zones of the AVF where low shear rates might occur, imposed the choice of a shear-thinning constitutive model for the blood. To this purpose we used the Carreau viscosity model that is implemented in FIDAP in the form

$$\mu = \mu_\infty + (\mu_0 - \mu_\infty)\,(1 + K^2 D^2)^{(n-1)/2} \qquad (4.1)$$

where $\mu_\infty$ is the limiting viscosity at infinite shear rate, $\mu_0$ is the limiting viscosity at zero shear rate, K is a constant and D is the second invariant of the strain rate tensor [15]. The value of $\mu_\infty$ was assumed as dependent on hematocrit ($H_t$) and plasma viscosity, as suggested by Quemada [16]. To calculate plasma viscosity we used the formula proposed by Kawai et al. [17] as a function of the plasma protein concentration ($C_p$). With actual blood analysis data (hematocrit $H_t$ = 35.1% and plasma proteins $C_p$ = 7.0 g/dl) the infinite viscosity was $\mu_\infty$ = 0.033 Poise. The other parameters of equation (1) were determined by curve-fitting procedure with the experimental data from Brooks et al. [18], who reported blood viscosity-shear rate relationships for a hematocrit of 35.9%, a value that is close to that measured in our present investigation. The resulting parameters were $\mu_0$ = 0.16, $K$ = 1 and $n$ = 0.4. Blood density was assumed to be $\rho$ = 1.045 g/cm$^3$.

As boundary conditions we imposed zero velocity at the vessel wall (no-slip condition), assumed to be rigid, and we left the velocity components at the outflow free in order to obtain zero stress in normal and tangential directions. At the AVF inflow (afferent side) we imposed time-dependent parabolic velocity profiles. The centerline velocity of these parabolas was derived from CDU investigation at the level of radial artery (Figure 5.6). The velocity spectrum represented in Figure 5.6 was obtained with a probe size comparable to the vessel diameter ($\approx$ 5 mm), and centerline velocity was derived from the maximum velocity as a function of time taking into account the difference in cross-sectional area between inflow and CDU transversal

section. Time-averaged flow rate in the radial artery was 11.9 mL/s (714 mL/min) and pulse frequency was 68 strokes/minute.

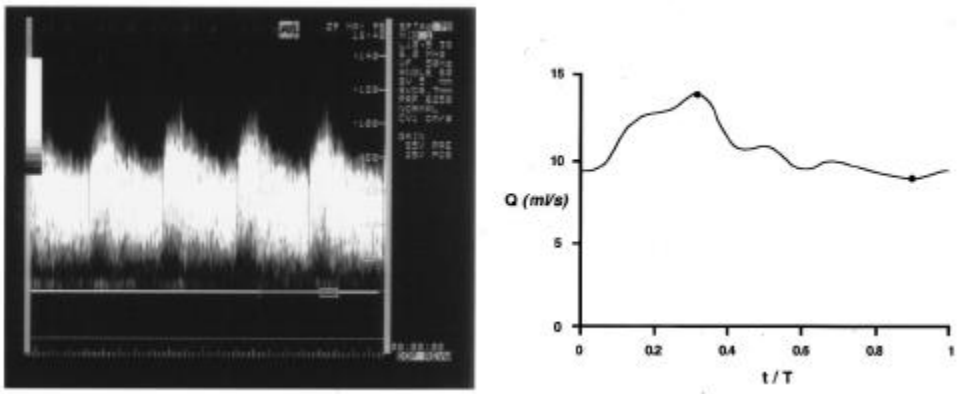


**Figure 5.6. Centerline velocity measured with CDU in the radial artery of the fistula. Pulse frequency was 68 beats/min; radial artery diameter was 5.8 mm; calculated mean flow rate was 11.9 mL/s. Maximum and minimum flow occur at period fraction t/T=0.32 and t/T=0.90.**

In view of the large number of mesh nodes, the numerical procedure was carried out using the segregated solution method, an algorithm that solves each conservation equation (velocity component and pressure) separately and in a sequential manner for each time step. Time integration was executed with the implicit, backward Euler method with 50 fixed time steps for each pulse cycle, and three complete flow cycles were calculated. For flow visualization, we used the post-processing module of the CFD package (FIPOST).

## 5.4. Results

Angiographic images of the AVF and location of the anastomosis are reported in Figure 5.2. The radial artery appears fairly uniform in radius and straight. There is marked narrowing of the vessel diameter in the area where the artery bent. Immediately after the anastomosis the cephalic vein showed an irregular shape, likely the result of vessel remodeling. More distally the cephalic vein had more uniform diameter. The 3-D meshwork generated reproduced in detail the geometry of the AVF (Figure 5.5). This mesh was used to solve the computational problem in order to estimate blood velocity field and derive wall shear stress along the peripheral surface of the vessel. Figure 5.7 shows representative blood velocity vectors calculated in the curvature plane of the fistula at time t/T = 0.32, that corresponds to maximum blood volume flow. Velocity profiles did not show recirculation flows on the arterial (descending) side of the AVF. As expected, velocity increases at the bend, due to restriction of the vessel cross-section. There was an important area of recirculation on the ascending side of the AVF, immediately after the anastomosis (Figure 5.7).

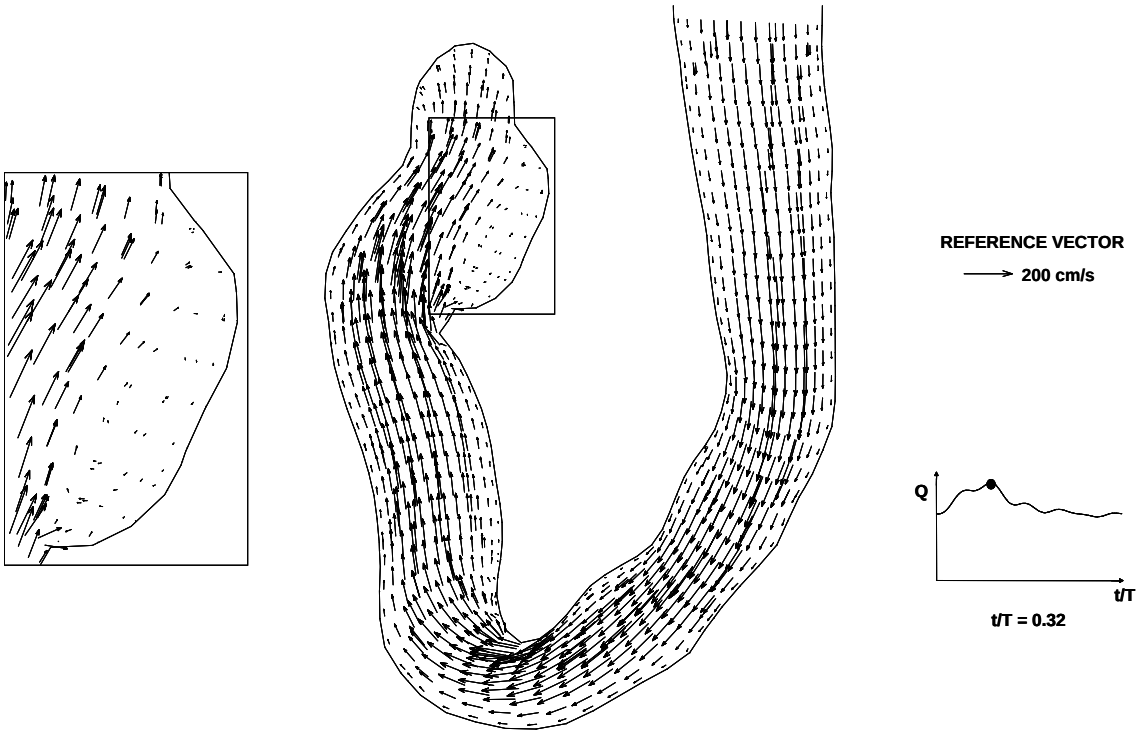


**Figure 5.7. Velocity vector plot at t/T=0.32 (maximum flow rate) in a plane that cuts the bending and anastomosis zones of the AVF.**

Axial velocity vector plots in four longitudinal planes at the level of radial artery (A), bending zone (B), anastomosis zone (C) and cephalic vein (D) are reported in Figure 5.8.

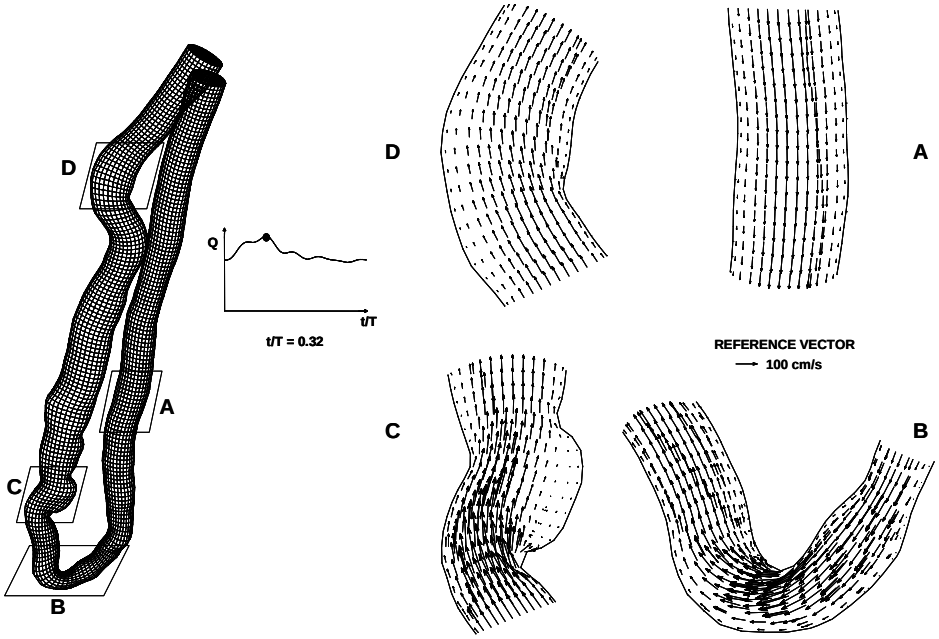


**Figure 5.8. Axial velocity vector plots in four planes that cut the AVF longitudinally at positions A, B, C, and D.**

Radial velocity vector plots at the specified vessel cross-sections, on the arterial (panels A and B) and venous side (panels C and D), at the time fraction t/T=0.32, are reported in Figure 5.9.

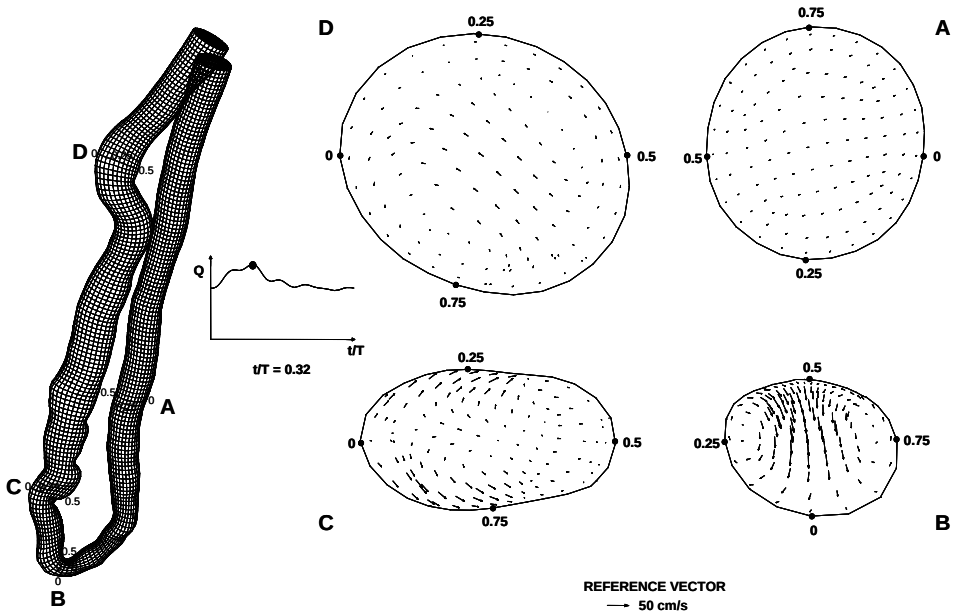


**Figure 5.9. Secondary velocity vector plot at four cross sections (A, B, C, D) of the AVF.**

We calculated Reynolds number in these four cross-sections considering blood as non-Newtonian fluid. To this purpose we used a characteristic shear rate ($\dot{\gamma}_c$), as proposed by Gijsen et al. [19]. For cylindrical tubes, the characteristic shear rate can be approximated as $\dot{\gamma}_c = 8\bar{v}/D$, where $\bar{v}$ is the average velocity and D is the tube diameter. The characteristic viscosity $\mu_c = \mu(\dot{\gamma}_c)$ was calculated using equation (1) and the Reynolds number as $Re = \rho \bar{v} D/\mu_c$. For the above cross-sections (A, B, C and D), mean diameter, $\dot{\gamma}_c$, $\mu_c$ and the resulting Reynolds number at the maximum flow rate (14.7 mL/s) are reported in Table 5.1. These Reynolds numbers are lower than the critical value for straight tubes with steady flow, however, as a result of curvature and diameter changes along the vessel, secondary motions are evident at cross-sections B and C and marginal in D.

**Table 5.1. Geometric and hemodynamic parameters in the four cross-sections of the AVF.**

| Section | Mean diameter | $\dot{\gamma}_c$ | $\mu_c$ | **Re** |
|---|---|---|---|---|
| | *(cm)* | *($s^{-1}$)* | *(Poise)* | |
| **A** | 0.63 | 587 | 0.0358 | 862 |
| **B** | 0.44 | 1,699 | 0.0345 | 1,275 |
| **C** | 0.60 | 692 | 0.0355 | 918 |
| **D** | 0.80 | 294 | 0.0372 | 658 |

Reported values are calculated for the maximum blood volume flow rate (14.7 mL/s). Legend: $\dot{\gamma}_c$, characteristic shear rate; $\mu_c$, characteristic viscosity. See text for detail of calculation and Figure 5.9 for cross-sections location.

The recirculation flow pattern at level C is clearly depicted in Figure 5.10, which presents trajectories of massless particles moving near the inner wall of the cephalic vein immediately after the anastomosis.

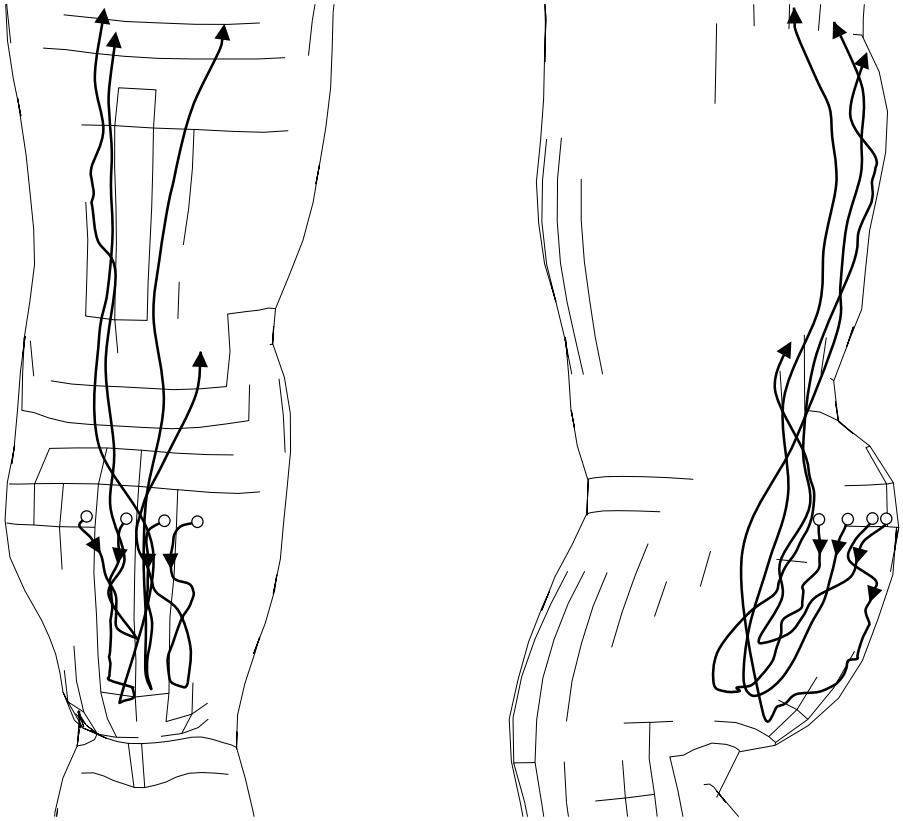

**Figure 5.10. Path plot of virtual massless particles moving near the wall on the ascending side of the fistula immediately after the arteriovenous anastomosis.**

These particles are introduced in the flow domain near the wall and the path motion of the particles is tracked on the basis of the computed flow field. As shown in Figure 5.10, these particles move initially in direction opposite to the main flow and then recirculate following the main blood stream. 3-D profiles of axial velocity in the four sections A, B, C, and D (see Figure 5.9) are represented in Figure 5.11.

At level A, blood flow is fully developed, axial velocity profile is almost parabolic, without secondary flows. At level B, blood acceleration is evident and the flow profile is skewed, characteristic for curved tubes [20]. Non-uniform geometry of the vessel wall near level C leads to secondary flows and recirculation, and the velocity profile shows negative and null values within the section area. At level D secondary flows were absent and axial velocity profile is close to parabolic.

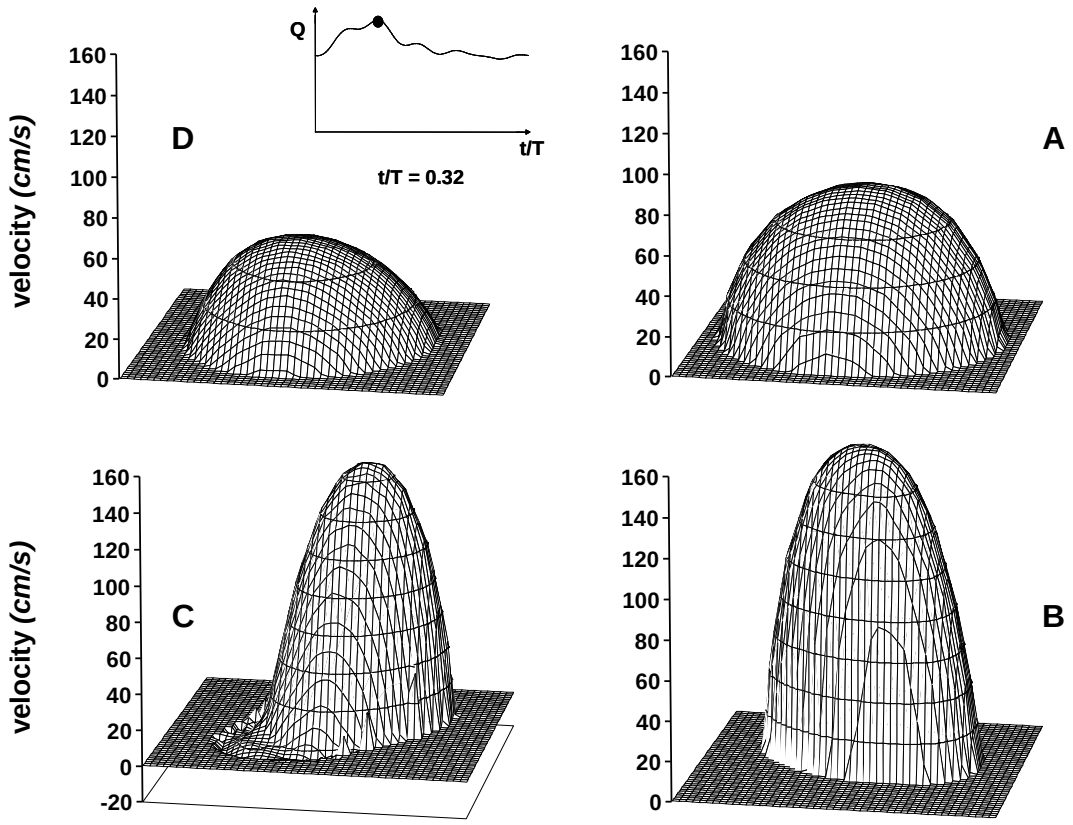


**Figure 5.11. Three-dimensional representation of axial velocity on the arterial side (A, B) near the anastomosis (C) and on the venous side (D) of the AVF at the maximum flow rate. See Figure 5.9 for the position of vessel cross-sections.**

For these four cross-sections, we calculated the magnitude of the wall shear stress along the perimeter corresponding to maximum (t/T=0.32) and minimum (t/T=0.90) blood volume flow rate. The value of wall shear stress was considered positive if the vector was directed in the main flow direction and negative if directed opposite to the main flow. As reported in Figure 5.12, wall shear stress on the radial artery (cross-section A) ranged between 20 and 36 dynes/cm$^2$, values almost within the physiological range [4]. On the contrary, shear stress was importantly elevated above the physiological range along the perimeter of section B ranging from 44 up to more than 350 dynes/cm$^2$, with an average of 194 and 134 dynes/cm$^2$ at t/T = 0.32 and t/T = 0.90, respectively. These values far exceed the physiological range by at least one order of magnitude. Near the anastomosis (C), there were regions of negative (-12 dynes/cm$^2$) as well as positive (116 dynes/cm$^2$) wall shear stress. In about 18% of this perimeter, wall shear stress remaines negative or null throughout the entire cardiac cycle. At location D (cephalic vein) the calculated wall shear stress returned within the physiological range with values ranging from 8 to 22 dynes/cm$^2$.

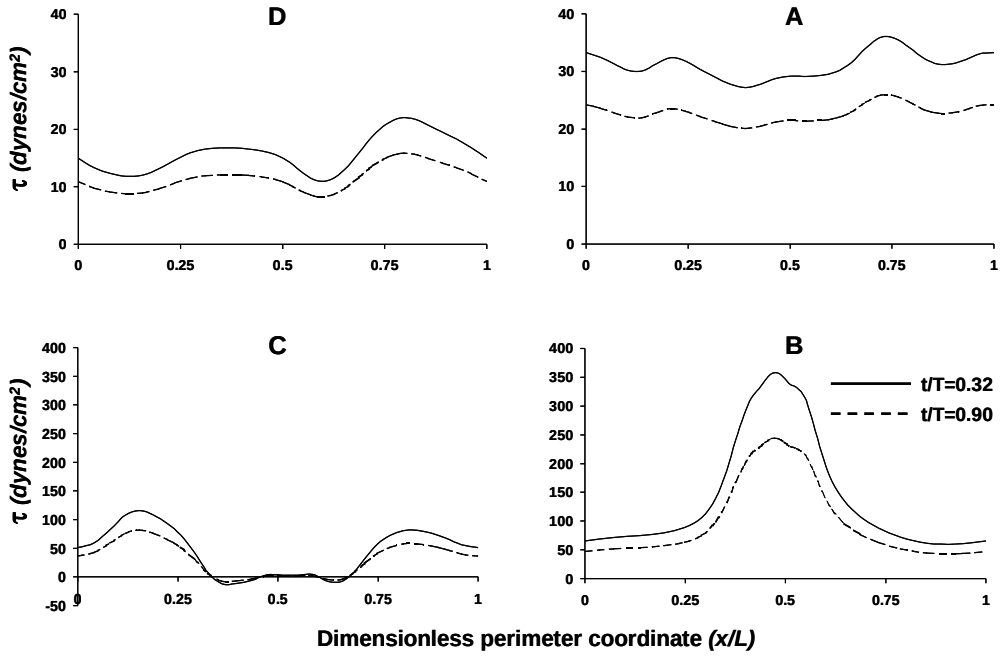


**Figure 5.12 Wall shear stress at the four cross-sections of the AVF; see Figure 5.9 for the position of the four cross-sections and of the dimensionless perimeter.**

At the inner side of the AVF, from section B to section C, the transition from high to low shear stress generates the highest shear stress gradient along the entire AVF surface. We calculated the directional derivative of the axial direction of wall shear stress along the line connecting position 0.5 of section B to position 0.5 of section C. The maximum value of the wall shear stress gradient along this line was 2,570 dynes/cm$^3$, at time fraction t/T = 0.32, corresponding to maximum blood volume flow. We also calculated the oscillatory shear index (OSI) along the perimeter of the four sections previously considered, as proposed by Moore et al. [25]. This index is null if the wall shear stress is entirely positive or entirely negative during cardiac cycle (no fluctuations) and tend to 0.5 if wall shear stress of opposite sign are present during cardiac cycle. OSI was null along the perimeter of cross-sections A, B and D and different than 0 only in two out of 27 points of the profile cross-section C. In these two points (at position 0.46 and 0.54) OSI was equal to 0.03 and to 0.45.

## 5.5. Discussion

The mechanisms involved in failure of AVF for haemodialysis access remain to be elucidated yet. About 5-15% [1] of all surgically created AVF fail before maturation and these "early" failures are generally regarded as technical failures, although hemodynamic parameters may also play a role. Yerdel and coworkers [2] found that the immediate success of a newly constructed AVF mainly depends on preoperative arterial inflow and subclavian venous flow. For early thrombosis, the skill of the surgeon seems to be a crucial factor [7]. Prischl and coworkers [21] also suggested that the surgeon has a significant effect on the patency of AVF. Age and diabetes mellitus are other significant risk factors for late fistula failure.

Hemodynamic conditions have been extensively indicated as playing a major role in vascular remodeling and neointima formation [6]. Flow disturbances and turbulence, which may develop at the venous side of the AVF, have also been documented to influence intimal-medial thickening [9] and endothelial cell turnover [22]. Local blood flow conditions seem to be important also in atherosclerotic plaque formation [24]. It has been documented that when wall shear stress is low and oscillating, and there are zones of shear stress spatial gradients, vessel walls are more prone to vascular damage. AVF involve complex hemodynamic conditions. The first factor influencing blood movement in these vessels is the shunt between arterial and venous circulation that greatly increases blood volume flow rate. Secondly, the non-uniform geometry of the anastomosis forces blood flow to change direction rapidly. As a result, blood flow conditions in these vessels are very different from the physiological state and can cause changes in the vascular wall responsible for vascular remodeling, narrowing or dilatation of the venous side and eventually for vessel occlusion.

To assess how physical forces affect these vessels, one should measure or estimate blood flow velocity and wall shear stress along the 3-D vascular structure. To obtain this result we combined DSA with CFD. The high spatial resolution of DSA enabled us to reconstruct a detailed 3-D geometry of the AVF using two orthogonal projections. Even though it is based on the simplifying assumption that cross-sections of the vessel were elliptical, the reconstructed model reproduced all the detail shown in the angiographic views, and the model allowed generation of the "patient-specific" 3-D meshwork. The technique we developed here can be usefully applied not only to AV fistulas for haemodialysis but for general purpose 3-D geometrical reconstruction of other arterial segments conventionally investigated with DSA. The required digital acquisitions can be obtained during conventional angiographic studies

with only minor changes to routine investigational protocols. Using this technique we have previously reconstructed 3-D geometric models of carotid bifurcation from back-projection of four DSA acquisitions [26]. The generation of 3-D patient-specific vascular models could be used for detailed functional investigation of diseased arterial segments.

Here we used CFD to investigate blood flow distribution in this reconstructed AVF. The dimension of the mesh elements averaged 0.53 mm for central cells and 0.18 mm for outer cells. In some areas (such as cross-section B) the minimum size of near-wall elements was 0.07 mm. The dimension of the these outer elements, that are crucial for shear stress calculations, indicate that this spatial resolution is far better than the best resolution of MR, that ranges between 0.3 and 0.4 mm. For the CFD analysis we considered the blood as a non-Newtonian fluid using the shear-thinning model of Carreau. On the other hand, a limitation of our numerical analysis of blood flow is related to the assumption of rigid walls of the AVF. Moving walls would make the problem a lot more complex and would need estimates on the mechanical properties of the vessel wall that are difficult to obtain. However, consideration of compliant walls in other arterial segments [27] did not result in major differences in the flow field as compared to consideration of rigid walls.

Using CFD analysis we visualized velocity profiles and calculated wall shear stress along the vessel wall. Shear stress in the radial artery was within the physiological range [4] and fairly uniform along the vessel perimeter (see Figure 5.12 - A). As expected, very high wall shear stresses, associated with high shear stress spatial gradients, develop in the bending zone (B), far exceeding the physiological range. Immediately after the anastomosis an irregular geometry of the vein is present, probably due to the mismatch between artery and vein diameters and to differences between the elastic properties of the vascular wall. In this region, rapid changes in cross-section area (level C) induce recirculation flow with positive and negative values of wall shear stress, and high shear stress gradients. More distally, at the level of the cephalic vein (D), the flow disturbances attenuate and wall shear stresses decrease and return within the physiological range, without flow recirculation.

Previous investigations have shown that areas of the circulation characterized by oscillation of wall shear stress tend to develop intima hyperplasia and to favor atherosclerotic disease. To quantify this condition it has been proposed to calculate an oscillatory shear index defined as the fraction of time for which wall shear stress is negative (i.e., in the opposite direction in respect to the main flow) [5]. In our flow simulation study the flow pulsatility was limited, actually peripheral resistances were shunted by the AV anastomosis and the flow rate remained sustained for the entire cardiac cycle. This condition resulted in null OSI along the

entire vessel wall surface. Only in focal points of cross-section C that is located on the venous side of the AVF near the anastomosis, we calculated OSI different than 0, but this was limited to less than 8% of the perimeter. These results would indicate that oscillations in wall shear stress may not be relevant for vascular wall changes in this *end-to-end* AV shunt. Another condition that has been shown to influence endothelial cell function is the presence of elevated spatial shear stress gradients. *In vitro* studies [28], [29] showed that endothelial cell function and growth is already altered for shear stress gradients higher than 800 dynes/cm$^3$. Our CFD analysis enabled us to identify areas of the AVF wall characterized by much more elevated wall shear stress gradients, up to 2,570 dynes/cm$^3$ (at the inner side of the bend towards the AV anastomosis). These high shear stress gradients may alter the functional state of the endothelial layer and probably of the underlying smooth muscle cells.

In the vessel we examined, exposure of the endothelial layer to non-physiological conditions could induce vessel remodeling, especially downstream from the anastomosis, with thickening of intima and media layers, and deposition of circulating cells and molecules on the vessel wall. It has been shown by Fillinger [9] that fluctuations of blood flow at the venous side of the AVF in an animal model are a strong predictor of intimal-medial thickening. These authors have shown that banding AV shunts allowed to reduce the mean Reynolds number from about 1,000 to about 400 and this protected against development of intima-media thickening on the venous side. Our analysis showed that the vessel wall of this AVF is subjected to very high shear stresses, flow recirculation and areas of elevated shear stress gradients, with values of Reynolds number ranging from 658 to 1,275. Thus, these wall shear stress disturbances may be responsible for venous wall dysfunction like remodeling, intima hyperplasia and possible thrombus formation in the long term.

The precise identification of the relations between local hemodynamic alterations and the response of the vascular wall is beyond the scope of this investigation and would need sequential observation. However, our experimental approach appears to be useful for the identification of areas of the vessel wall critically exposed to non-physiological mechanical stress. For instance, at the venous side of the AVF, the recirculation of blood flow indicates an area of possible dilatation of the venous side, remodeling and intimal-medial thickening. This type of information on the local blood flow in AVF could be used to gain a better understanding of pathological conditions that develop in these vessels with time, and to cast more light on ways to ensure more lasting AVF patency. Our approach, together with the latest developments in the field of computer programs for 3-D representation and CFD, will allow functional investigation of diseased arterial segments at the level of individual patients, to predict areas

of flow instability for early detection of vessel wall damage. More in general, this approach could further enhance our understanding of the relation between hemodynamic conditions and development of vascular diseases.

## 5.6. Acknowledgments

We would like to thank Dr. S. Rota and Dr. G. Belloni who helped during clinical investigation and Dr. A. Veneziani and Dr. L. Antiga for help in computer based 3-D reconstruction. We also thank J. Bagott for editorial assistance during preparation of the manuscript.

# 5.7. Annex at Chapter 5

### 5.7.1. Introduction

A short introduction is needed: this new part of the **Chapter** was not covered in the published article, it was specifically requested by a member of the Doctorate Committee. Since the main article is rather outdated, originally published in 2001, the main request was to update the numerical modeling of that VA case to the current *state-of-the-art*.

### 5.7.2. Methods

Numerical methods were updated to the same used in the computational study presented in **Chapter 4,** based on the study published in 2015. Briefly, a new high-resolution CFD simulation for the *end-to-end* vascular access case was performed using *OpenFOAM* v.2.3.1, an open-source CFD based on the finite-volume method [30].

The original hexahedral patient-specific mesh previously used was refined by using *refineMesh*, a mesh utility that is part of the *OpenFOAM* toolbox. Refining the mesh resulted in 274,320 hexahedral cells, having low non-orthogonality and low skewness of, with the volume ranging from $9.9\ 10^{-7}$ to $10.5\ 10^{-5}$ $cm^3$. The 3-D surface of the *end-to-end* AVF model and details of the volume mesh for CFD simulation are presented in Figure 5.13.

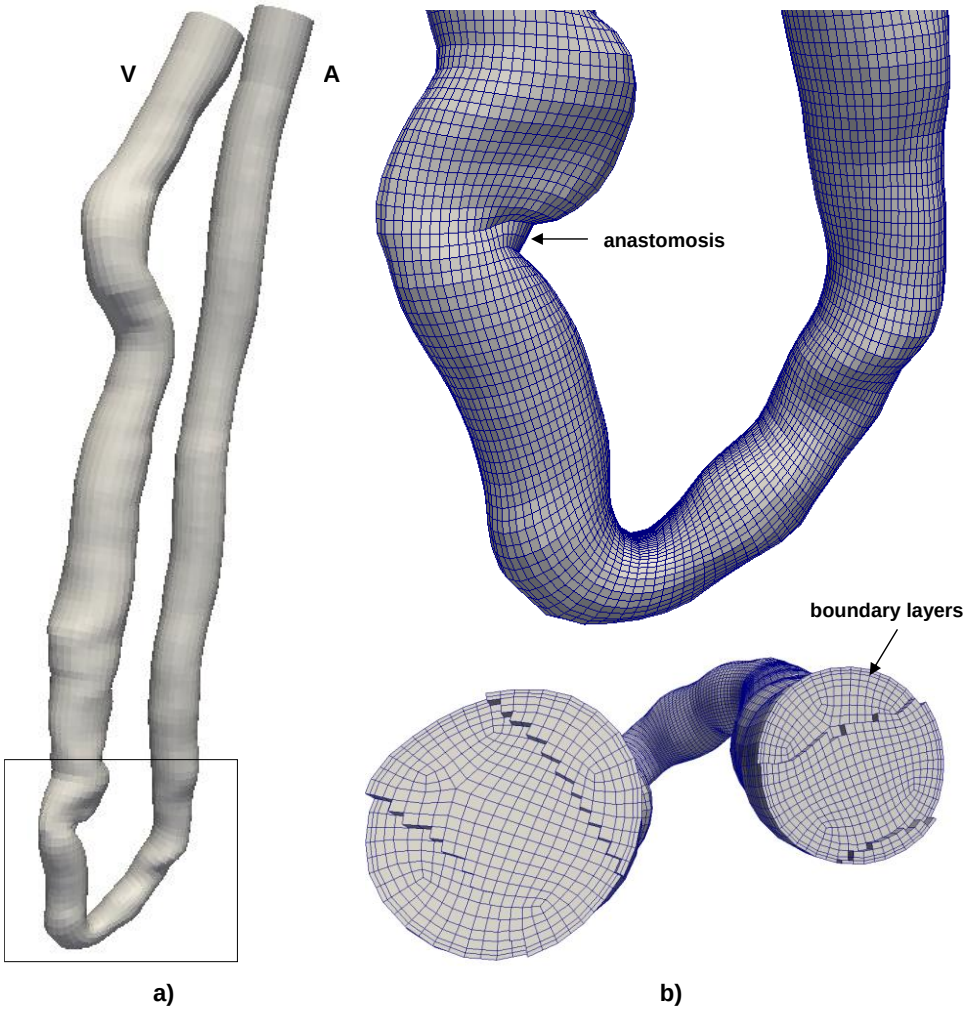


**Figure 5.13. Patient-specific model of the *end-to-end* AVF: a) 3-D surface of the model; b) detail of the surface and volume meshwork showing internal cells and the boundary layers near the wall. Legend: A, (radial) artery; V, (cephalic) vein.**

We considered the non-Newtonian behavior of blood by using of the Bird-Carreau rheological model implemented in *OpenFOAM* with the same parameters used previously (i.e., $\mu_\infty$ = 0.33 Poise, $\mu_0$ = 0.16 Poise, $k$ = 1 s and $n$ = 0.4, based on patient's hematocrit and plasma proteins). Blood density was also assumed as previously $\rho$ = 1.045 g/cm$^3$.

As boundary conditions, we prescribed the blood volumetric flow rate at the inlet artery with the waveforms derived from Figure 5.6. A traction-free (zero stress in the normal and tangential directions) condition was applied at the vein outlet and no-slip condition was applied at the walls, which were considered rigid. For the pulsatile simulation, we used *pimpleFoam*, a transient solver for incompressible flows and first order Euler time integration scheme. This solver adjusts automatically the time step based on a user-defined maximum Courant–Friedrichs–Lewy (CFL) number. We used CFL = 1, which for this specific case resulted in 10,814 variable time steps for a cycle, corresponding to a mean temporal resolution of 0.092

ms (range 0.050 to 0.143), and then saved the results for post-processing in 1,000 equal time steps for each cycle. Three complete cardiac cycles were solved in order to damp the initial transients of the fluid and only the results of the third cycle were considered for data processing.

In the post-processing phase, we characterized the CFD-predicted flow and the related near-wall disturbed flow. In particular, reciprocating disturbed flow was localized using oscillatory shear index (OSI) [31] and multidirectional disturbed flow by means of the transversal WSS (transWSS) metric [32].

### 5.7.3. Results

Representative 3-D velocity profiles in the artery, the artery curvature, immediate after the anastomosis and more distally on the vein, corresponding to peak-systolic and end-diastole time-points are shown in Figure 5.14.

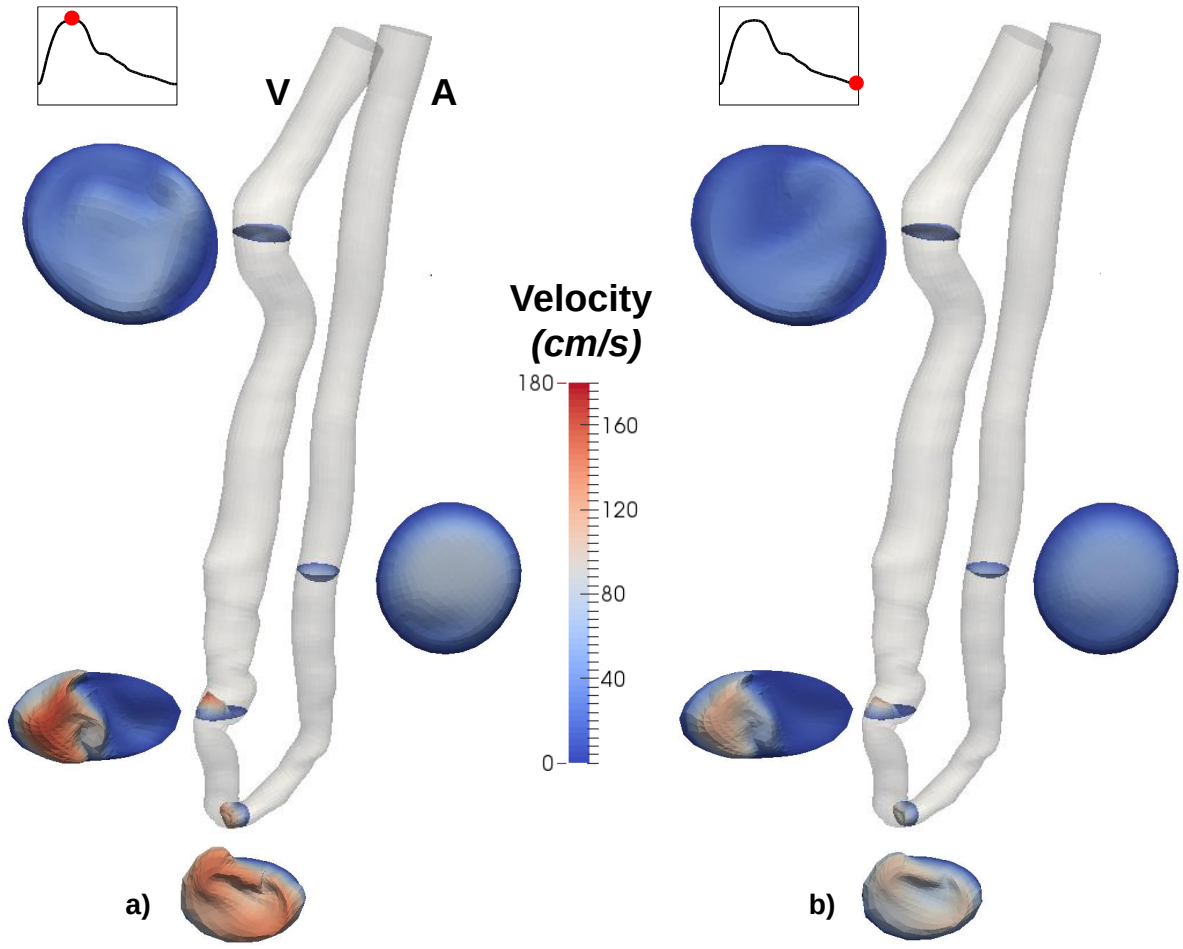


**Figure 5.14. Three-dimensional representation of the velocity profiles on the arterial side, near the anastomosis and on the venous side of the AVF, corresponding to peak-systolic and end-diastole time-points. Legend: A, artery; V, vein.**

The velocity profile in the artery has a parabolic shape, representative for laminar flow. At contrary, the velocity profiles in the bending zone and in the vein have complex shapes, with ridges skewed towards the wall. These profiles reveal development of vortexes and important secondary flows at peak-systole, which are damped more distally on the vein or in the diastolic phase of the cardiac cycle (see cross-section images in Figure 5.14). To better characterize the CFD-predicted flow phenotype, we represented in Figure 5.15 a volume rendering of the velocity magnitude, corresponding to peak-systolic and end-diastole time-points.

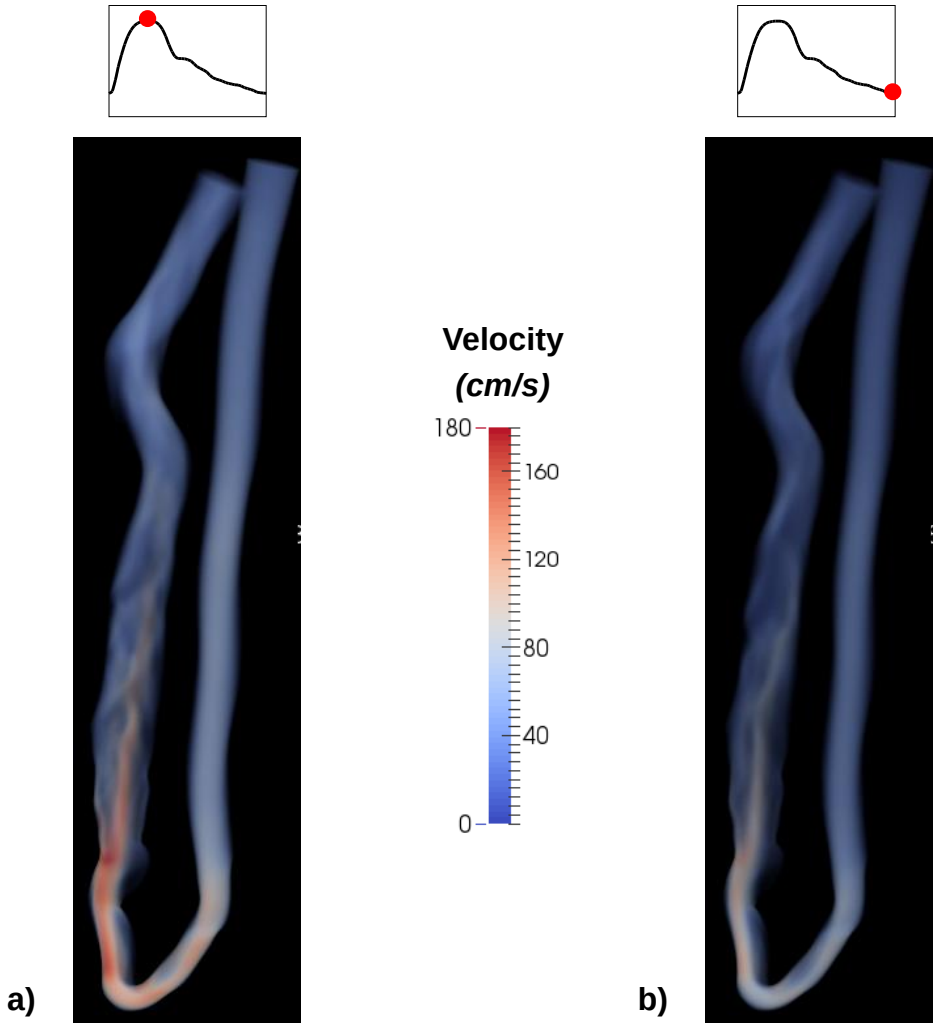


**Figure 5.15. Volume rendering of blood velocity magnitude inside the *end-to-end* AVF, corresponding to peak-systolic and end-diastole time-points.**

As shown well in Figure 5.15, transitional laminar-to-turbulent flow starts to develop on the venous side of the AVF, immediately after the anastomosis. The transitional flow is more pronounced at systolic peak, but is still evident during the diastole.

The WSS distribution on the AVF at peak-systole and end-diastole are presented in Figure 5.16.

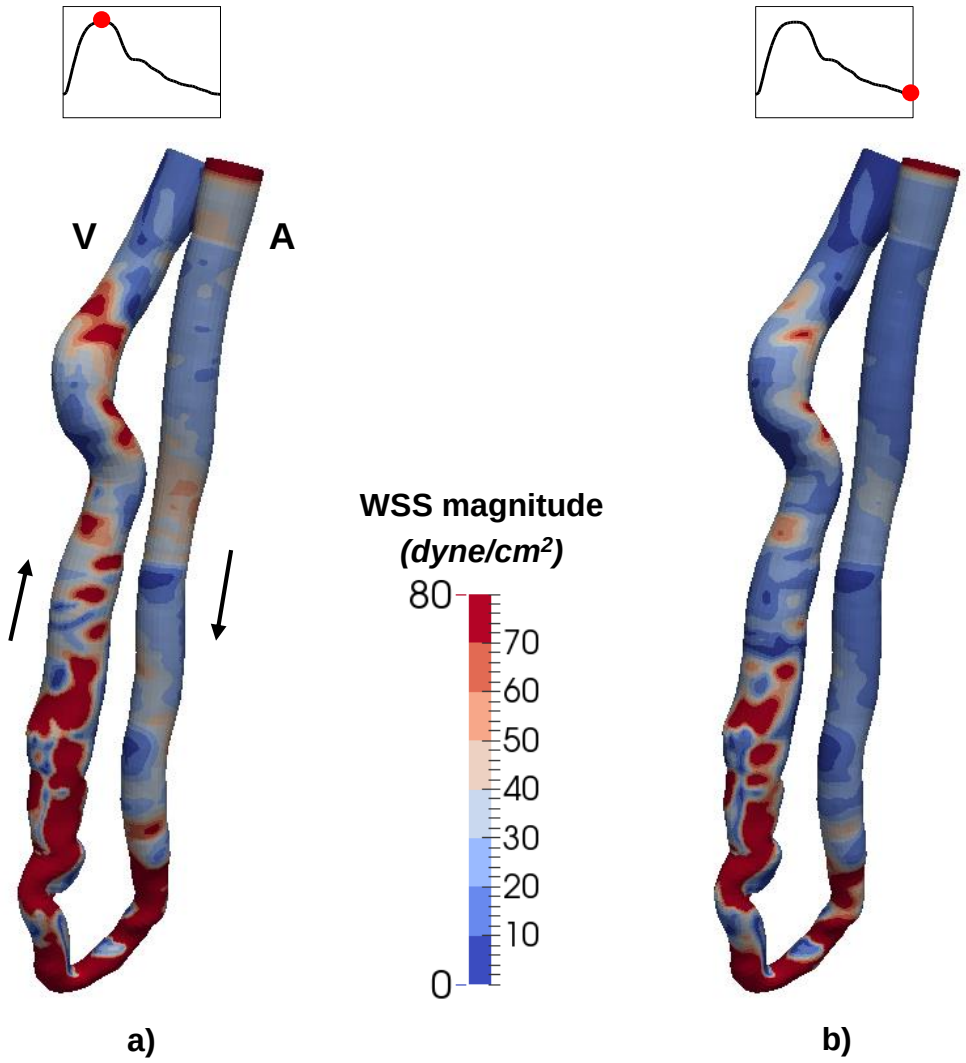


**Figure 5.16. Wall shear stress patterns on the *end-to-end* AVF walls, corresponding to peak-systolic (a) and end-diastole (b) time-points. Legend: A, artery, V, vein; arrows indicate direction of blood flow.**

A big portion of the AVF surface, especially on the bending zone and on the outer wall of the vein is subjected to very high WSS (in red color, > 70 dyne/cm$^2$). However, areas of low WSS are along the artery, and also localized on the vein. In particular, even if the blood flow rate is at its maximum, low WSS areas are still located in focal sites on the vein (see Figure 5.16a).

CFD-predicted near-wall disturbed flow patterns on the AVF walls are presented in Figure 5.17.

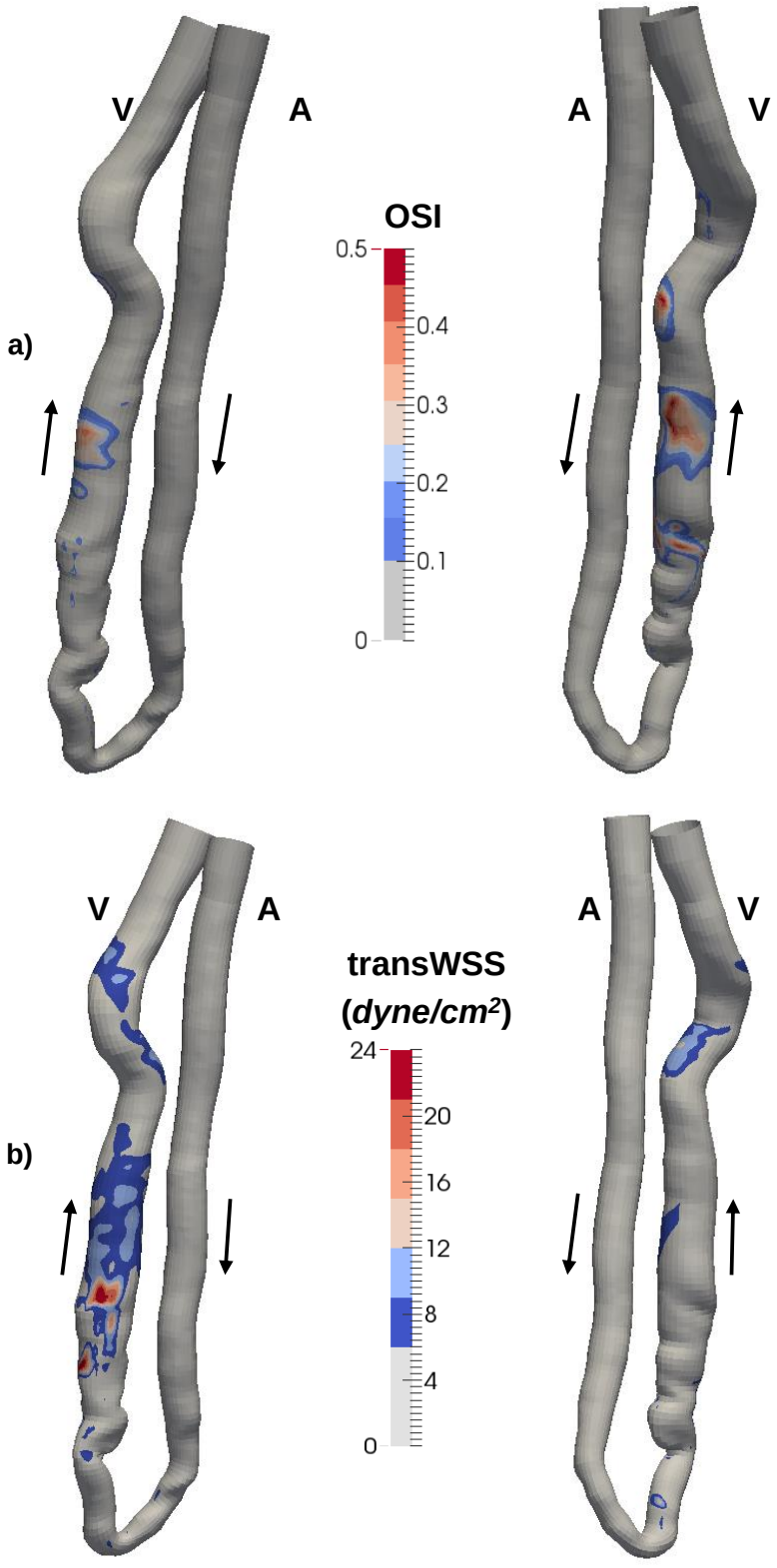


**Figure 5.17. Disturbed flow patterns on the *end-to-end* AVF walls: OSI (a) and transWSS (b). Values of OSI between 0 and 0.1 and of transWSS below 6 dyne/cm$^2$ were represented in light grey to emphasize the patterns of disturbed flow. Legend: A, artery, V, vein; OSI, oscillatory shear stress; transWSS, transversal WSS. Arrows indicate direction of blood flow. Left, front-view; right, rear-view.**

Reciprocating shear disturbed flow zones, revealed by high OSI, as reported in Figure 5.17a, are located either on the inner or the outer wall of the vein, after the anastomosis. Multidirectional flow, as characterized by medium-to-high (> 10 dyne/cm$^2$) transWSS in Figure 5.17b is located on the inner and outer venous wall, and in a lesser extent, more distally after the vein curvature. Such patterns of transWSS indicate that the shear vectors change direction throughout the cardiac cycle, while they remain approximately parallel to the main direction of flow on the arterial wall.

### 5.7.4. Discussion

We characterized the flow filed by high resolution CFD in this patient-specific case of *end-to-end* AVF. Our CFD-predicted flow (Figures 5.14 and 5.15) show transition from laminar to turbulence after the anastomosis, that vanishes gradually more distally in the vein. By solving the numerical solution with a high temporal resolution, we could catch the transition from laminar to turbulent flow that develops in the venous side, in line with similar findings of other authors [33],[34].

It is obvious that flow instabilities representative of transitional flow, are related to high frequency oscillations in the velocity field present in the venous side and that oscillations of the velocity vectors in the vein result in disturbed near-wall flow. By using OSI surface maps, we identified the presence of reciprocating disturbed flow areas either on the inner or the outer wall of the vein, with a wider area on the inner wall, in line with our previous findings in AVF idealized models presented in **Chapter 2**. Our study revealed also the multi-directionality of WSS on the venous wall, which corroborated our finding in a patient-specific *side-to-end* RC AVF model presented in **Chapter 4**.

Actual *state-of-the-art* high-resolution CFD applied to this patient-specific *end-to-end* VA case revealed development of transitional flow in the venous side, not found in the original manuscript of 2001, most probably due to inadequate numerical modeling.

In conclusion, we have found that the venous limb is subjected to multidirectional hemodynamic shear stress and simultaneously develops reciprocating disturbed flow in some focal points. This may have implications in the understanding of the mechanisms responsible for the initiation of neointimal hyperplasia in the vascular access.

## 5.8. References


[1] Feldman, H.I., Kobrin, S. and Wasserstein, A., 1996, "Haemodialysis Vascular Access Morbidity", *Journal of the American Society of Nephrology*, Vol. 7, pp. 523-535.

[2] Yerdel, M.A., Kesenci, M., Yazicioglu, K.M., Döseyen, Z., Türkcapar, A.G. and Anadol, E., 1997, "Effect of Haemodynamic Variables on Surgically Created Arteriovenous Fistula Flow", *Nephrology Dialysis Transplantation*, Vol. 12, pp. 1684-1688.

[3] Kanterman, R.Y., Vesely, T.M., Pilgram, T.K., Guy, B.W., Windus, D.W. and Picus, D., 1995, "Dialysis Access Grafts: Anatomic Location of Venous Stenosis and Results of Angioplasty", *Radiology*, Vol. 195, pp. 135-139.

[4] Giddens, D.P., Zarins, C.K. and Glagov, S., 1993, "The Role of Fluid Mechanics in The Localization and Detection of Atherosclerosis", *Journal of Biomechanical Engineering*, Vol. 115, pp. 588-594.

[5] Ku, D.N., Giddens, D.P., Zarins, C.K. and Glagov, S., 1985, "Pulsatile Flow and Atherosclerosis in the Human Carotid Bifurcation", *Arteriosclerosis*, Vol. 5 (3), pp. 293-302.

[6] Salam, T.A., Lumsden, A.B., Suggs, W.D. and Ku, D.N., 1996, "Low Shear Stress Promotes Intimal Hyperplasia Thickening", *Journal of Vascular Investigation*, Vol. 2(1), pp. 12-22.

[7] Hehrlein, C., 1995, "How do AV Fistulae Lose Function? The Role of Haemodynamics, Vascular Remodeling, and Intimal Hyperplasia", *Nephrology Dialysis Transplantation*, Vol. pp. 1287-1290.

[8] Dobrin, P.B., Littooy, F.N. and Endean, E.D., 1989, "Mechanical Factors Predisposing to Intimal Hyperplasia and Medial Thickening in Autogenous Vein Grafts", *Surgery*, Vol. 105, pp. 393-400.

[9] Fillinger, M.F., Reinitz, E.R., Schwartz, R.A., Resetarits, D.E., Paskanik, A.M. and Bredenberg, C. E., 1989, "Beneficial Effects of Banding on Venous Intimal-Medial Hyperplasia in Arteriovenous Loop Grafts", *The American Journal of Surgery*, Vol. 158(2), pp. 87-94.

[10] Girerd, X., London, G., Boutouyrie, P., Mourad, J.J., Safar, M. and Laurent, S., 1996, "Remodeling of the Radial Artery in Response to a Chronic Increase in Shear Stress", *Hypertension*, Vol. 27(3), pp. 799-803.

[11] Vitali, A., Salmoiraghi, P., Butti, I., Pompei, L., Sarti, E., Caverni, L., Petroboni, E., Merli, R. and Remuzzi, A., 2000, " Localization of Cerebral Arterovenous Malformations Using Digital Angiography ", *Medical Physics*, Vol. 27(9), pp. 2024-2030.

[12] Schroeder, W., Martin, K. and Lorensen, B., 1998, *The Visualization Toolkit: An Object-Oriented Approach to 3D Graphics*, 2nd Ed, Prentice Hall, New Jersey.

[13] Lorensen, E. and Cline, H.E., 1987, "Marching Cubes: A High Resolution 3D Surface Construction Algorithm", *Computer Graphics*, Vol. 21 (4), pp. 163-169.

[14] Deen, W.M., 1998, *Analysis of Transport Phenomena*, Oxford University Press, New York.

[15] FIDAP User's manual, 1998, *FIDAP 8*, Fluent Incorporated, 10 Cavendish Court, Lebanon, NH.

[16] Skalak, R. and Chien, S., 1987, "The Rheology and Tube Flow of Blood", in *Handbook of Bioengineering*, McGraw-Hill.

[17] Kawai, H., Fukada, E., Ibe, T. and Shono, H., 1965, "A New Capillary Viscometer for Measuring the Viscosity of Small Amounts of Blood", in *Proceedings, Fourth International Congress on Rheology*, A. L. Copley, ed., Interscience, New York, pp. 281-297.

[18] Brooks, D.E., Goodwin, J.W. and Seaman, G.V.F., 1970, "Interactions among Erythrocytes under Shear" *J Appl Physiol*, Vol. 28, pp. 172-177.

[19] Gijsen, F.J.H., Brands, P.J., van de Vosse, F.N. and Janssen, J.D., 1998, "Assessment of Wall Shear Rate Measurements with Ultrasound", *Journal of Vascular Investigation*, Vol. 4, pp. 187-196

[20] Caro, C.G., Parker, K.H. and Doorly, D.J., 1995, "Essentials of Blood Flow", *Perfusion*, Vol. 10(3), pp. 131-134.

[21] Prischl, F.C., Kirchgatterer, A., Brandstätter, E., Wallner, M., Baldinger, C., Roithinger, F.X. and Kramar, R., 1995, "Parameters of Prognostic Relevance to the Patency of Vascular Access in Haemodialysis Patients", *J Am Soc Nephrol*, Vol. 6, pp. 1613-1618.

[22] Davies, P.F., Remuzzi, A., Gordon, E.J., Dewey, C.F.Jr., and Gimbrone, M.A.Jr., 1986, "Turbulent Fluid Shear Stress Induces Vascular Endothelial Cell Turnover in Vitro", *Proc. Natl. Acad. Sci.*, Vol. 83, pp.2114-2117.

[23] Friedman, M.H., Deters, O.J., Bargeron, C.B., Hutchins, G.M. and Mark, F.F., 1986, "Shear-Dependent Thickening of the Human Arterial Intima", *Atherosclerosis*, Vol. 60, pp. 161-171.

[24] Nerem, R.M., 1991, "Vascular Fluid Mechanics, the Arterial Wall, and Atherosclerosis", *Journal of Biomechanical Engineering*, Vol. 114, pp. 274-282.

[25] Moore Jr., J.E., Xu, C., Glagov, S., Zarins, C.K. and Ku, D.N., 1994, "Fluid Wall Shear Stress Measurements in a Model of the Human Abdominal Aorta: Oscillatory Behavior and Relationship to Atherosclerosis", *Atherosclerosis*, Vol. 110, pp. 225-240.

[26] Remuzzi, A., Ene-Iordache, B., Veneziani, A., Pata, R., Caverni. L. and Belloni, G., 1996, "Three-dimensional Geometrical Models of Carotid Bifurcation from Digital Angiography", *Books of Abstracts*, Sloten, J.V., Lowet G., Van Audekercke, R. and Van der Perre, G. Eds., 10th Conference of the European Society of Biomechanics, Leuven, August 28-31, 1996.

[27] Perktold, K. and Rappitsch, G., 1995, "Computer Simulation of Local Blood Flow and Vessel Mechanics in a Compliant Carotid Artery Bifurcation Model", *J Biomech*, Vol. 28(7), pp. 845-856.

[28] DePaola, N., Gimbrone Jr., M.A., Davies, P.F. and Dewey Jr., C.F., 1992, "Vascular Endothelium Responds to Fluid Shear Stress Gradients", *Arteriosclerosis and Thrombosis*, Vol. 12(11), pp. 1254-1257.

[29] DePaola, N., Davies, P.F., Pritchard,W.F., Florez, L., Harbeck, N., and Polacek, D.C., 1999, "Spatial and Temporal Regulation of Gap Junction Connexin43 in Vascular Endothelial Cells Exposed to Controlled Disturbed Flows In Vitro", *Proc Natl Acad Sci*, Vol. 96, pp.3154-3159.

[30] OpenFOAM Foundation. OpenFOAM http://www.openfoam.org/

[31] He X and Ku DN. Pulsatile flow in the human left coronary artery bifurcation: average conditions. *J Biomech Eng* 1996;118:74-82.

[32] Peiffer V, Sherwin SJ, Weinberg PD. Computation in the rabbit aorta of a new metric - the transverse wall shear stress - to quantify the multidirectional character of disturbed blood flow. *J Biomech* 2013;46(15):2651-8.

[33] McGah PM, Leotta DF, Beach KW, Eugene Zierler R, Aliseda A. Incomplete restoration of homeostatic shear stress within arteriovenous fistulae. *J Biomech Eng* 2013;135(1):011005.

[34] Lee SW, Smith DS, Loth F, Fischer PF, Bassiouny HS. Importance of flow division on transition to turbulence within an arteriovenous graft. *J Biomech* 2007;40(5):981-92.

# CHAPTER 6

# Adaptation of the radial artery after the creation of *end-to-end* AVF for haemodialysis

This chapter is based on:

Ene-Iordache B, Mosconi L, Antiga L, Bruno S, Anghileri A, Remuzzi G, Remuzzi A.

**Radial artery remodeling in response to shear stress increase within arteriovenous fistula for haemodialysis access**

***Endothelium* 10(2): 95-102, 2003**

## 6.1. Abstract

It is known that changes in blood volume flow induce vascular remodeling and that shear stress, the tractive force acting on the vessel wall due to blood flowing, influences endothelial cells function. The aim of the present study was to investigate the relation between changes in pulsatile shear forces and arterial remodeling in response to chronic elevation in blood volume flow within the radial artery. We studied vessel diameter, flow rate and shear stress in the radial artery of uremic patients before and after surgical creation of a native arteriovenous fistula for haemodialysis access. For this purpose, we used echo-color-Doppler ultrasound to perform diameter and blood velocity measurements. Time-function blood volume flow rate and wall shear stress were calculated based on arterial diameter, center-line velocity wave-form and blood viscosity, using a numerical method developed according to Womersley's theory for unsteady flow in tubes.

Our results confirmed that the radial artery diameter increases in response to a chronic increase in blood volume flow. Moreover, it seems that the arteries dilate in such a way as to maintain the peak wall shear stress constant, indicating that endothelial cells sense the maximum rather than the mean wall shear stress. This finding may lead to further understanding of the mechanisms responsible for endothelial response to physical stimulation by flowing blood.

## 6.2. Introduction

Evidences that lesions occur at specific sites in the arterial tree, like branches and bifurcations, have led to the idea of an important role of local blood flow conditions in the onset and progression of arterial wall disorders. In human pathological conditions there is now consensus about the role of shear stress, the drag force exerted by flowing blood on the vascular wall, as a pathogenic factor for atherosclerosis [1], [2], [3]. The location of arterial lesions at the carotid bifurcation [1] and in the abdominal aorta [4] correlates with regions where wall shear stress (WSS) is low and oscillating. It is not clear yet how local hemodynamic conditions influence intimal hyperplasia, the major cause of failure for bypass grafts and restenosis post-endarterectomy and angioplasty [5]. High WSS inhibits, and low WSS favors the development of intimal hyperplasia. Intimal thickness is predominant in areas of low WSS, like the anastomotic floor and toe, suggesting once again a decisive role of blood flow conditions in vessel wall injury.

Systemic arteries adapt their lumen to changes in blood volume flow rate, and reduce or dilate, respectively, when the flow decreases or increases. It has been proposed that changes in arterial diameter keep WSS within a narrow, so-called "physiological" range [6]. The mechanism of arterial enlargement or narrowing seems to be regulated by the endothelial cells that have been identified as transducers of wall shear stress by many in vitro studies [7], [8]. Similarly, in vivo studies in animals [9], [10], [11] have shown that the vascular adaptive response to changes in blood volume flow tend to maintain a constant WSS. Despite difficulties in experimental setting and measurements, in the last few years many studies have investigated the influence of WSS on arterial regulation in humans, most of them in superficial arteries like the brachial [12], radial or carotid arteries [13], [14]. Kubis et al [15] used ultrasound (US) technique to study adaptive changes of the common carotid arteries in patients with internal carotid occlusion. They found the diameter of the common carotid on the occluded side was smaller than the contralateral vessel. This is believed to be the arterial wall's response to a chronic decrease in blood volume flow, so as to keep WSS within the "physiological" range.

In many reports [1], [2] the shear stress acting on endothelial cells is considered normal when it is between 10 and 20 dyn/cm$^2$. These values are usually time-averaged shear stress acting on the luminal side of the arterial wall. However, in large and medium size arteries WSS changes markedly during the cardiac cycle, from peak values higher than 30 dyn/cm2 to null

during diastole. Thus, it is not known whether vascular adaptation of WSS is related to conservation of mean, maximum or minimum values over cycle period.

To study the arterial wall's dynamic response to changes in blood volume flow, the arteriovenous shunt represents a suitable in vivo experimental condition [11]. In patients with end-stage renal disease (ESRD) an arteriovenous fistula (AVF) is usually created between native vessels to provide vascular access (VA) for haemodialysis. Radiocephalic fistulas cause sudden increases in blood volume flow, and changes the waveform of blood velocity, thus representing an interesting condition of time-related changes in WSS. In a previous work Girerd et al. [16] studied the radial artery diameter adaptation to the increase in blood volume flow due to AVF. It has been shown that in the radial artery of patients with a distal AVF for haemodialysis, the lumen diameter increased to maintain almost constant mean WSS, as compared to the mean WSS estimated in the contralateral radial artery. Despite precise measurements of arterial diameter, this study only estimated mean WSS considering steady flow and constant (Newtonian) viscosity of blood. Since blood volume flow rate in radial artery with or without AVF is markedly pulsatile and blood is a non-Newtonian fluid, we designed the present study to investigate more in detail the relation between dynamic changes in pulsatile WSS and changes in arterial diameter in response to chronic elevation of blood volume flow within the radial artery. We estimated vessel diameter, blood volume flow rate and WSS in the radial artery of uremic patients before and after surgical creation of a radiocephalic AVF for haemodialysis access. We used echo-color-Doppler ultrasound (US) to obtain diameter and blood velocity measurements in the radial artery, and then used a mathematical model [17] to calculate pulsatile blood volume flow and WSS in the radial artery proximal to the AVF. Non-Newtonian blood viscosity was also considered in the model. These measurements allow to shed more light on the mechanisms involved in endothelial-mediated remodeling of the arterial wall.

# 6.3. Methods

## 6.3.1. Patient Population

We recruited 43 consecutive ESRD patients (29 males, 14 females, aged 21-77 years), referred to start haemodialysis treatment in the Nephrology and Dialysis Unit at the Ospedali Riuniti di Bergamo. The study was approved by the Ethical Committee of the Clinical Research Center for Rare Diseases Aldo e Cele Daccò and all patients were enrolled after signed informed consent.

A primary native fistula was created at the wrist by end-to-end anastomosis of the radial artery to the adjacent cephalic vein [18]. The study involved four visits, scheduled one day before surgery, then 10, 40 and 100 days after. At each visit a blood sample was taken from the contralateral arm to determine hematocrit (Ht) and total plasma protein concentration (Cp), further used for calculating blood viscosity, and US examination of the AVF was done. Not all the patients could finish the study. Reasons for early study termination were fistula failure (10), HIV (1), stroke (1) or lost to follow-up (3). Thus, the results presented hereafter refer to those patients (N=28) who completed the whole study.

## 6.3.2. US Examination

US examinations were done with a 12-5 MHz linear array transducer on an HDI 5000 (ATL Ultrasound, Bothell, WA) unit. The radial artery was scanned in longitudinal sections 2-10 cm above the wrist, after at least 5 min of rest in the supine position. Depth and gain settings were optimized to identify the vessel wall-to-lumen interface. Arterial flow velocity was measured using pulsed-wave Doppler, keeping an incidence angle of about 60°. The velocity spectrum was measured at the vessel's axis with the minimum size of sample volume (1 mm) in order to record center-line velocity profile. Luminal diameter and blood velocity measurements were taken on the radial artery, 5-6 cm from the wrist during the baseline visit (pre-surgery), and then at the same location during subsequent visits, corresponding to 2-3 cm proximal to the fistula.

### 6.3.3. WSS Calculation

Velocity spectrum images from the US were transferred to the memory of a personal computer. The maximum velocity contour was traced manually, then converted into numerical data (cm/s) using a general-purpose image analysis software (NIH Image v1.62, NIH, Bethesda, MD). Values of four pulse cycles were averaged in order to obtain final center-line velocity waveform.

In 1955 Womersley [19] presented an analytical model for calculation of unsteady (pulsatile) flow for incompressible, Newtonian fluid in rigid, circular straight tubes. Womersley's theory can be used to develop simple mathematical algorithms for calculating parameters related to unsteady flow like velocity profiles, time-dependent flow, pressure gradient and wall shear stress [20]. We developed a computer program to calculate blood volume flow rate and WSS on the basis of center-line velocity. As input parameters we used the radial artery diameter, heart rate and blood viscosity calculated as a function of plasma protein concentration and hematocrit. Details of the theoretical model used to calculate blood volume flow rate and WSS has been described previously [17].

### 6.3.4. Statistical Analysis

Data are expressed as mean ± standard deviation (SD). Data were analyzed with the ANOVA for repeated measures (SAS v 8.0, SAS Institute Inc., Cary, NC). Tukey post-hoc procedure was used to determine statistically significant differences between visits. Statistical significance was assumed at a value of $P < 0.05$.

## 6.4. Results

Surgical anastomosis between the radial artery and cephalic vein caused a substantial reduction in peripheral resistance and a rise in blood volume flow due to the high pressure gradient between arterial and venous pressures. As shown in Figure 6.1, the resistance index (RI, measured during echo-Doppler examination as 1 – [minimum diastolic velocity / maximum systolic velocity]), dropped immediately after surgery and then remained constant in time.

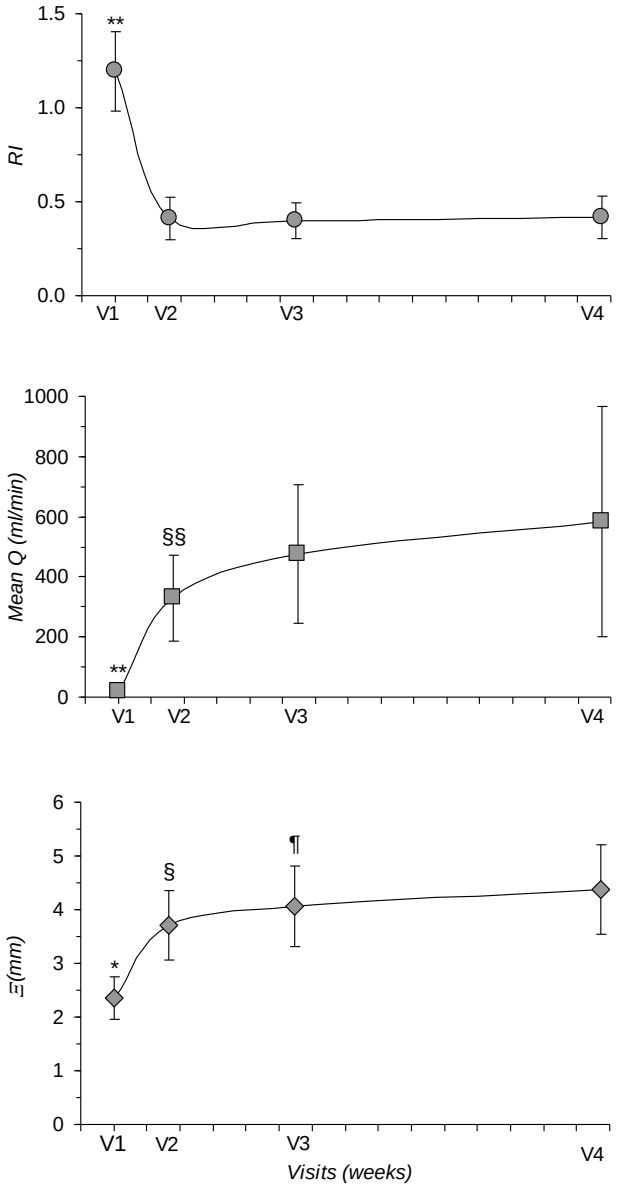


**Figure 6.1. Resistance index (RI), mean blood volume flow (Q), and measured diameter (ϕ) in the normal radial artery (visit 1) and in the arteriovenous fistula at visits 2, 3 and 4 for 28 ESRD patients. *P*<0.05: * vs. V2, V3, V4; § vs. V3, V4; ¶ vs. V4 ; *P*<0.01: ** vs. V2, V3, V4; §§ vs. V3, V4.**

Mean blood volume flow in the radial artery averaged 18±14 ml/min at baseline and rose considerably 10 days after surgery (averaging 329±142 ml/min), and further increased to 476±232 and 583±382 ml/min after 40 and 100 days, respectively. This increase was associated with a significant increase in lumen diameter of the radial artery, that averaged 2.4±0.4 mm before surgery and 3.7±0.7, 4.1±0.8 and 4.4±0.8 mm, at the three visits after surgery ($P$<0.05).

The calculated time-dependent WSS in the radial artery of all 28 subjects at the four visits are presented in Figure 6.2, as mean (black line), pulse-averaged value (dashed line) and range (gray band).

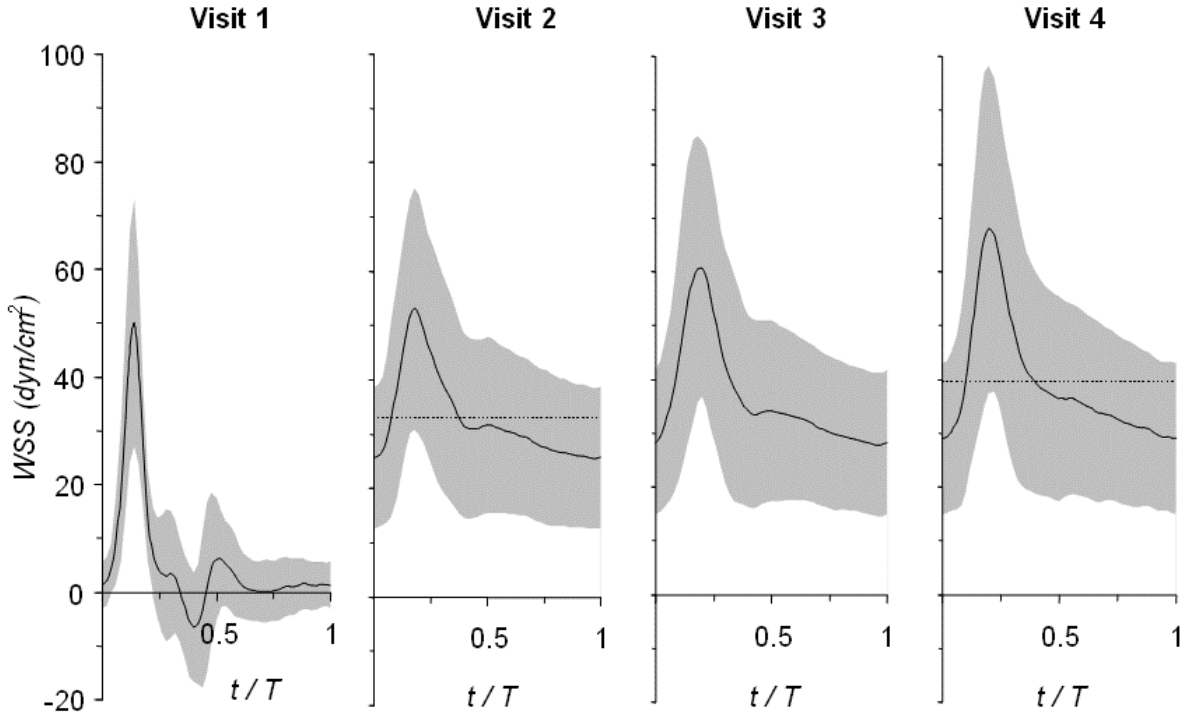


**Figure 6.2. One cycle, time-dependent, wall shear stress calculated in the radial artery before (visit 1) and after creation of the AVF (visits 2, 3, 4) for 28 ESRD patients.**

Averaged values for the measured and calculated parameters at the four visits are reported in Table 6.1. Hematocrit was comparable at visits 1 and 2 but rose significantly at visits 3 and 4. This could be explained by concomitant treatment with erythropoietin as these patients start dialysis therapy. Plasma protein concentration was constant at all four visits, so blood viscosity progressively increased after visit 2 (see Table 6.1), with the increased $H_t$.

**Table 6.1. Main parameters measured and calculated for the radial artery of 28 patients with AVF.**

| N=28 | | V1 | V2 | V3 | V4 |
|---|---|---|---|---|---|
| Time | *days* | -1 | 10 ± 4 | 38 ± 6 | 102 ± 8 |
| Ht | *%* | 30.3 ± 3.4 ‡‡ | 29.9 ± 3.7 § | 32.6 ± 4.0 ¶¶ | 37.4 ± 5.2 |
| Cp | *g/dl* | 6.2 ± 0.8 | 6.3 ± 0.7 | 6.5 ± 0.7 | 6.5 ± 0.8 |
| μ | *cP* | 2.8 ± 0.4 ‡‡ | 2.8 ± 0.4 §§ | 3.0 ± 0.4 | 3.3 ± 0.5 |
| ϕ | *mm* | 2.4 ± 0.4 * | 3.7 ± 0.7 § | 4.1 ± 0.8 ¶ | 4.4 ± 0.8 |
| Q min | *ml/min* | -29 ± 36 ** | 253 ± 126 §§ | 367 ± 194 | 445 ± 310 |
| Q mean | *ml/min* | 18 ± 14 ** | 329 ± 142 §§ | 476 ± 232 | 584 ± 382 |
| Q max | *ml/min* | 121 ± 78 * | 478 ± 218 § | 700 ± 322 | 869 ± 566 |
| RI | - | 1.19 ± 0.21 ** | 0.41 ± 0.11 | 0.40 ± 0.10 | 0.42 ± 0.12 |
| WSS min | *dyn/cm²* | -12 ± 9 * | 25 ± 13 | 27 ± 14 | 28 ± 14 |
| WSS mean | *dyn/cm²* | 6 ± 4 * | 33 ± 16 | 37 ± 17 | 39 ± 18 |
| WSS max | *dyn/cm²* | 45 ± 14 † | 54 ± 21 ‖ | 62 ± 23 | 69 ± 30 |
| WSR min | *s⁻¹* | -441 ± 308 ** | 895 ± 494 | 899 ± 454 | 855 ± 368 |
| WSR mean | *s⁻¹* | 213 ± 140 * | 1200 ± 586 | 1226 ± 519 | 1189 ± 472 |
| WSR max | *s⁻¹* | 1641 ± 470 * | 1980 ± 810 | 2095 ± 724 | 2094 ± 750 |
| | *P<0.05:* | ** vs. V2, V3, V4*<br>*† vs. V3, V4* | *§ vs. V3, V4*<br>*‖ vs. V4* | *¶ vs. V4* | |
| | *P<0.01:* | *** vs. V2, V3, V4*<br>*†† vs. V3, V4*<br>*‡‡ vs. V4* | *§§ vs. V3, V4* | *¶¶ vs. V4* | |

***Legend***: AVF, arteriovenous fistula; Ht, hematocrit; Cp, total protein concentration; μ, viscosity; ϕ, radial artery diameter; Q, blood volume flow rate; RI, resistance index; WSS, wall shear stress; WSR, wall shear rate.

According to our calculations, the increase in blood volume flow after creation of the AVF, led to a large increase in WSS, that very likely acted as a mechanical stimulus for wall remodeling, with a corresponding increase in artery diameter. Mean WSS was significantly higher at all visits than at the pre-surgery visit (6±4 at baseline vs. 33±16, 37±17 and 39±18 dyn/cm$^2$, $P$<0.05). Although from visits 2 to 4 mean WSS continued to rise, the differences were not statistically significant. The minimum WSS followed a pattern similar to the mean WSS. In contrast, despite a large increase (>18 fold) in blood volume flow rate between visits 1 and 2, maximum WSS during the cardiac cycle increased only from 45±14 to 54±21 dyn/cm$^2$ and this difference did not reach statistical significance. Later, at visits 3 and 4, maximum WSS rose slightly, averaging 62±23 and 69±30 dyn/cm$^2$ at 40 and 100 days after surgery, respectively.

It is interesting to note that mean wall shear rate (WSR) rose six fold after fistula creation, then remained constant throughout the observation period (Table 6.1). Thus, although blood volume flow rate increased in time from visit 2 to visit 4 (Figure 6.1), the distribution of blood volume flow velocity gradients near the wall did not change. As shear stress is the product of blood viscosity and shear rate, the slight increase in WSS estimated from visit 2 to visit 4 was exclusively due to the increase in blood viscosity.

## 6.5. Discussion

Ultrasound investigation is becoming the method of choice for the evaluation [21] and management of AVF in ESRD patients [22]. We used echo-color-Doppler to investigate radial artery diameter and center-line blood velocity profiles, before and after creation of the AVF, and calculated blood volume flow and WSS wave-form. The surgical maneuver of shunting between radial artery and cephalic vein produces an important increase in blood volume flow and consequently sudden changes in hemodynamic conditions. We investigated the arterial response during this massive change in WSS to evaluate the mechanism of endothelial response and consequent arterial remodeling. It has to be considered that surgery was performed in end-stage renal failure patients, in which the vascular response may be compromised in some degree. Even if the uremic condition may principally affect endothelial function, we postulate that, due to the initial stage of uremia, the endothelial functions are not affected to such a critical point to be impaired. The echographic examinations and the related computations we performed were fast, and provided a detailed picture of WSS in relation to time. An important point in the method we used is the precision in estimating arterial diameter. Using new-generation ultrasound units, the error involved in measuring radial artery diameter was probably less than 10%, with a consequent margin of error for WSS of the same magnitude. Considering the variability of the phenomena under investigation this can be considered acceptable.

Our investigation showed that, as expected, after creation of the AVF, blood volume flow in the radial artery increased substantially, more than 18 times the baseline value. Before AVF creation mean blood volume flow in the radial artery averaged 18±14 ml/min, while ten days post-operatively mean blood volume flow increased to 329±142 ml/min, and increased during the following observation time. Similar blood volume flow rates were reported by Sivanesan et al. [23] in end-to-side radiocephalic fistulas. In addition, on the basis of these flow and vessel diameter data, WSS calculated in the radial artery were similar to those we previously estimated [18] on the radial side of a 25-month-old end-to-end AVF, using more detailed geometric modeling and computational fluid dynamics analysis.

Our present data show that the rapid increase in radial artery blood volume flow after AVF surgery was associated with concomitant increase in vessel diameter, with a tendency to increase up till the third month after surgery. This stage is usually known as “maturation” of the fistula [24] because during this time both artery and vein dilate and the vein wall thickens,

allowing the repeated needle punctures required for dialysis. In well functioning AVF, this is presumably due to a kind of "vicious circle", since the flow rate increase leads to an increase in arterial diameter, resulting in even higher blood volume flow and further enlargement of the vessel until equilibrium is reached. We tried to clarify the effect of a sustained blood volume flow increase on the adaptation of arterial wall, and specifically the role of endothelial cells as mechano-sensors of arterial response.

As reported by Girerd et al. [16], our study confirmed that the internal diameter of the radial artery increases in response to the chronic increase in blood volume flow. However, mean WSS did not remain constant after AVF surgery but rather increased from 6±4 to 33±16 dyn/ $cm^2$ in average (see Table 6.1). This is different from the observation of Girerd et al that reported constant WSS before and after AVF surgery. This difference may be related to different methods used to calculate the WSS, Hagen-Poiseuille equation versus the Womersley theory we used. It has been shown [25] that the difference in flow rate according to Poiseuille's law and following Womersley's equation for oscillating flow depends non-linearly on the non-dimensional Womersley number $\alpha=R(\omega\rho/\mu)^{0.5}$, where R is the vessel radius, $\omega$ is the angular frequency of the oscillation, $\rho$ is blood density and $\mu$ is blood viscosity. The approximation made by Poiseuille's law is acceptable only for values of $\alpha < 1$, but when $\alpha$ becomes greater than 1, the oscillating flow differs considerably from that predicted by the Poiseuille equation [25]. We calculated a mean value of $\alpha = 2.05$ in the normal radial artery (pre-surgery) and $\alpha = 3.18$ ten days after creation of the AVF, thus supporting our choice of the Womersley model.

The time-function WSS during the cardiac cycle showed different patterns for mean and maximum WSS changes after creation of the AVF. Pre- and post-surgery mean WSS were significantly different ($P<0.05$, see Table 6.1), but maximum WSS remained almost constant, despite substantial increase in radial artery blood volume flow. The finding that peak WSS, rather than mean WSS, is kept constant in human arteries despite major changes in blood volume flow, through an increase in vessel diameter, suggests that the key parameter sensed by endothelial cells is not the mean WSS, as previously indicated [6], but rather the peak WSS during the cardiac cycle. This observation is further supported by the relative changes in mean and maximum WSS during the observation time. As reported in Figure 6.3, after surgery mean WSS was more than seven times the baseline value while maximum WSS was only 30% higher than baseline. Even larger relative differences in mean WSS were found at visits 3 and 4, while maximum WSS remained almost constant.

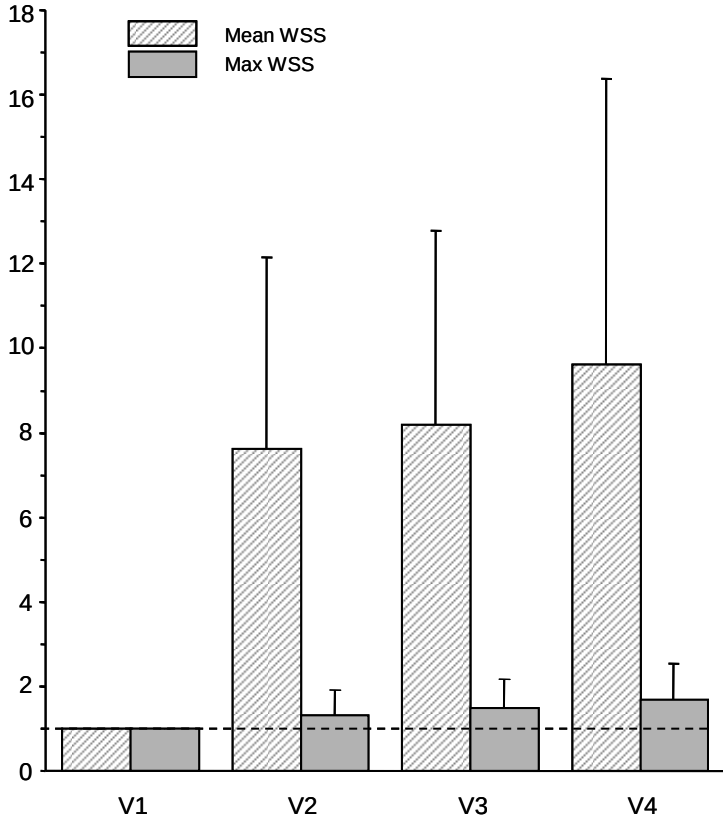


**Figure 6.3. Relative increase of mean and maximum wall shear stress at the three visits post-AVF surgery respect to baseline (pre-surgery: visit 1).**

The biological mechanisms responsible for endothelial cells response to shear stress have been extensively studied for more than twenty years. Most of these studies, however, have employed steady flow conditions with constant shear stress over time [26], [27]. The results of our study, suggesting that endothelial cells in the human radial artery mainly sensed peak shear stress, indicate a potential new mechanism by which endothelial cell function is altered as a response to physical action of blood volume flow. Actually, some experimental studies on endothelial cells in vitro do demonstrate that these cells sense steady and pulsatile shear stress differently. Endothelial cell monolayers exposed to different flow environments differed in their intracellular calcium levels [28], [29], nitric oxide production [30] and cell morphology [31]. Bongrazio et al. [32] showed that genes involved in flow-dependent vascular adaptation are regulated differently in steady or transient flow conditions (see [7] for a review).

The signals transmitted within the cells by time fluctuations in shear forces are at the moment largely unknown. It has been shown that fluid shear stress acting on the luminal surface of endothelial cell membrane [33], induces changes in plasma membrane viscosity and likely affects associated transmembrane proteins that are believed to act as mechano-receptors. We can speculate that such changes might be maximal at peak shear values and may act as main determinant of intracellular biochemical signals.

The observation that the level of peak shear stress determines endothelial cell response to flow can be useful in predicting the effect of chronic changes in arterial perfusion, as in partially stenotic arteries or after reconstructive vascular surgery to improve arterial perfusion. In these conditions, analysis of fluid dynamics within the blood vessel may show how chronic changes in blood volume flow are related to arterial adaptations, considering that vessel remodeling will tend to keep the maximum WSS constant. If applied to clinical conditions, these theoretical analyses may be useful in interpreting the evolution of pathological conditions when planning vascular surgery [34].

In summary, the present results confirm that in humans, major increases in arterial blood volume flow lead to increases in arterial diameter, so as to keep constant peak WSS resulting from pulsatile blood. This may be important for experimental studies aimed at elucidating the mechanisms by which endothelial cells respond to shear forces induced by flowing blood, and predicting arterial adaptation in normal and in pathological conditions.

## 6.6. References


[1] Ku DN, Giddens DP, Zarins CK, Glagov S: Pulsatile flow and atherosclerosis in the human carotid bifurcation. *Arteriosclerosis* 5 (3):293-302, 1985.

[2] Malek AM, Alper SL, Izumo S: Hemodynamic shear stress and its role in atherosclerosis. *JAMA* 282:2035-2042, 1999.

[3] Pasterkamp G, de Kleijn DP, Borst C: Arterial remodeling in atherosclerosis, restenosis and after alteration of blood flow: potential mechanisms and clinical implications. *Cardiovasc Res* 45:843-852, 2000.

[4] Moore JEJ, Xu C, Glagov S, Zarins CK, Ku DN: Fluid wall shear stress measurements in a model of the human abdominal aorta: oscillatory behavior and relationship to atherosclerosis. *Atheroscl*. 110:225-240, 1994.

[5] Neville RF, Sidawy AN: Myointimal hyperplasia: basic science and clinical considerations. *Seminars in Vascular Surgery* 11:142-148, 1998

[6] Giddens DP, Zarins CK, Glagov S: The role of fluid mechanics in the localization and detection of atherosclerosis. *J Biomech Eng* 115:588-594, 1993.

[7] Malek AM, Izumo S: Control of endothelial cell gene expression by flow. *J Biomech* 28:1515-1528, 1995.

[8] Davies PF: Mechanisms involved in endothelial responses to hemodynamic forces. [Review] [18 refs]. *Atherosclerosis* 131 Suppl:S15-7, 1997.

[9] Langille BL, O'Donnell F: Reductions in arterial diameter produced by chronic decreases in blood flow are endothelium-dependent. *Science* 231:405-407, 1986.

[10] Salam TA, Lumsden AB, Suggs WD, Ku DN: Low shear stress promotes intimal hyperplasia thickening. *J Vasc Invest* 2(1):12-22, 1996.

[11] Zarins CK, Zatina MA, Giddens DP, Ku DN, Glagov S: Shear stress regulation of artery lumen diameter in experimental atherogenesis. *J Vasc Surg* 5:413-420, 1987.

[12] Gnasso A, Carallo C, Irace C, De Franceschi MS, Mattioli PL, Motti C, Cortese C: Association between wall shear stress and flow-mediated vasodilation in healthy men. *Atheroscl* 156:171-176, 2001

[13] Gnasso A, Carallo C, Irace C, Spagnuolo V, De Novara G, Mattioli PL, Pujia A: Association between intima-media thickness and wall shear stress in common carotid arteries in healthy male subjects. *Circ* 94:3257-3262, 1996.

[14] Samijo SK, Willigers JM, Barkhuysen R, Kitslaar PJ, Reneman RS, Brands PJ, Hoeks AP: Wall shear stress in the human common carotid artery as function of age and gender. *Cardiovasc Res* 39:515-522, 1998.

[15] Kubis N, Checoury A, Tedgui A, Levy BI: Adaptive common carotid arteries remodeling after unilateral internal carotid artery occlusion in adult patients. *Cardiovasc Res* 50:597-602, 2001.

[16] Girerd X, London G, Boutouyrie P, Mourad J, Safar M, Laurent S: Remodeling of the radial artery in response to a chronic increase in shear stress. *Hypertens* 27(3):799-803, 1996.

[17] Remuzzi A, Ene-Iordache B, Mosconi L, Bruno S, Anghileri A, Antiga L, Remuzzi G: Radial artery wall shear stress evaluation in patients with arteriovenous fistula for haemodialysis access. *Biorheol* 40:423-430, 2003.

[18] Womersley JR: Method for the calculation of velocity, rate of flow and viscous drag in arteries when the pressure gradient is known. *J Physio*l 127:553-563, 1955.

[19] He X, Ku DN, Moore JEJ: Simple calculation of the velocity profiles for pulsatile flow in a blood vessel using Mathematica [published erratum appears in Ann Biomed Eng 1993 Sep-Oct;21(5):557-8]. *Ann Biomed Eng* 21:45-49, 1993.

[20] Nonnast-Daniel B, Martin RP, Lindert O, M¦gge A, Schaeffer J, Lieth HVD, SÜchtig E, Galansky M, Koch K, Daniel WG: Colour Doppler ultrasound assessment of arteriovenous haemodialysis fistulas. *Lancet* 339:143-145, 1992.

[21] Bay WH, Henry ML, Lazarus JM, Lew NL, Ling J, Lowrie EG: Predicting hemodialysis access failure with

color flow Doppler ultrasound. *Am J Nephrol* 18:296-304, 1998.

[22] Sivanesan S, How TV, Bakran A: Characterizing flow distributions in AV fistulae for haemodialysis access. *Nephro Dial Transplant* 13:3108-3110, 1998.

[23] Ene-Iordache B, Mosconi L, Remuzzi G, Remuzzi A: Computational fluid dynamics of a vascular access case for hemodialysis. *J Biomech Eng* 123:284-292, 2001.

[24] England REM, Jackson A: Imaging of dialysis access: a review of 67 failing fistulas investigated by intravenous digital subtraction angiography. *The British Journal of Radiology* 66:32-36, 1993.

[25] Nichols WW, O'Rourke MF: McDonald's blood flow in arteries. Theoretical, experimental and clinical principles. London, Arnold, 1998.

[26] Davies PF: Flow-mediated endothelial mechanotransduction. Physiol Rev 75:519-560, 1995.

[27] Barakat AI, Davies PF: Mechanisms of shear stress transmission and transduction in endothelial cells. [Review]. *Chest* 114:58S-63S, 1998.

[28] Helmlinger G, Berk BC, Nerem RM: Calcium responses of endothelial cell monolayers subjected to pulsatile and steady laminar flow differ. Am.J.Physiol. 269:C367-C375, 1995.

[29] Helmlinger G, Berk BC, Nerem RM: Pulsatile and steady flow-induced calcium oscillations in single cultured endothelial cells. *J Vasc Res* 33:360-369, 1996.

[30] Noris M, Morigi M, Donadelli R, Aiello S, Foppolo M, Todeschini M, Orisio S, Remuzzi G, Remuzzi A: Nitric oxide synthesis by cultured endothelial cells is modulated by flow conditions. *Circ Res* 76:536-543, 1995.

[31] Helmlinger G, Geiger RV, Schreck S, Nerem RM: Effects of pulsatile flow on cultured vascular endothelial cell morphology. *J Biomech Eng* 113:123-131, 1991.

[32] Bongrazio M, Baumann C, Zakrzewicz A, Pries AR, Gaehtgens P: Evidence for modulation of genes involved in vascular adaptation by prolonged exposure of endothelial cells to shear stress. *Cardiovasc Res* 47:384-393, 2000.

[33] Haidekker MA, L'Heureux N, Frangos JA: Fluid shear stress increases membrane fluidity in endothelial cells: a study with DCVJ fluorescence. *Am J Physiol Heart Circ Physiol* 278:H1401-1406, 2000.

[34] Taylor CA, Draney MT, Ku JP, Parker D, Steele BN, Wang K, Zarins CK: Predictive medicine: computational techniques in therapeutic decision-making. *Computer Aided Surgery* 4:231-247, 1999.

# CHAPTER 7

# Discussion and conclusions

## 7.1. General discussion

In the present work we characterized the blood flow field that develop after the surgical creation of the arteriovenous fistulae (AVF) used as vascular access (VA) for haemodialyisis (HD). In particular, we carefully considered the patterns of haemodynamic wall shear stress (WSS) towards a better understanding of its role in the mechanisms of local remodeling (stenosis formation) and vascular adaptation. To this end, we performed computational fluid dynamics (CFD) studies in idealized *side-to-end* and *end-to-end* radial-cephalic AVF models with proper shape and dimensional modeling, as well as in real geometries with patient-specific boundary conditions. We also applied a numerical model based on Womersley's theory for pulsatile flow in tubes to estimate the local WSS in the radial artery of ptients with newly-created *end-to-end* radial-cephalic AVF, and subsequently followed-up during the HD treatment. Briefly, our findings may be summarized in the following paragraphs.

In the AVF for HD, due to the high blood flow rates, irregular vessel geometry, and pulsatility of blood throughout the cardiac cycle, transitional flow with complex secondary and vortical components develop after the anastomosis. This type of flow induce near-wall multidirectional and reciprocating disturbed flow on the juxta-anastomotic vein, and reciprocating disturbed flow on the distal artery in case of *side-to-end* AVF.

In those uremic patients having already impaired endothelial function due to the final stage of renal disease and risk factors such as aging, cardiovascular disease, diabetes, and obesity, the disturbed flow that develops after the surgical creation of the AVF will act as an additional event for the pathogenesis of neointimal hyperplasia, enhancing its development, and leading to immediate failure or to non-maturation of the fistula.

The radial artery diameter enlarges in response to the permanent increase in blood volume flow after the surgical creation of the AVF. Our findings indicate that, at least in the radial artery, the peak shear stress rather than its pulse cycle time-average is the key factor in driving vessel dilatation upon chronic augmentation of the blood flow.

### 7.1.1. Local remodeling in the AVF

Among the events that may contribute to neointima formation, the hemodynamic shear stress at the AVF anastomosis was investigated in our studies (**Chapters 2 to 5**).

The first two studies were performed in idealized models of the AVF to characterize the general flow patterns in such high-flow conduits. The computational study presented in **Chapter 2** was aimed at investigating the haemodynamic flow field and the patterns of wall shear stress in forearm AVF, known to be the major determinant of vascular remodeling and disease in the arterial tree. By using CFD simulations within idealized 3-D models of *side-to-end* and *end-to-end* radial cephalic anastomoses, we have found that WSS patterns are different between the two types of anastomoses and that in the *side-to-end* arterial limb these depend on the flow division ratio and blood direction in the distal artery, i.e. antegrade or retrograde. Zones of low and oscillating WSS that lead to development of intimal hyperplasia were found on the AF and on the inner wall of the SS. We concluded that the zones of low and oscillatory wall shear stress were located in the same sites where luminal reduction was documented in previous experimental studies [13], thus pioneering the pivotal role of disturbed flow in triggering intimal hyperplasia in vascular access.

Based on these findings, in a parametric idealized model of *side-to-end* AVF, we further studied whether the anastomosis angle might influence the pattern of disturbed flow (**Chapter 3**). The model of wrist *side-to-end* radial-cephalic AVF described in this chapter simulates the intra-operative haemodynamic conditions of a newly created AVF. We evaluated the flow distribution in four equivalent meshes having anastomotic angles of 30°, 40°, 60° and 90° in order to study the effects of angle on the local patterns of low and oscillating WSS. Using the relative residence time (RRT) as indicator of disturbed flow, we localized the disturbed flow in the same areas where flow recirculation and stagnation occur, mainly on the SS and at the AF. Quantification of these areas showed that, the smaller the angle, the smaller is the area of low and oscillating WSS. These results suggest that an acute anastomosis angle should be preferred to minimize the risk of neointimal hyperplasia in *side-to-end* radial-cephalic AVF.

We also performed image-based CFD studies in realistic models of AVF, simulating patient-specific blood characteristics and pulsatile volumetric flows (**Chapters 4 and 5**).

In the CFD study presented in **Chapter 4**, we performed a transient simulation in a case of patient-specific, *side-to-end* radial-cephalic AVF. To this aim, we used image-based CFD with patient-specific blood volumetric flow derived from Doppler examinations. Our findings indicate that the results obtained with idealized models of AVF in **Chapters 2 and 3** may

provide useful information regarding the general pattern of disturbed flow, if correct dimensional and boundary conditions are used. We have found that the SS of the vein is a conduit subjected to high multidirectional hemodynamic shear stress and simultaneously develops reciprocating disturbed flow in some focal points. This combination may enhance the pathogenesis of intimal hyperplasia that leads to stenosis and subsequent failure of the VA.

In the CFD study presented in **Chapter 5**, we performed a transient simulation in a case of patient-specific, *end-to-end* radial-cephalic AVF. To this aim, we used DSA images for 3-D reconstruction of the AVF and echo-Doppler ultrasound to measure blood flow velocity in the radial artery. We obtained detailed spatial and temporal information on the flow characteristics, with areas of the vessel wall exposed to non-physiologic WSS, very high on the bending zone, and low on the inner wall after the anastomosis. Reciprocating disturbed flow, as localized by high OSI, develops more on the inner wall, while multidirectional disturbed flow dvelops more on the outer wall of the cephalic vein.

### 7.1.2. Vascular adaptation in AVF

Beside intimal hyperplasia, it is well known that WSS is the physiological stimulus for vascular adaptation upon changes in blood flow. We have previously developed a computational model based on Womersley's theory to estimate haemodynamic parameters like WSS and blood volume flow starting from center-line velocity waveforms measured by Doppler ultrasound in the radial artery [7]. In **Chapter 6** the above computational model was employed in a pilot study in 28 ESRD patients undergoing surgery for placement of wrist radial-cephalic AVF. The radial artery of these patients was examined by ultrasound to gather diameter and blood velocity measurements, 1 day before and then at 10, 40 and 100 days after fistula creation. Time-function blood volume flow and WSS were calculated for these follow-up visits. The results confirmed that the radial artery diameter increases in response to a chronic increase in blood flow in uremic patients. Moreover, it seems that the radial artery dilates in such a way as to maintain the peak wall shear stress constant, suggesting that EC sense the maximum rather than the time-averaged WSS. This finding may lead to further understanding of the mechanisms responsible for endothelial response to physical stimulation by flowing blood.

## 7.3. Main findings and some application of them

Our findings in the article presented in **Chapter 3** were acknowledged in an Editorial Comment in April 2013 issue of ***Nephrology Dialysis Transplantations*** [8]. In the Editorial our study was introduced this way: *"In this issue of NDT, Ene-Iordache et al. (1) present their study 'Effect of anastomosis angle on the localization of disturbed flow in side-artery-to-end-vein fistulae for haemodialysis access'. Many nephrologists may be astonished to find such a specialized article highlighting a small detail of surgical technique. For the authors of this editorial, experienced nephrologists and active in access surgery over a period of many years, the work of Ene-Iordache et al. represents a landmark in the field of the unremarkable, widely unknown, rarely published if ever, but absolutely determining aspects of arteriovenous fistula (AVF) creation - worthwhile to talk about*."

The two studies presented in **Chapter 2** and **3** are interconnected and the key message of the two articles is represented by the statement that "~30° anastomoses represent the solution which minimizes the disturbed flow zones in *side-to-end* radial-cephalic arteriovenous anastomoses". The most important implication of our studies is to inform clinicians about the optimal angle that minimizes the development of intimal hyperplasia resulting from the response of the endothelium to disturbed haemodynamic shear, because changes in anastomosis angle is amenable to surgical manipulation. As shown above, some debate on this was started among the VA community [8] and our hope is to further continue in this research until they will include indication on the anastomotic angle in the specific guidelines for selection and placement of haemodialysis access [1-3]. To further confirm our hypotheses, the next step would be to demonstrate similar findings *in vivo* in longitudinal studies in patients with AVF having acute anastomotic angle. Nevertheless, recent clinical results obtained with the "piggyback" straight-line onlay technique (pSLOT) anastomosis [11] seem very encouraging in this direction by confirming the superiority of acute angle anastomoses over the traditional *side-to-end* approach in terms of improvement in AVF maturation, reduction of juxta-anastomotic stenosis events and increase of vascular access survival.

The work presented in **Chapter 5** has pioneered the image-based CFD studies in patient-specific AVF used as VA for haemodialysis.

In contrast to the classical, widely applied, Poiseuille theory yielding constant haemodynamic shear in time, the pulsatile WSS waveforms obtained in **Chapter 6**, allowed us to formulate a new hypothesis for artery remodeling. Major increases in the blood volume flow lead to increases in the radial artery diameter to maintain constant the peak rather than the mean WSS. Of note, a group of researchers from Maastricht [15], [16] obtained the same finding in the brachial arteries of HD patients followed for one year. While these observations were made in arteries of uremic patients, they may have major implications in understanding the mechano-transduction phenomena that trigger arterial remodeling in general. Recent studies *in vitro* on endothelial cells (EC) undergoing pulsatile shear stress [17], [18] seem to confirm our results and make us believe that such phenomenon may apply also in other arteries, but this hypothesis has to be demonstrated in clinical setting in other conduits.

An interesting application of our finding was the implementation of an algorithm for vascular adaptation over time based on the level of peak WSS in the pulse wave propagation model *pyNS* [14] developed under the ARCH FP7 framerwork. This translated into a better prediction of diameter and blood volume flow in the complete arm vascular network of the VA arm based on pre-operative patient-specific data [10]. The clinical validation of this computational tool was performed in 63 patients with newly primary AVF creation, prospectively followed in the ARCH clinical study [4], [5].

## 7.4. Study limits and further research

### 7.4.1. Study limits

Vascular access can be provided using native vessels or synthetic grafts as was described in the introductory **Chapter 1**. In this thesis we have studied only cases of autogenous AVF surgically created between the radial artery and cephalic vein in the lower arm. This preference was dictated by the fact that in Europe, and more specifically in Italy, radial-cephalic AVF is widely used, and consequently most of our subjects were patients with a VA of this type. Moreover, even in US in the last years the native AVF is becoming the first alternative for new dialysis patients while reducing AVG and CVC use, as requested by the "Fistula First Breakthrough Initiative" [10].

Some of the methods used in the studies presented in this dissertation have intrinsic limits. For example, all our numerical simulations assumed rigid blood vessel walls and a "laminar" model of turbulence.

The numerical model employed in **Chapter 6** is based on Womersley's theory derived from straight, cylindrical and rigid-walled tubes. Of course, this is not the case of arteries and veins employed for VA, but at least this model yields results for pulsatile WSS waveforms, that are more accurate than the constant WSS obtained using the classical Poiseuille formula.

### 7.4.2. Future research

Other types of anastomoses for VA not covered here, like for example *side-to-side* in the lower arm, autogenous and synthetic grafts in the upper arm, are worth investigating to assess whether disturbed flow develops .

Future research and developments may arise from the limits that were underlined above. Patient-specific CFD simulations including models of vessel wall elasticity, i.e. Fluid-Structure Interaction (FSI) simulations would need to be performed to confirm the findings on disturbed flow in the AVF for haemodialysis.

Also, the transitional flow that develops in the venous limb with such high blood voume flows, indicate that further computational investigations should include Direct Numerical Simulation (DNS) or turbulence models.

## 7.5. Take home messages

- Numerical studies revealed fast transition from laminar-to-turbulent flow in the juxta-anastomotic vein, in line with the well known chaotic flow observed by echo-Doppler ultrasound. The high frequency oscillations of the velocity field induce similar haemodynamic stresses on the wall.

- Some areas of the juxta-anastomotic vein wall are characterized by multidirectional disturbed flow and simultaneously develop reciprocating disturbed flow in some focal points, both conditions known as mechanistic links between the haemodynamic stress and the response of the endothelial layer in wall disease.

- Although it remains to be proved, it is plausible that also the high-frequency temporal WSS gradients elicited by the turbulent flow in the juxta-anastomotic vein could be of importance for the understanding of mechanobiology of neointimal hyperplasia, which may have major implications also in the understanding of vascular wall pathogenesis mechanisms in cardiovascular research.

- The vascular adaptation upon chronic changes of blood flow in laminar pulsatile flow in the radial artery is driven by the peak WSS rather than its time-averaged value.

- We used CFD simulations set with high-temporal resolution and minimally dissipative solvers that may run in the time setting of a clinical investigation. Such CFD simulations should be further used in image-based, patient-specific, longitudinal pilot studies that will allow stronger inference conclusions.

# 7.6. References


[1] NKF/KDOQI Vascular Access Work Group. Clinical practice guidelines for vascular access. *Am J Kidney Dis*, 2006; 48 Suppl 1:S176-S247.

[2] NKF/KDOQI Vascular Access Work Group. Clinical practice guidelines for vascular access. *Am J Kidney Dis*, 2006;48 Suppl 1:S248-S273.

[3] Tordoir JHM, Canaud B, Haage P, Konner K, Basci A, Fouque D, Kooman J, Martin-Malo A, Pedrini L, Pizzarelli F, Tattersall J, Vennegoor M, Wanner C, ter Wee P, Vanholder R. EBPG on Vascular Access. *Nephrol Dial Transplant*, 2007;22 Suppl 2:ii88-117.

[4] Clinical study protocol for the ARCH project - computational modeling for improvement of outcome after vascular access creation. Bode A, Caroli A, Huberts W, Planken N, Antiga L, Bosboom M, Remuzzi A, Tordoir J; ARCH project consortium. *J Vasc Access*, 2011; 12(4):369-76.

[5] Caroli A, Manini S, Antiga L, Passera K, Ene-Iordache B, Rota S, Remuzzi G, Bode A, Leermakers J, van de Vosse F, Vanholder R, Malovrh M, Tordoir J and Remuzzi A on behalf of the ARCH project Consortium. Validation of patient specific hemodynamic computational model for surgical planning of vascular access in hemodialysis patients. *Kidney Int* 2013; 84(6):1237-45.

[6] Manini S, Passera K, Huberts W, Botti L, Antiga L, Remuzzi A. Computational model for simulation of vascular adaptation following vascular access surgery in haemodialysis patients. *Comput Meth Biomech Biomed Eng*, 2014; 17(12):1358-67.

[7] Remuzzi A, Ene-Iordache B, Mosconi L, Bruno S, Anghileri A, Antiga L, Remuzzi G: Radial artery wall shear stress evaluation in patients with arteriovenous fistula for hemodialysis access. *Biorheol* 40:423-430, 2003.

[8] Konner K, Lomonte C, Basile C. Placing a primary arteriovenous fistula that works - more or less known aspects, new ideas. *Nephrol Dial Transplant*, 2013; 28(4):781-4.

[9] Passera K, Manini S, Antiga L, Remuzzi A. Patient-specific model of arterial circulation for surgical planning of vascular access. *J Vasc Access*, 2013; 14(2):180-9.

[10] Fistula First Breakthrough Initiative (FFBI). Available at: http://www.fistulafirst.org. Accessed January 19, 2013.

[11] Bharat A, Jaenicke M, Shenoy S. A novel technique of vascular anastomosis to prevent juxta-anastomotic stenosis following arteriovenous fistula creation. *J Vasc Surg*, 2012; 55(1):274-80.

[12] Fan L, Karino T. Effect of a disturbed flow on proliferation of the cells of a hybrid vascular graft. *Biorheology*, 2010; 47(1):31-8.

[13] Sivanesan S, How TV, Bakran A. Sites of stenosis in AV fistulae for haemodialysis access. *Nephrol Dial Transplant*, 1999; 14:118–120.

[14] pyNS - Python vascular Network Solver. Available at: https://github.com/archTk/pyNS. Accessed January 19, 2013.

[15] Dammers R, Tordoir JH, Welten RJ, Kitslaar PJ, Hoeks AP. The effect of chronic flow changes on brachial artery diameter and shear stress in arteriovenous fistulas for hemodialysis. *Int J Artif Organs* 2002; 25(2):124-8.

[16] Dammers R, Tordoir JH, Kooman JP, Welten RJ, Hameleers JM, Kitslaar PJ, Hoeks AP. The effect of flow changes on the arterial system proximal to an arteriovenous fistula for hemodialysis. *Ultrasound Med Biol* 2005; 31(10):1327-33.

[17] Bao X, Lu C, Frangos JA: Temporal gradient in shear but not steady shear stress induces PDGF-A and MCP-1 expression in endothelial cells: role of NO, NF kappa B, and egr-1. *Arterioscler Thromb Vasc Biol*. 1999;19(4):996-1003.

[18] White CR, Haidekker M, Bao X, Frangos JA: Temporal gradients in shear, but not spatial gradients, stimulate endothelial cell proliferation. *Circ* 2001;103 (20):2508-2513.

# ACKNOWLEDGMENTS

I had the idea of this Doctorate while I was participating to the ARCH FP7 project, a project consisting of many participants from Italy, Slovenia, UK, Belgium and of course, The Netherlands. There, I met young people like Nils Planken, Wouter Huberts, Maarten Merkx, Wilco Kroon and Koen Van Canneyt involved in PhD programs with their Institutions. We collaborated on various scientific topics and meet all together during the project meetings we had. It was thus possible to taste some specific beers from UK, Belgium and The Netherlands: it has been a pleasure working with you !

Thus, it is not casually that the Leaders of the ARCH project are now my supervisors. First and foremost, I would like to thank Frans van de Vosse and Andrea Remuzzi for their dedicated supervision and to Wouter Huberts for encouraging me in this idea. Furthermore, I acknowledge the members of my Doctorate Committee for their thorough review of my thesis; specifically, I really appreciated the critical comments on the draft of this thesis of Tammo Delhaas and Gabriele Dubini.

In addition, I wish to thank Gabriele Dubini for giving me the opportunity to work with graduate students from Politecnico di Milano, like Luca Cattaneo, Cristina Semperboni and Michela Bozzetto, which made the life in our Lab more noisy and funny, and with whom it was a pleasure to collaborate with.

During the work for this Doctorate, I was pleasantly surprised to be contacted by Klaus Konner from Köln University Hospital. Thank you for encouraging my studies !

I would like to collectively thank the members of our Biomedical Engineering Department at Mario Negri Institute, to my Lab girls Anna Caroli, Michela Bozzetto and Kanishka Sharma and my Lab boys Sergio Carminati, Davide Martinetti and Flavio Suardi. For this thesis in particular, a special thank goes to Davide for the cover design and to Anna for the precious recommendations from her Doctorate experience.

Finally, the affection of my family was my main fuel to achieve these results, especially the complete support of my mother and my wife. My love goes to Mara, with us since chapter 3 of this thesis, without any doubt the best chapter of our lives. (*Faccio io ! ....Faccio io ! ....Oggi è difficile lavorare con tua moglie !*)

# ABOUT THE AUTHOR

# CURRICULUM VITAE

**Bogdan ENE-IORDACHE** was born on January 18, 1966 in Ploiesti, Romania. He now lives in Italy and owns double citizenship, Romanian and Italian.

After finishing the National College *Mihai Viteazul* in Ploiesti in 1984, he studied Mechanical Engineering at the *Petroleum & Gas* University in Ploiesti. In 1990 he graduated the *Chemical, Petrochemical and Refinery Equipment* section with a thesis entitled "Mechanical project of a reactor for gas oil hydrogenation".

After a one-year working experience in a petroleum refinery in Ploiesti, in 1992 he moved to Bergamo, Italy, where he joined the Bioengineering Lab at the *Mario Negri* Institute for Pharmacological Research. In January 2000, he became head of the new Biomedical Technologies Laboratory created as part of the Department of Biomedical Engineering.

His main interests are on cardiovascular haemodynamics (computational fluid dynamics in large blood vessels), randomized clinical trials (data management and statistics), and renal research (epidemiology of chronic kidney disease, morphometry of glomerular capillary). He published more than 40 papers on these research topics, reaching an *h-index* of 21 and *i10-index* of 29 (by Google Scholar, as of May 2014).

From May 2014 he started a PhD project at TU/e of which the results are presented in this dissertation.

**Contact information:**

**Bogdan Ene-Iordache**
Laboratory of Biomedical Technologies
*Mario Negri* Institute for Pharmacological Research
Via G.B. Camozzi, 3
24020 Ranica (BG)
Italy

Phone: +39-035-4535390
Fax: +39-035-4535371
Mail to: bogdan.ene-iordache@marionegri.it
Webpage: http://villacamozzi.marionegri.it/~bogdan

# LIST OF PUBLICATIONS

## Publications in peer reviewed Journals

1. Ene-Iordache B, Semperboni C, Dubini G and Remuzzi A. Disturbed flow in a patient-specific arteriovenous fistula for hemodialysis: Multidirectional and reciprocating near-wall flow patterns. **J Biomech, 48(10):2195-200, 2015**.
2. Ruggenenti P, Ruggiero B, Cravedi P, Vivarelli M, Massella L, Marasà M, Chianca A, Rubis N, Ene-Iordache B, Rudnicki M, Pollastro RM, Capasso G, Pisani A, Pennesi M, Emma F and Remuzzi G; for the Rituximab in Nephrotic Syndrome of Steroid-Dependent or Frequently Relapsing Minimal Change Disease or Focal Segmental Glomerulosclerosis (NEMO) Study Group. Rituximab in steroid-dependent or frequently relapsing idiophatic nephrotic syndrome. **J Am Soc Nephrol, 25(4):850-63, 2014.**
3. Remuzzi A and Ene-Iordache B. Novel paradigms for dialysis vascular access: upstream hemodynamics and vascular remodeling in dialyis access steonosis. **Clin J Am Soc Nephrol, 8(12):2186-93, 2013**.
4. Gallieni M, Ene-Iordache B, Aiello A, Tucci B, Sala V, Brahmochary Mandal SK, Doneda A, Stella A, Carminatti S, Perico N and Genovesi S. Hypertension and kidney function in an adult population of West Bengal, India: role of body weight, waist circumference, proteinuria and rural area living. **Nephrology, 18(12):798-807, 2013**.
5. Caroli A, Manini S, Antiga L, Passera K, Ene-Iordache B, Rota S, Remuzzi G, Bode A, Leerrmakers J, van de Vosse FN, Vanholder R, Malovrh M, Tordoir J and Remuzzi A. Validation of a patient-specific hemodynamic computational model for surgical planning of vascular access in hemodialysis patients. **Kidney Int, 84(6):1237-45, 2013**.
6. Ene-Iordache B, Cattaneo L, Dubini G and Remuzzi A. Effect of anastomosis angle on the localization of disturbed flow in 'side-to-end' fistulae for haemodialysis access. **Nephrol Dial Transplant, 28(4):995-1005, 2013.**
7. Codreanu I, Sali V, Gaibu S, Suveica L, Popa S, Perico N, Ene-Iordache B, Carminati S, Feehally J and Remuzzi G. Prevalence of hypertension and diabetes and coexistence of chronic kidney disease and cardiovascular risk in the population of the Republic of Moldova. **Int J Hypertens, 951734, 2012**.
8. Cravedi P, Sharma SK, Bravo RF, Islam N, Tchokhonelidze I, Ghimire M, Pahari B, Thapa S, Basnet A, Tataradze A, Tinatin D, Beglarishvili L, Fwu CW, Kopp JB, Eggers P, Ene-Iordache B, Carminati S, Perna A, Chianca A, Couser WG, Remuzzi G and Perico N. Preventing renal and cardiovascular risk by renal function assessment: insigths from a cross-sectional study in low-income countries and the USA. **BMJ Open, 2012 Sep 22;2(5)**.
9. Ruggenenti P, Porrini E, Motterlini N, Perna A, Illiev IP, Dodesini AR, Trevisan R, Bossi A, Sampietro G, Capitoni E, Gaspari F, Rubis N, Ene-Iordache B, Remuzzi G; for the BENEDICT Study investigators. Measurable urinary albumin predicts cardiovascular risk among normoalbuminuric patients with type 2 diabetes. **J Am Soc Nephrol, 2012 Oct;23(10):1717-24**.
10. Ruggenenti P, Gaspari F, Cannata A, Carrara F, Cella C, Ferrari S, Stucchi N, Prandini S, Ene-Iordache B, Diadei O, Perico N, Ondei P, Pisani A, Buongiorno E, Messa P, Dugo M, and Remuzzi G, for the GFR-ADPKD Study Group. Measuring and estimating GFR and treatment effect in ADPKD patients: results and implications of a longitudinal cohort study. **PLoS ONE 7(2):e32533, 2012**.
11. Ene-Iordache B and Remuzzi A. Disturbed flow in radial-cephalic arteriovenous fistulae for haemodialysis: low and oscillating shear stress locates the sites of stenosis. **Nephrol Dial Transplant 27(1):358-368, 2012**.

12. Ruggenenti P, Lauria G, Iliev IP, Fassi A, Ilieva AP, Rota S, Chiurchiu C, Pongrac D, Sghirlanzoni A, Lombardi R, Penza P, Cavaletti G, Piatti ML, Frigeni B, Filipponi M, Rubis N, Noris G, Motterlini N, Ene-Iordache B, Gaspari F, Perna A, Zaletel J, Bossi A, Dodesini AR, Trevisan R and Remuzzi G. Effects of manidipine and delapril in hypertensive patients with type 2 diabetes: the DEMAND randomized clinical trial. **Hypertension 58(5):776-783, 2011**.

13. Ruggenenti P, Perticucci E, Trevisan R, Dodesini A R, Gambara V, Ene-Iordache B, Carminati S, Rubis N, Gherardi G, Perna A, Cravedi P, Remuzzi A, Remuzzi G, The Remission Clinic Task Force. The Remission Clinic approach to halt the progression of kidney disease. **J Nephrol 24(3): 274-281, 2011**.

14. Piccinelli M, Bacigaluppi S, Boccardi E, Ene-Iordache B, Remuzzi A, Veneziani A and Antiga L. Geometry of the ICA and recurrent patterns in location, orientation and rupture status of lateral aneurysms: an image-based computational study. **Neurosurgery 68(5):1270-1285, 2011**.

15. Ruggenenti P, Fassi A, Parvanova A, Petrov I, Chiurchiu C, Rubis N, Gherardi G, Ene-Iordache B, Gaspari F, Perna A, Cravedi P, Bossi A, Trevisan R, Motterlini N, Remuzzi G for the BENEDICT-B Study Investigators. Effects of Verapamil addded-on Trandolapril therapy in hypertensive type 2 diabetes patients with microalbuminuria: the BENEDICT-B randomized trial. **J Hypertens 29(2): 207-216, 2011**.

16. Sharma KS, Hequn Z, Togtokh A, Ene-Iordache B, Carminati S, Remuzzi A, Wiebe N, Ayyalasomayajula B, Perico N, Remuzzi G and Tonelli M. Burden of CKD, proteinuria, and cardiovascular risk among Chinese, Mongolian, and Nepalese participants in the International Society of Nephrology screening programs. **Am J Kidney Dis 56(5):915-927, 2010**.

17. Ruggenenti P, Perna A, Tonelli M, Loriga G, Motterlini N, Rubis N, Ledda F, Rota S, Satta A, Granata A, Battaglia G, Cambareri F, David S, Gaspari f, Stucchi N, Carminati S, Ene-Iordache B, Cravedi P and Remuzzi G. Effects of add-on Fluvastatin therapy in patients with chronic proteinuric nephropathy on dual RAS blockade: the ESPLANADE trial. **Clin J Am Soc Nephrol 5(11):1928-1938, 2010**.

18. Ruggenenti P, Cattaneo D, Rota S, Iliev I, Parvanova A, Perna A, Diadei O, Ene-Iordache B, Ferrari S, Bossi A, Trevisan R, Belviso A and Remuzzi G. Effects of combined Ezetimibe and Simvastatin therapy as compared to Simvastatin alone in patients with type 2 diabetes: a prospective, randomized, double-blind clinical trial. **Diab Care, 33(9):1954-1956, 2010**.

19. Ruggenenti P, Iliev I, Filipponi M, Tadini S, Perna A, Ganeva M, Ene-Iordache B, Cravedi P, Trevisan R, Bossi A and Remuzzi G. Effect of trandolapril on regression of retinopathy in hypertensive patients with type 2 diabetes: a prespecified analysis of the BENEDICT Trial. **J Ophthalmology ID 106384, 1-9, 2010**.

20. Perico N, Antiga L, Caroli A, Ruggenenti P, Fasolini G, Cafaro M, Ondei P, Rubis N, Diadei O, Gherardi G, Prandini S, Panozo A, Bravo RF, Carminati S, Leon FR, Gaspari F, Cortinovis M, Motterlini N, Ene-Iordache B, Remuzzi A and Remuzzi G. Sirolimus therapy to halt the progression of ADPKD. **J Am Soc Nephrol 21(6), 1031-1040, 2010**.

21. Botti L, Piccinelli M, Ene-Iordache B, Remuzzi A and Antiga L. An adaptive mesh refinement solver for large-scale simulation of biological flows. **Int J Numer Meth Eng Biomed 26(1):86-100, 2010**.

22. Ene-Iordache B, Carminati S, Antiga L, Rubis N, Ruggenenti P, Remuzzi G and Remuzzi A. Developing regulatory-compliant electronic case report forms for clinical trials: experience with the DEMAND trial. **J Am Med Inform Assoc 16(3): 404-408, 2009**.

23. Lavinio A, Ene-Iordache B, Nodari I, Girardini A, Cagnazzi E, Rasulo F, Smielewski P, Czosnyka M and Latronico N. Cerebrovascular reactivity and autonomic drive following traumatic brain injury. **Acta Neurochir Suppl 102: 3-7, 2008**.

24. Antiga L, Piccinelli M, Ene-Iordache B, Remuzzi A and Steinman D. An image-based modeling framework for patient-specific computational hemodynamics. **Med Biol Eng Comput 46(11): 1097-1112, 2008**.

25. Ruggenenti P, Iliev I, Costa, G, Parvanova A, Perna A, Giuliano G, Motterlini N, Ene-Iordache B and Remuzzi G. Preventing left ventricular hypertrophy by ACE inhibition in hypertensive patients with type 2 diabetes: a pre-specified analysis of the BENEDICT Trial. **Diab Care 31(8): 1629-1634, 2008**.

26. Remuzzi G, Cravedi P, Costantini M, Lesti M, Ganeva M, Gherardi G, Ene-Iordache B, Gotti E, Donati D, Salvadori M, Sandrini S, Segoloni G, Federico S, Rigotti P, Sparacino V and Ruggenenti P for the MYSS Follow-up Study Group. Mycophenolate mofetil versus azathioprine for prevention of chronic allograft dysfunction in renal transplantation: the MYSS follow-up trial. **J Am Soc Nephrol, 18(6): 1973-1985, 2007.**

27. Ruggenenti P, Perna A, Ganeva M, Ene-Iordache B and Remuzzi G. Impact of blood pressure control and angiotensin-converting enzyme inhibitor therapy on new-onset microalbuminuria in type 2 diabetes: a post-hoc analysis of the BENEDICT trial. **J Am Soc Nephrol 17: 3472-3481, 2006**.

28. Antiga L, Piccinelli M, Fasolini G, Ene-Iordache B, Ondei P, Bruno S, Remuzzi G and Remuzzi A. Computed tomography evaluation of ADPKD progression: a progress report. **Clin J Am Soc Nephrol 1: 754-760, 2006**.

29. Dodesini AR, Lepore G, Neotti C, Ene-Iordache B, Remuzzi A and Trevisan R. Blood pressure and lipids in an Italian outpatient cohort of type 2 diabetic patients: comparison with the general population. **Nutrition, Metabolism & Cardiovascular Diseases 16(6): e1-e3, 2006**.

30. Gotti E, Perico N, Gaspari F, Cattaneo D, Lesti MD, Ruggenenti P, Segoloni G, Salvadori M, Rigotti P, Valente U, Donati D, Sandrini S, Federico S, Sparacino V, Mourad G, Bosmans JL, Dimitrov BD, Ene-Iordache B and Remuzzi G. Blood Cyclosporine level soon after kidney transplantation is a major determinant of rejection: insights from the Mycophenolate Steroid-Sparing trial. **Transpl Proc 37(5): 2037-2040, 2005**.

31. Ruggenenti P, Remuzzi A, Ondei P, Fasolini G, Antiga L, Ene-Iordache B, Remuzzi G and Epstein FH. Safety and efficacy of long-acting somatostatin treatment in autosomal dominant polycistic kidney disease. **Kidney Int 68(1): 206-216, 2005.**

32. Ruggenenti P, Perna A, Loriga G, Ene-Iordache B, Turturo M, Lesti M, Perticucci E, Chakarsky IN, Leonardis D, Garini G, Sessa A, Basile C, Alpa M, Scanziani R, Sorba G, Zoccali C and Remuzzi G for the REIN-2 Study Group. Blood-pressure control for renoprotection in patients with non-diabetic chronic renal disease (REIN-2): multicentre, randomised controlled trial. **Lancet 365(9463): 939-946, 2005.**

33. Ruggenenti P, Fassi A, Ilieva AP, Bruno S, Iliev IP, Brusegan V, Rubis N, Gherardi G, Arnoldi F, Ganeva M, Ene-Iordache B, Gaspari F, Perna A, Bossi A, Trevisan R, Dodesini AR, Remuzzi G for the Bergamo Nephrologic Diabetes Complications Trial (BENEDICT) Investigators. Preventing microalbuminuria in type 2 diabetes. **NEJM 351(19): 1941-1951, 2004.**

34. Remuzzi G, Lesti M, Gotti E, Ganeva M, Dimitrov BD, Ene-Iordache B, Gherardi G, Donati D, Salvadori M, Sandrini S, Valente U, Segoloni G, Mourad G, Federico S, Rigotti P, Sparacino V, Bosmans JL, Perico N, Ruggenenti P. Mycophenolate mofetil versus azathioprine for prevention of acute rejection in renal transplantation (MYSS): a randomised trial. **Lancet 364(9433): 503-512, 2004.**

35. Antiga L, Ene-Iordache B, Remuzzi A. Computational geometry for patient-specific reconstruction and meshing of blood vessels from MR and CT angiography. **IEEE Trans Med Imaging 22(5): 674-684, 2003.**

36. Ene-Iordache B, Mosconi L, Antiga L, Bruno S, Anghileri A, Remuzzi G, Remuzzi A. Radial artery remodeling in response to shear stress increase within arteriovenous fistula for hemodialysis access. **Endothelium 10(2): 95-102, 2003.**

37. Ruggenenti P, Flores C, Aros C, Ene-Iordache B, Trevisan R, Ottomano C, Remuzzi G. Renal and metabolic effects of insulin lispro in type 2 diabetic subjects with overt nephropathy. **Diabetes Care 26(2): 502-509, 2003.**

38. Remuzzi A, Ene-Iordache B, Mosconi L, Bruno S, Anghileri A, Antiga L, Remuzzi G. Radial artery wall shear stress evaluation in patients with arteriovenous fistula for hemodialysis access. **Biorheology 40(1-3): 423-30, 2003.**

39. Ene-Iordache B, Bruno S, Remuzzi A and Remuzzi G. Effect of hemodynamic conditions on arteriovenous fistula for hemodialysis access. **Contrib Nephrol 137: 54-59, 2002.**

40. Antiga L, Ene-Iordache B, Caverni L, Cornalba GP, Remuzzi A. Geometric reconstruction for computational mesh generation of arterial bifurcations from CT angiography. **Comput Med Imaging Graph 26(4): 227-235, 2002.**

41. Antiga L, Ene-Iordache B, Remuzzi G, Remuzzi A. Automatic generation of glomerular capillary topological organization. **Microvasc Res 62(3): 346-354, 2001.**

42. Ene-Iordache B, Mosconi L, Remuzzi G, Remuzzi A. Computational fluid dynamics of a vascular access case for hemodialysis. **J Biomech Eng 123(3): 284-292, 2001.**

43. Remuzzi A and Ene-Iordache B. Capillary network structure does not affect theoretical analysis of glomerular size selectivity. **Am J Physiol 268: F972-F979, 1995.**

44. Ene-Iordache B and Remuzzi A. Numerical analysis of blood flow in reconstructed glomerular capillary segments. **Microvasc Res 49: 1-11, 1995.**

45. Ene-Iordache B, Imberti O, Foglieni O, Remuzzi G, Bertani T and Remuzzi A. Effects of angiotensin-converting enzyme inhibition on glomerular capillary wall ultrastructure in MWF/Ztm rats. **J Am Soc Nephrol 5: 1378-1384, 1994.**

## Collaborator in the following studies

1. Caroli A, Perico N, Perna A, Antiga L, Brambilla P, Pisani A, Visciano B, Imbriaco M, Messa P, Cerutti R, Dugo M, Cancian L, Buongiorno E, De Pascalis A, Gaspari F, Carrara F, Rubis N, Prandini S, Remuzzi A, Remuzzi G, Ruggenenti P; ***ALADIN study group***. Effect of long-acting somatostatin analogue on kidney and cyst growth in autosomal dominant polycystic kidney disease (ALADIN): a randomised, placebo-controlled, multicentre trial. **Lancet 382(9903):1485-95, 2013**.
2. Rurali E, Noris M, Chianca A, Donadelli R, Banterla F, Galbusera M, Gherardi G, Gastoldi S, Parvanova A, Iliev I, Bossi A, Haefliger C, Trevisan R, Remuzzi G, Ruggenenti P; BENEDICT Study Group. ADAMTS13 predicts renal and cardiovascular events in type 2 diabetic patients and response to therapy. **Diabetes 62(10):3599-609, 2013**.
3. Martinelli I, Ruggenenti P, Cetin I, Pardi G, Perna A, Vergani P, Acaia B, Facchinetti F, La Sala GB, Bozzo M, Rampello S, Marozio L, Diadei O, Gherardi G, Carminati S, Remuzzi G, Mannucci PM; ***HAPPY Study Group***. Heparin in pregnant women with previous placenta-mediated pregnancy complications: a prospective, randomized, multicenter, controlled clinical trial. **Blood 119(14):3269-75, 2012**.
4. Zoccali C, Ruggenenti P, Perna A, Leonardis D, Tripepi R, Tripepi G, Mallamaci F, Remuzzi G; ***REIN Study Group***. Phosphate may promote CKD progression and attenuate renoprotective effect of ACE inhibition. **J Am Soc Nephrol 22(10):1923-30, 2011**.
5. Bode A, Caroli A, Huberts W, Planken N, Antiga L, Bosboom M, Remuzzi A, Tordoir J; ***ARCH project consortium***. Clinical study protocol for the ARCH project - computational modeling for improvement of outcome after vascular access creation. **J Vasc Access 12(4):369-76, 2011.**
6. De Cosmo S, Motterlini N, Prudente S, Pellegrini F, Trevisan R, Bossi A, Remuzzi G, Trischitta V, Ruggenenti P; ***BENEDICT Study Group***. Impact of the PPAR-gamma2 Pro12Ala polymorphism and ACE inhibitor therapy on new-onset microalbuminuria in type 2 diabetes: evidence from BENEDICT. **Diabetes 58(12):2920-9, 2009**.
7. The BENEDICT Group. BErgamo NEphrologic DIabetes Complications Trial (BENEDICT): design and baseline characteristics. **Control Clin Trials 24(4): 442-461, 2003**.

## Conference papers

1. Ene-Iordache B, Antiga L, Soletti L, Caverni L, Remuzzi A. Validation of a 3D reconstruction method for carotid bifurcation models starting from angio CT images. 6th International Symposium on Computer Methods in Biomechanics & Biomedical Engineering, **Madrid, Spain, February 2004.**
2. Antiga L, Ene-Iordache B and Remuzzi A. Centerline computation and geometric analysis of branching tubular surfaces with application to blood vessel modeling. 11-th International Conference in Central Europe on Computer Graphics, Visualization and Computer Vision 2003, **Plzen, Czech Republic, February 2003.**

## Divulgence articles

1. Barcella L, Ene-Iordache B, Scarpato M, Beccaria L, Citterio A, Baraldo G and Daina E. Registri di malattie rare: esperienza della Regione Lombardia. **Ricerca & Pratica, November/Dicember 2009.**
2. Ruggenenti P, Ene-Iordache B, Remuzzi G. Excellent survival using kidney transplants from older donors. **Diabetic Microvascular Complications Today, March/April 2006.**
3. Antiga L, Bogdan Ene-Iordache and Remuzzi A. Personalized blood flow simulations. **FluentNews 27, Fall 2003.**

ISBN: 978-90-386-3906-2